[redacted]

JET PROPULSION LABORATORY
CALIFORNIA INSTITUTE OF TECHNOLOGY
PASADENA, CALIFORNIA

FINAL REPORT

ON

QUASI-ISOTROPIC SPACECRAFT ANTENNA SYSTEM

for

National Aeronautics and Space Administration
Jet Propulsion Laboratory
Pasadena, California

[illegible]
by

Dalmo Victor Company
Division of Textron, Inc.
Belmont, California

November 5, 1964
(Revised May 24, 1965)
(Second Revision June 30, 1965)

Prepared by:

Kenneth A. Green
Microwave Design Engineer

John R. Wood
Senior Microwave Engineer

Kenneth A. Green
for Victor Galindo
Senior Microwave Engineer

Approved by:

John B. Damonte
Manager, Microwave Engineering

R D Murie
Robert D. Murie
Chief Engineer

This work was performed for the Jet Propulsion Laboratory, California Institute of Technology, sponsored by the National Aeronautics and Space Administration under Contract NAS7-100.

65-430

PERSONNEL AND AREAS OF RESPONSIBILITY

Kenneth A. Green - Microwave Design Engineer
Antenna design and development and project coordination

Frank L. Hennessey - Senior Microwave Engineer
Consultant on antenna design

John R. Wood - Senior Microwave Engineer
Logic and switching design and development

Victor Galindo - Senior Microwave Engineer
Antenna theoretical analysis

Joseph O. Carter - Mathematical Consultant
Computer programming

Walter A. Read - Microwave Design Engineer
Pattern measurements

Arthur W. Jeong - Microwave Design Engineer
Circuitry fabrication and testing

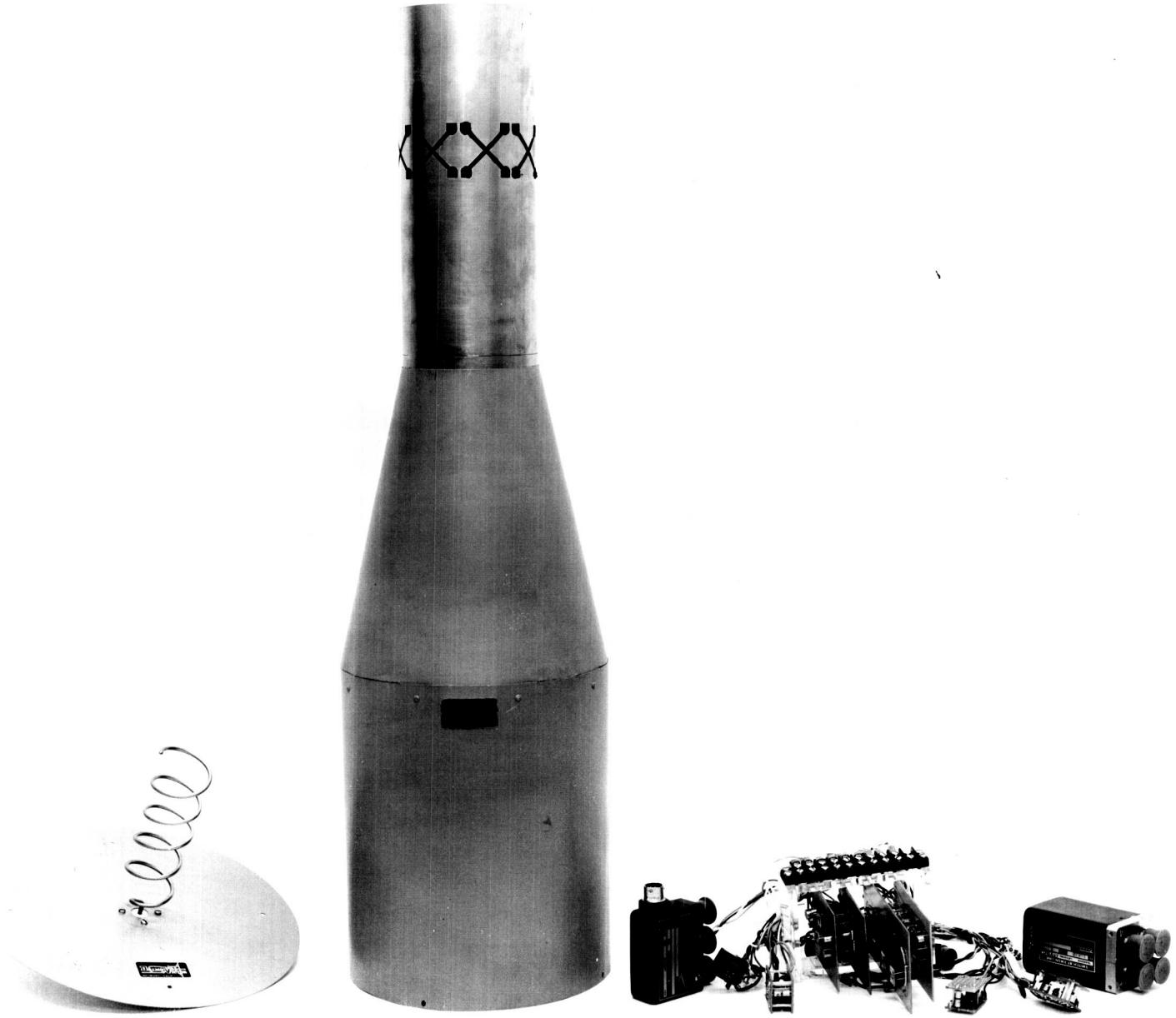

FRONTISPIECE - OVERALL VIEW OF ANTENNAS AND LOGIC

ABSTRACT

This report describes in detail the results of a study and development program leading to a spacecraft quasi-isotropic antenna system for space telemetry.

Two antennas are employed with an automatic logical switching system to assure right circularly polarized spherical pattern coverage at near isotropic gain.

The principal antenna provides right circularly polarized coverage over the maximum area theoretically possible and can easily be adapted to any 10 per cent band from 1 to 10 Gc.

The switching logic, which is designed to operate with one or two receivers and one transmitter, will assure a closed loop telemetry path through the better antenna. Several modes of operation maximize reliability for a given weight.

Author

TABLE OF CONTENTS

TABLE OF CONTENTS (Cont'd)

TABLE OF CONTENTS (Cont'd)

LIST OF ILLUSTRATIONS

LIST OF ILLUSTRATIONS (Cont'd)

LIST OF ILLUSTRATIONS (Cont'd)

LIST OF ILLUSTRATIONS (Cont'd)

at 45° to the input mode, with 90° differential phase shift to the orthogonal components. The radiating section is eight crossed slot elements equispaced on a circumference one-eighth of a wavelength from a short circuit.

The secondary (fill-in) antenna is a right circularly polarized, axial mode helix. Its beamwidth is adjusted to give optimum null-fill-in. A quarter wave transformer on the input allows a good impedance match to 50 ohm coaxial line.

C. Logic

The logic portion of this study presents three modes of operation of a spacecraft communication system. A means of ground control is presented which operates independently of this switching logic. Consideration has been given to providing a fail-safe failure mode.

In Mode I, the system consists of a single receiver and two separate antennas. The logic insures that the best antenna is being used.

In Mode II, two receivers are used in conjunction with two antennas. Here the logic functions to keep the best receiver teamed up with the best antenna and connected to the "on-line" output. If a receiver should happen to fail, the Mode II system becomes a Mode I system.

Mode III adds an additional high gain steerable antenna with an acquisition mode to a Mode II system. The Mode III logic, when activated, first provides a means of establishing lock on this tracking antenna without disturbing the transmit communication link. After lock is established, the logic then permits the transmitter to be switched to the high gain antenna. When not activated, Mode III operates as a Mode II system.

The ground control mode permits the switching function performed by this logic automatically to be individually performed by a ground command. The ground control is possible anytime the spacecraft is in contact with the ground station. Ground control permits switching sequences not wired into the logic. The operator is provided with controls and information that enable him to provide the logic function.

Consideration has been given to providing the best system possible in the event of a failure. This is accomplished by providing an optimum rest state and reverting to a simpler mode or the ground control mode in the event of a failure.

II. PROGRAM GOALS

A. Modes of Operation

1. Mode I

This mode uses one transmitter, one receiver, and two antennas. The logic operates two coaxial relays. One first determines which antenna is used by the receiver; the other then switches the transmitter to that antenna.

2. Mode II

This mode uses one transmitter, two receivers, and two antennas. The logic includes all of Mode I, plus an extra relay at receiver outputs which must also be controlled.

3. Mode III

This mode is a Mode II system plus a remotely selected, steerable, high-gain antenna. Logic is essentially unchanged, except that remote control is mandatory here, optional in Modes I and II.

A demonstration of the feasibility of the logic for the above modes does not require a complete system, but merely one of each type of module, so that the various operations can be simulated. In particular, the relays give complete input/output isolation, so that any given relay can be tested with all others simulated by loads plus a fixed coaxial system.

In fact, given the receiver AGC characteristics, the entire logic **system can be exercised without any RF equipment whatsoever.** This is what was actually done in testing the logic.

B. Pattern Coverage Requirements

The pattern coverage desired from the principal antenna is different for lunar and planetary missions. Definition follows:

1) Lunar Missions - Case I

The gain of the right circularly polarized pattern is to be greater than -4 db from isotropic over the angular range

of 0 to 140° from the spacecraft roll axis. Zero degrees is defined as the spacecraft apex.

2) Planetary Missions - Case II

The gain of the right circularly polarized pattern is to be greater than +1 db from isotropic between 0 and 65° from the spacecraft roll axis and greater than -3 db between 65 and 120°. Zero degrees can be defined as either end of the spacecraft.

The RCP gain in the fill-in region is to be greater than -6 db over the area not specified for coverage by the principal antenna for either case.

Laboratory test models of the two antennas for Case I are to be fabricated and tested, but Case II need not be demonstrated.

C. Other Requirements

In addition to the various modes of operation and pattern coverage requirements, the antenna system is designed to meet or demonstrate its adaptability to the following specifications.

1) Frequency
Receive at 2113 ±5 Mc
Transmit at 2295 ±5 Mc

2) VSWR
VSWR to be 1.4:1 maximum on both antennas.

3) Power Handling
The system shall be capable of transmitting 50 watts of RF power.

4) Power Consumption
The logic shall operate with a maximum of 3.5 watts of average power.

5) System Weight
The antennas, logic, switches, and cables shall not exceed eight pounds total weight.

6) Environment

The design approach shall be amendable to design for one year in space environment.

7) Reliability

The system reliability shall be maximized and a logic failure mode shall be provided.

8) Simplicity

The design shall be simple and practical. All fabrication techniques shall be within the state-of-the-art.

9) Ranger Spacecraft

Patterns shall be performed for various spacecraft configurations to demonstrate the system's application on a full scale mockup for a Ranger spacecraft.

III. ANALYSES OF THE PROBLEMS

A. Limitations on Patterns

1. Theoretical

It has been theoretically demonstrated that a singularly polarized pattern cannot be isotropic[1, 2, 3]. A typical example of an antenna that demonstrates this is Riblet's[4] spherical antenna. This is basically a set of crossed dipoles (turnstile) fed such that the radiation is right circular in one hemisphere and left circular in the other. The polarization around the boundary of the two hemispheres is linear.

Other examples of attempts to produce singularly polarized isotropic patterns are given below.

Bell Telephone Laboratories had a problem similar to ours on the Telstar Experiment. Due to the shape, small size of the satellite, and the large amount of space available for the antenna, a unique solution was found[5] that provided an equatorial circularly polarized pattern with nulls at both ends of the satellite's spin axis. The antenna consisted of a ring of circularly polarized horns, all fed in phase, that encompassed the satellite. This technique could not be applied to a spacecraft the size and shape of the Ranger. It would also be too heavy.

Bugnolo[6] has also used the supporting structure (satellite) as part of the radiating element and obtained results similar to the Telstar antenna, but with linear polarization. The -3 db gain coverage factor was 87 per cent. (Coverage factor is defined in the next section.)

The fact that one antenna cannot yield right circularly polarized isotropic coverage means that a minimum of two antennas must be used. To avoid pattern interference, a switch must be employed to utilize only one antenna at a time. To maximize reliability, the switching action must be minimized; hence, one antenna should cover as much space as possible and no more than two antennas should be used.

2. A Measure of Isotropy

The normal parameters of gain, 3 db beamwidth and minor lobe level do not apply to antennas that approach isotropic coverage.

To evaluate such an antenna, we can specify a required gain level for the desired polarization over a sphere or portions of a sphere, then record and plot a three dimensional gain contour map and note the angular limits of regions that fall below the specified level, and finally, calculate the coverage factor[7] (C. F.). For our purposes, C. F. can be defined as the area in which the gain is equal to or greater than that specified compared to the area for which a gain has been specified.

$$\text{C. F.} = \left[1 - \frac{\int_{\phi_1}^{\phi_2} \int_{\theta_1}^{\theta_2} \sin\theta \, d\theta \, d\phi}{\int_{\phi_3}^{\phi_4} \int_{\theta_3}^{\theta_4} \sin\theta \, d\theta \, d\phi} \right] 100\%$$

where ϕ_1, ϕ_2, θ_1, θ_2 specify area that does not meet specified gain and ϕ_3, ϕ_4, θ_3, θ_4 define area for which a specified gain is required.

NOTE: If more than one area is below specified gain, the numerator of the second term is the sum of the individual areas.

For full spherical coverage, the denominator of the second term = 4π steradians.

An example of the use of coverage factor can be made using the specifications for the principal Case I antenna. Since $\phi_3 = 0$, $\phi_4 = 360°$, $\theta_3 = 0$ and $\theta_4 = 140°$, the area over which coverage is specified is

$$A_s = \int_0^{360} \int_0^{140} \sin\theta \, d\theta \, d\phi = 3.53\pi \text{ steradians}$$

If we assume measured gain contours show the right circular gain to be above -4 db over all the region specified except for the area bounded by $0° \leq \phi \leq 360°$ and $20° \leq \theta \leq 30°$

Then;

$$\int_0^{360} \int_{20}^{30} \sin\theta \, d\theta \, d\phi = 0.148\pi \text{ steradians}$$

Now

$$\text{C.F.} = \left[1 - \frac{0.148\pi}{3.53\pi} \right] 100\% = \underline{\underline{95.8\%}}$$

3. Spacecraft Shadowing

Theoretically, a full 100% coverage can be obtained from one antenna if more than one sense of polarization is accepted. However, the antenna must have an input terminal and be mounted on a vehicle to have any practical value. This vehicle will shadow (block) the antenna and limit the coverage obtainable.

An antenna that possesses the theoretical maximum single polarization coverage can be mounted on a resonable size spacecraft without serious pattern deterioration if,

1) the spacecraft is positioned to shadow only the null region of the antenna's principal polarization pattern, and

2) the spacecraft has no protruding elements that will reflect the incorrect polarization back into the region covered by the antenna.

When reflection or diffraction from the spacecraft creates unacceptable deterioration to the primary antenna coverage, the problem can usually be overcome by redesigning the spacecraft to deflect the unwanted energy into or near the null region. Then the secondary antenna can be designed to provide greater gain than any of the diffraction lobes. This may result in an enlarged secondary antenna coverage area, but 100% coverage can be obtained in two sections, with only two antennas.

B. Environmental Considerations

The requirements of a simple, practical, lightweight, highly reliable antenna system that can be adapted to operate for one year in space greatly restrict the types of designs that can be considered.

Ideally, the antennas, which are external to the spacecraft, should be all metal, self-supporting, possess no moving parts or protruding elements. A basic spherical or cylindrical shape would allow very thin walled material and still maintain strength.

IV. POSSIBLE SOLUTIONS

A. Types of Antennas

1. Crossed Slots in Rectangular Waveguide

One of the possible solutions considered to meet the goals of Section II and overcome the problems of Section III is the quadrature array of rectangular waveguides with topwall crossed slot radiators. Simmons[8] has described the use of a crossed slot in the top wall of a rectangular waveguide as a circularly polarized radiating element. Four of these waveguides can be arrayed in a quadrangle to provide a full 360° coverage in the omni plane. This provides only four elements in the omni plane and, as noted in Section V-B-1-f, the ripple in the pattern exceeds 3 db. Other disadvantages of this type of element are:

1) each rectangular waveguide requires a traveling wave with a load at the end that absorbs 10 to 20% of the total power;

2) the four-way power divider to feed each waveguide is a difficult component to design compact and lightweight;

3) total weight is estimated as excessive.

2. Coax-Fed Slot-Dipoles

A smaller, lighter weight design is the coaxial waveguide with longitudinal slots and probe-fed dipoles. This design was not given detailed consideration for the following reasons:

1) The phase centers of the slots and dipoles cannot be made to coincide so they cannot be circularly polarized over a very broad angular range.

2) Adjusting each element's conductance and phase would be extremely difficult.

3) The dipole support should be thin dielectric and the design would not be mechanically sound.

3. Slot-Fed Parallel Plates on Circular Waveguide

One of the more practical designs originally considered is an array of 45° inclined slots around a circular waveguide with a rotating H_{11} mode. The slots feed circular discs (parallel plates) whose spacing is set to provide 90° differential phase shift between the TEM and the TE (vertical and horizontal) modes excited by the 45° inclined slots.

A disadvantage of this design is the enlarged diameter of the radiating section (outer edge of the parallel plates). Generally, the larger the circumference around an omni antenna, the greater the ripple in the pattern. Another possible problem could develop due to mutual coupling of the various modes excited between the parallel plates.

This design was chosen as a backup to the one selected as the best approach.

4. Crossed Slots in a Circular Waveguide

The design selected as the best approach to the omni-directional, circularly polarized antenna problem is a ring array of crossed slot radiators on a circular waveguide. The waveguide is fed with a circularly polarized H_{11} mode and terminated with a short circuit. This design is extremely simple. Since it is no larger than the waveguide itself, it will be the lightest possible unit. The cylindrical design with no protruding or delicate pieces will result in a very strong and highly reliable design.

Since this design is the one actually developed, complete analysis, both theoretical and experimental, is given in Section V-B of this report.

5. Secondary Antenna

The secondary antenna to fill in the null (region not covered by the omni antenna) cannot be selected until the null region is defined. However, several well known designs can be utilized depending on the beamwidth required.

For half power beamwidths between 20 and 60 degrees, an axial mode helix[9] would be a good choice.

A conical spiral[10] has approximately 60 degrees beamwidth and it is more constant with frequency changes.

An Archimedes spiral[11] (planar spiral) has approximately 80 degrees beamwidth and is also broadband. This design, however, has the disadvantage of requiring a balanced-to-unbalanced impedance transformer.

B. Switching

1. Solid State Relays

The use of solid state switches was considered. However, these were rejected on the following counts:

a) continuous holding power necessary

b) type of power - (high current/low voltage, plus low current/high voltage) - meant added power supplies, cancelling weight and size advantages

c) insertion loss higher than mechanical relays

2. Mechanical Relays

Mechanical relays have several advantages. Their power handling, insertion loss, and isolation are superior to those of solid state devices. Latching configurations are available, saving on power consumption. In addition, use of latching relays simplifies the logic; since they "remember" which position they hold, the logic does not need to do so itself. Mechanical relays are slower than solid state switches, but this does not seem a disadvantage when the desired time delay between loss of signal and switch action is considered.

C. Logic

The logic constraints did not allow much leeway as to the general logic pattern. The mechanization of this pattern, however, allows a number of options to be considered. The logic can be broken down into:

1) a decision element which determines what actions are needed, and when they have been satisfactorily completed

2) a timer to produce required delays, etc.

3) gate circuits to route orders correctly

4) control circuits to operate the coaxial relays

Transistors are a natural for the decision element. Ordinary (bipolar) transistors were used in the breadboarded module. In case the AGC loading of this unit is excessive, or the environment is expected to contain high radiative conditions, field-effect transistors could be substituted easily. While magnetic amplifiers would possibly improve the reliability, the added oscillator needed to power them would probably cancel this advantage.

Diode-transistor logic was selected for the gating circuits. This type of circuit is easy to design, gives good isolation and consistent results. In effect, it allowed remaining circuits to be designed separately, by absorbing the interface problems.

The timer selected consisted of a one-minute clock plus a binary counter. Bipolar transistors were used in both. Consideration was given to the use of magnetic counters, since these would combine period immunity with higher (than 2) counts per stage. Such devices at present are not readily available --particularly in the required size. Conversion, at a later date, to such a counter would not significantly affect the remainder of logic, assuming size to be compatible.

The coaxial relay control circuit finally selected uses controlled switches to operate the relays. The relays selected include a switch to interrupt coil current as soon as relay has transferred, so these switches are satisfactory. Required size and drive power is reduced by an order of magnitude, as a result. No alternatives --miniature relays, conventional transistors, etc., were found that could match their performance. The controlled switches were themselves tripped by pulses from conventional transistors. No particular advantages were noted in the possibility of using field effect transistors here, since low driving impedances are involved.

Conventional sized components were used in the breadboard circuit, since the required package size could be met with them. Considering power levels, micro-size resistors and transistors could be used, together with welded-contact techniques, to further miniaturize the circuits if desired. This would have to be done carefully, however, to avoid loss of reliability.

D. Conclusions

After preliminary evaluation of four types of omni antennas, it was determined that only two could be expected to meet the requirements and that one was obviously superior. It was decided to place full emphasis on the crossed slots in circular waveguide design, since it is basically the same structure as the parallel plate design without the disadvantage of the plates.

A survey of the coaxial switch suppliers and comparison of the best solid state (diode) switches with mechanical latching relays revealed the superiority of the mechanical relays for space applications. Lower power consumption and insertion loss are the chief reasons.

The well defined logic requirements left little choice in the block diagram layout of the switching circuitry.

V. ANTENNAS - CASE I

A. Introduction

Development of the antennas for Case I was the major part of this study program. Sections II-B (pattern coverage and gain requirement) and III-A, -B and -C (analysis of the problem) define the type of antennas required. Section IV-A (possible solutions) concludes that only one of the possible omni-antenna designs was worthy of detailed analysis and development. The following gives the complete theoretical analysis and development details of the crossed slots in Circular Waveguide-Omni Antenna. The selection of the helix as the secondary antenna and details of its development are also included.

B. Omni Antenna

1. Mode and Radiation Theory

a. General Discussion

The fundamental element of the omnidirectional antenna will be a ring of crossed slots or holes located circumferentially around a circular cylinder such as is illustrated in Figure V-1. Each crossed slot or hole will be a circularly polarized radiator of a given sense, the preferred sense. In order to obtain adequate coverage in the northern direction (see Figure V-1) for this sense of polarization, the slots or holes will be phased progressively around the cylinder so that the sense of the ring is the preferred sense in the northern direction.

Actually, each slot will radiate a linear polarization in both the northern and southern directions. The progressive phasing around the cylinder, 360° phase for one revolution about the cylinder, causes the contributions from each slot to add constructively for one sense of circular polarization, the preferred sense, and to add destructively for the other sense in the north pole direction. Toward the south pole the sense of polarization reverses.

It is possible to make extremely accurate theoretical calculations for the radiation field of such a ring of slots or holes on a cylinder provided the cylinder is assumed to be infinite in length and no interfering, scattering objects exist in space. Such calculations have been made and verified by Silver and Saunders[12]. The work of Silver and Saunders is applicable for cylinders of small radius. Although their theory is exact for any cylinder radius, their solution is in

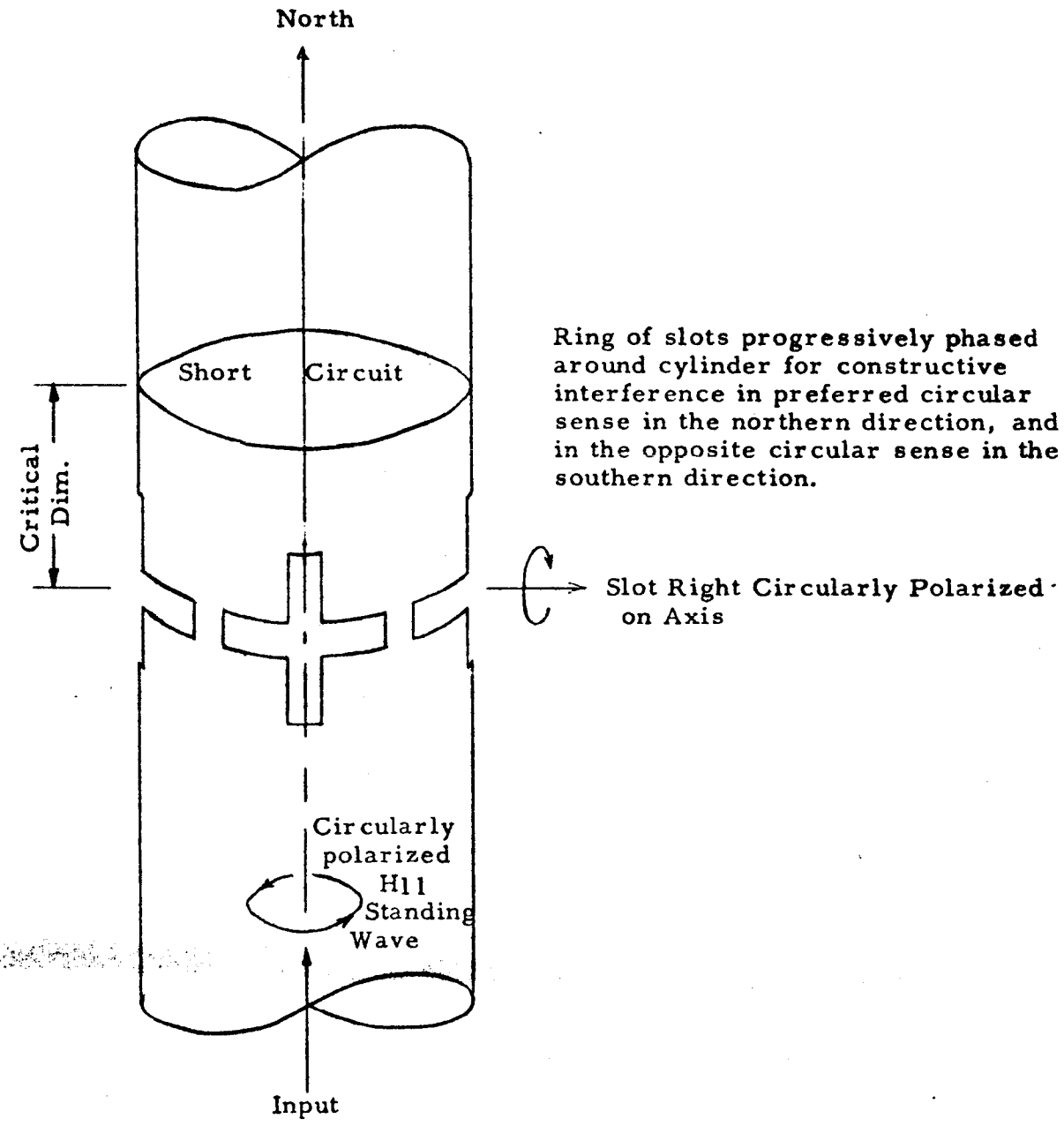

FIGURE V-1

FUNDAMENTAL RING ELEMENT

the form of a modal series which converges very slowly for large cylinder radii. For radii of approximately two or three wavelengths or less their solution is easily applied (depending upon the computer machinery available). It will be seen shortly that our method of exciting these slots will permit a small radius allowing us to use the theory of Reference 12. From the point of view of the exterior problem, that is the radiation problem exclusive of the excitation problem, we will show that the radius of the cylinder has little effect on the elevation pattern (θ plane) resulting from the fundamental ring element and very little on the azimuth pattern (ϕ direction, see Figure V-2), providing enough slots or holes exist in the ring element. The interior or excitation problem makes the radius a more sensitive parameter for the system. This effect is investigated theoretically and found to cause no problem over a substantial bandwidth.

The assumption of infinite length is not a serious one for the exterior problem, since it will be seen that the field decays rapidly away from the slots along the cylinder. There are no surface or leaky waves excited, since this cylinder will support neither. Hence, a total cylinder length of a few wavelengths is adequate for the problem.

The presence of scattering objects of great size on the other hand will obviously be serious in their effects. The presence of the space vehicle by itself is not too serious because of its location near the south pole and can be improved by arraying techniques which are discussed in another section. The practicality of these techniques will depend on the specific space vehicle involved. Such obstacles as a large paraboloid antenna or solar panels protruding far out from the south pole pose a problem which must be overcome by other techniques, as discussed later.

For the exterior problem, we will develop the formulas necessary to determine the radiation fields of rings, of slots and holes and make extensive numerical calculations of such fields. We will make extensive calculations which include the frequency characteristics of the modal system exciting the slots and holes. As mentioned previously, the pure exterior problem which assumes a perfect excitation as a function of frequency indicates the system is very broad band. When the excitation system is included more realistically, the frequency dependency results are obtained and the inherent capabilities of the system are carefully defined theoretically. In both cases, ignoring slot and hole resonance characteristics, the system proves itself to be

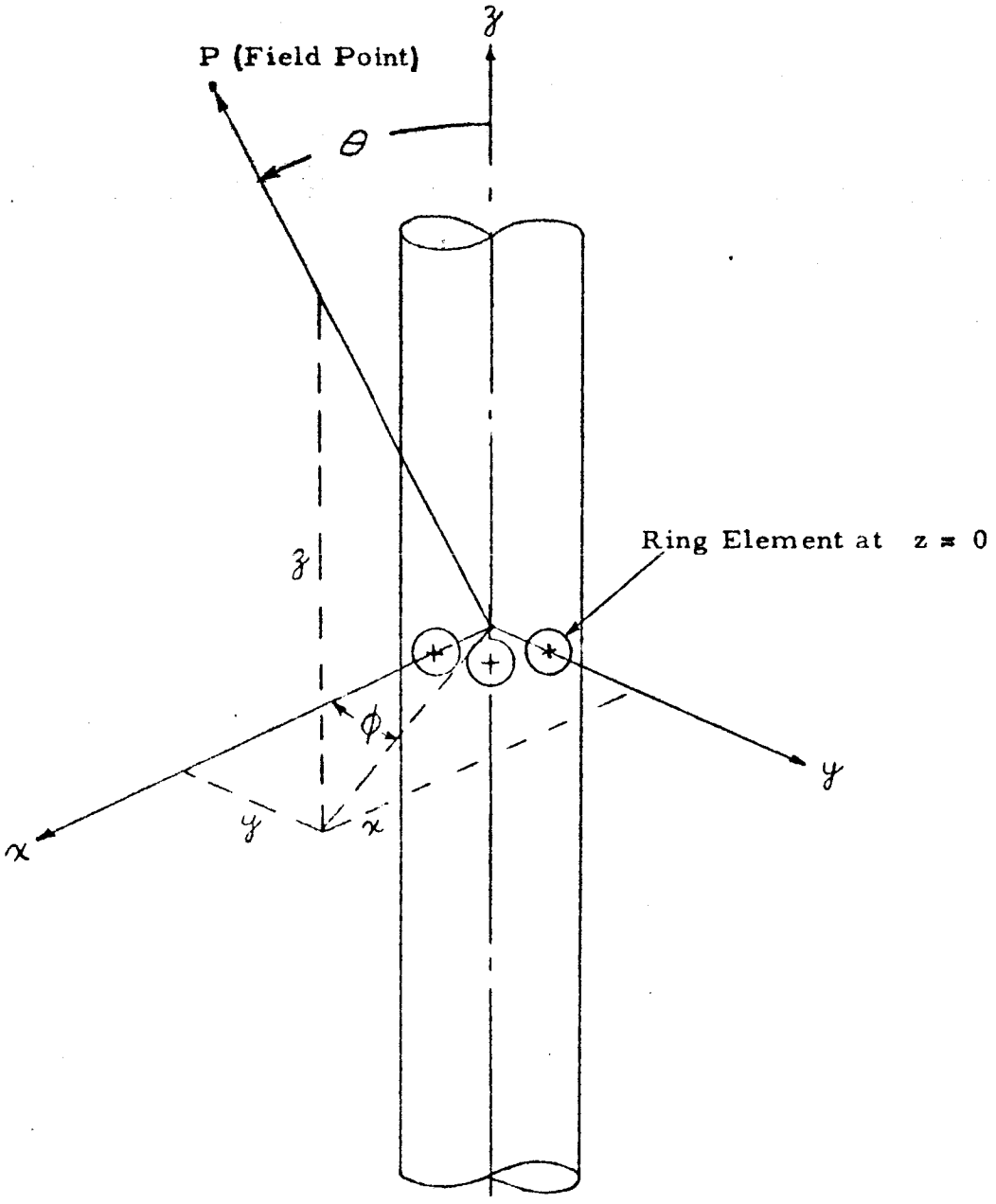

FIGURE V-2

COORDINATE SYSTEM FOR EXTERIOR PROBLEM

inherently wide band. That is, a 20 per cent bandwidth is intrinsically readily obtainable. For low conductances, crossed slots in rectangular waveguides have been shown to be very broad band by Simmons[13]. No great change is expected in this system, although slot resonances do present bandwidth problems if high efficiencies (i.e., high conductances) are required from a few slots.

It has been found that the desired excitation of the slots can be obtained by a standing circularly polarized mode in the cylinder. This mode is obtained by two crossed H_{11} (TE_{11}) circular modes in phase quadrature. The theory is developed in detail in the next section. With this modal excitation of the ring element, it is possible to use the series solution obtained by Silver and Saunders. The practical problem of developing such a modal set in the waveguide is also discussed in a later section.

b. Mode Theory for Cylindrical Circularly Polarized Omni Antenna Feed

In this section we will mathematically describe the modal system required in the cylindrical waveguide. This modal system will excite the ring of crossed slots (or holes) depicted in Figure V-1 with a circularly polarized wall current on the inside of the guide. The proper circumferential phase depends on the ring of slots being located an appropriate distance from the short circuit. The precise conditions for obtaining the correct wall current distribution at the slots will be discussed.

The notation which will be used is that of Marcuvitz[14]. A cylindrical (circular) coordinate system is used. If

J_ϕ = circumferential wall current density

and J_z = longitudinal wall current density

then the wall boundary condition

$$\vec{J} = \hat{n} \times \vec{H} = \hat{r} \times \vec{H}$$

(where $\hat{n}$ and $\hat{r}$ are unit vectors normal to the cylinder walls) yields for these currents (see Marcuvitz[14])

$$J_\phi = -H_z = +j\eta \frac{\lambda \chi'_i}{2\pi a} V_i'' \sqrt{\frac{\epsilon_m}{\pi}} \frac{\chi'_i}{\sqrt{\chi'^2_i - m^2}} \frac{\cos m\phi}{a}$$

and

$$J_z = H_\phi = I_i'' \sqrt{\frac{\epsilon_m}{\pi}} \frac{m}{\sqrt{\chi_i'^2 - m^2}} \frac{\sin m\phi}{a}$$

where

$i = m, n = 1, 1$ for the dominant H_{11} mode,

$\chi_i' = 1.841$ for $i = m, n$;

ϵ_m = Neumann Constant (= 1 for m = 0, = 2 for $m \neq 0$),

λ_{c_i} = cutoff wavelength = $(2\pi a/1.841)$,

a = radius (inside) of cylinder,

$$k_{c_i}'' = \frac{2\pi}{\lambda_{c_i}} = \frac{1.841}{a},$$

K_i'' = guide propagation constant $= \sqrt{k^2 - k_{c_i}''^2}$

$$= \sqrt{\left(\frac{2\pi}{\lambda}\right)^2 - \left(\frac{1.841}{a}\right)^2} = \frac{2\pi}{\lambda_{g_i}''},$$

$\mathcal{J}$ = intrinsic space impedance = $\frac{1}{\eta} = \sqrt{\frac{\mu}{\epsilon}}$ = 377 ohms,

and I_i'' and V_i'' are related excitation coefficients for the i^{th} mode.

The excitation coefficient I_i'' is readily obtained from V_i'' for any mode by

$$I_i'' = \frac{1}{-j K_i'' Z_i''} \left(\frac{d}{dz} V_i''\right)$$

where

$$Z_i'' = \frac{\mathcal{J} k}{K_i''}$$

so that

$$I_i'' = \frac{1}{-j \mathcal{J} k} \left(\frac{d}{dz} V_i''\right) = j \frac{\lambda K_i''}{2\pi(377)} \left\{ \frac{d}{d(K_i'' z)} V_i'' \right\}.$$

With the appropriate substitutions we find that

$$J_{\phi} = j\ A\ V_i''\ \cos\ \phi$$

and

$$J_z = j\ B \left(\frac{d}{d(K_i'' z)}\ V_i'' \right) \sin\ \phi$$

where

$$A = \left[\sqrt{\frac{2}{\pi}}\ \frac{(1.841)^2\ \lambda}{2\pi a^2\ (377) \sqrt{(1.841)^2 - 1}} \right] ,$$

and

$$B = \left[\sqrt{\frac{2}{\pi}}\ \frac{\sqrt{\left(\frac{2\pi}{\lambda}\right)^2 - \left(\frac{1.841}{a}\right)^2}\ \lambda}{2\pi a\ (377)\ \sqrt{(1.841)^2 - 1}} \right] ,$$

and

$$(B/A) = \left[\frac{\sqrt{\left(\frac{2\pi}{\lambda}\right)^2 - \left(\frac{1.841}{a}\right)^2}\ a}{(1.841)^2} \right] .$$

For our purposes, only the ratio (B/A) is of significance.

A traveling H_{11} (TE_{11} circular waveguide mode) wave in the cylindrical waveguide will not produce a ring of circularly polarized wall currents. In this case, for

$$V_i'' = e^{-j K_i'' z} ,$$

we find

$$J_{\phi} = j\ A \cos\ \phi\ e^{-j K_i'' z}$$

and

$$J_z = B \sin\ \phi\ e^{-j K_i'' z} .$$

Since (B/A) is a real constant, there are only four points in ϕ, around the ring, that have circularly polarized wall currents. They are

$$A \sin\ \phi = \pm B \cos\ \phi ,$$

where for the + sign we obtain ϕ_{RC} with one sense of circular polarization and with a π rotation, $\phi_{RC} = \phi_{LC} + \pi$, we obtain the ϕ_{LC} solution for the other sense of circular polarization.

Consider now a 90° rotated H_{11} mode in phase quadrature with the original mode. We obtain the space quadrature by transforming

$$\phi \longrightarrow \phi + \pi/2$$

and noting

$$\cos(\phi + \pi/2) = -\sin\phi$$

and

$$\sin(\phi + \pi/2) = +\cos\phi$$

The phase quadrature is obtained by operating on the original equations with $j = \sqrt{-1}$. We find for the new wall currents of the rotated H_{11} mode

$$J_\phi^r = A \sin\phi \, e^{-j K_i'' z}$$

and

$$J_z^r = j B \cos\phi \, e^{-j K_i'' z}$$

The total wall current for this traveling circularly polarized H_{11} mode is found by combining the equations

$$J_\phi^T = J_\phi + J_\phi^r$$

and

$$J_z^T = J_z + J_z^r$$

with the result that

$$J_\phi^T = j A \, e^{-j\phi} \, e^{-j K_i'' z}$$

and

$$J_z^T = j B \, e^{-j\phi} \, e^{-j K_i'' z}$$

We note that the phase dependence, $e^{-j\phi}$, of the above modal combination is appropriate for excitation of the ring element. The polarization is, however, linear and tilted at an angle ψ,

where

$$\psi = \arctan\left(\frac{J_z^T}{J_\phi^T}\right) = \arctan\ (B/A)$$

(B/A was given earlier as a constant depending on the frequency and guide radius only.) The current angle for this modal system is depicted in Figure V-3. If ψ was made equal to 45°, the above result suggests that a wave traveling in the opposite direction,

$$V_i'' = e^{+j K_i'' z}$$

would combine at half-wavelength ($\lambda_{g_i}''/2$) intervals to give circularly polarized wall currents of a given sense and with the same desired ϕ-dependence

$$e^{-j\phi}$$

Actually, the circularly polarized current can be obtained independent of the ratio (B/A), but dependent on the z-position in the guide as indicated. Furthermore, although the sense of circular polarization does not change at $\lambda/2$ intervals, the phase does alternate.

A wave traveling oppositely, in z, to our original wave is a standing wave. Therefore we have as the excitation voltage coefficient

$$V_i'' = \sin K_i'' z$$

and

$$\frac{d}{d(K_i'' z)} V_i'' = \cos K_i'' z$$

Therefore, we find that a single <u>standing</u> H_{11} mode results in the currents

$$J_\phi = jA \cos\phi \sin K_i'' z$$

and

$$J_z = jB \sin\phi \cos K_i'' z$$

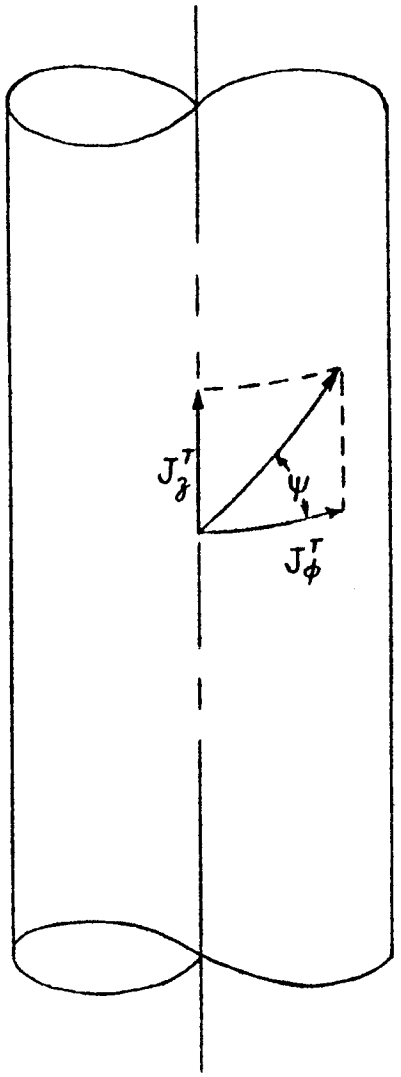

FIGURE V-3

TILTED LINEAR WALL CURRENT

The rotated H_{11} standing mode that is in phase quadrature with the original standing mode has wall currents

$$J_{\phi}^{r} = A \sin \phi \sin K_i'' z$$

and

$$J_z^r = -B \cos \phi \cos K_i'' z$$

Combining J_{ϕ} with J_{ϕ}^{r} and J_z with J_z^r gives, for the total wall current due to a standing circularly polarized H_{11} mode in the circular guide, the results

$$J_{\phi}^{T} = j A e^{-j\phi} \sin K_i'' z$$

and

$$J_z^T = -B e^{-j\phi} \cos K_i'' z$$

The above currents have the desired ϕ dependence. Taking the above current ratio

$$(J_z^T / J_{\phi}^T) = j (B/A \text{ ctn } K_i'' z)$$

we see that the condition for a circularly polarized wall current is

$$\pm 1 = (B/A) \text{ ctn } K_i'' z$$

where the $\pm$ sign is chosen appropriately for the desired circular sense of rotation.

The correct z positions for a given sense of circular polarization is seen to be, therefore

$$z = \frac{\pm 1}{\sqrt{\left(\frac{2\pi}{\lambda}\right)^2 - \left(\frac{1.841}{a}\right)^2}} \arctan \left[\frac{a\sqrt{\left(\frac{2\pi}{\lambda}\right)^2 - \left(\frac{1.841}{a}\right)^2}}{(1.841)^2} \right]$$

The ratio (J_z^T / J_{ϕ}^T) varies from $-\infty$ to $+\infty$ as z varies over $(\lambda_{g_i}'' / 2)$. Hence any polarization is obtainable and repeats identically every $(\lambda_{g_i}'' / 2)$. The precise position of a given polarization with respect to a zero or short in the line depends upon (B/A) or the frequency and quide radius. It will be shown later that this change causes no deterioration of the ring element pattern over a wide bandwidth.

Although the currents are circularly polarized in the same sense every ($\lambda''_{g_i}/2$) along z on the guide, the formulas for J_ϕ^T and J_z^T show clearly that the phase of this circularly polarized excitation for the slot ring element alternates between 0° and 180° every $\lambda''_{g_i}/2$.

c. Radiation Fields of Axial and Circumferential Slots in a Cylinder

1) General

The mode theory discussed in the previous section showed how a ring of right circularly polarized wall currents on the inside of the cylinder could be excited. It was assumed that the cylinder was perfect. That is, the radiating apertures were assumed not to affect the internal mode. When these apertures (slots, holes, etc.) are cut into the wall, then the currents are disturbed.

In the exterior problem which will now be discussed we have a similar approximation. We assume that over an arbitrary aperture in the cylindrical waveguide there exists a known tangential electric field distribution

$$E_\phi = f_1(\phi, z)$$

and

$$E_z = f_2(\phi, z)$$

in cylindrical coordinates as illustrated in Figure V-4. This distribution will be the same as that which was assumed for the undisturbed currents on the interior wall of the waveguide. Once given $f_1(\phi, z)$ and $f_2(\phi, z)$ we can solve the exterior problem to determine the radiated far field pattern.

Ideally, we should solve the interior and exterior problems simultaneously to arrive at a true solution to both problems. As a by-product of this solution, the slot or hole admittances would also be determined. In general, it is beyond the state-of-the-art to solve this type of problem exactly, although Stevenson[15] has done this approximately for slots in thin walled rectangular guide and Silver[16] has shown how a solution could be approached. In general practice the assumptions indicated above have proven excellent, expecially for narrow slots in thin walled guides. Very good results are obtained herein also. Silver and Saunders[17]

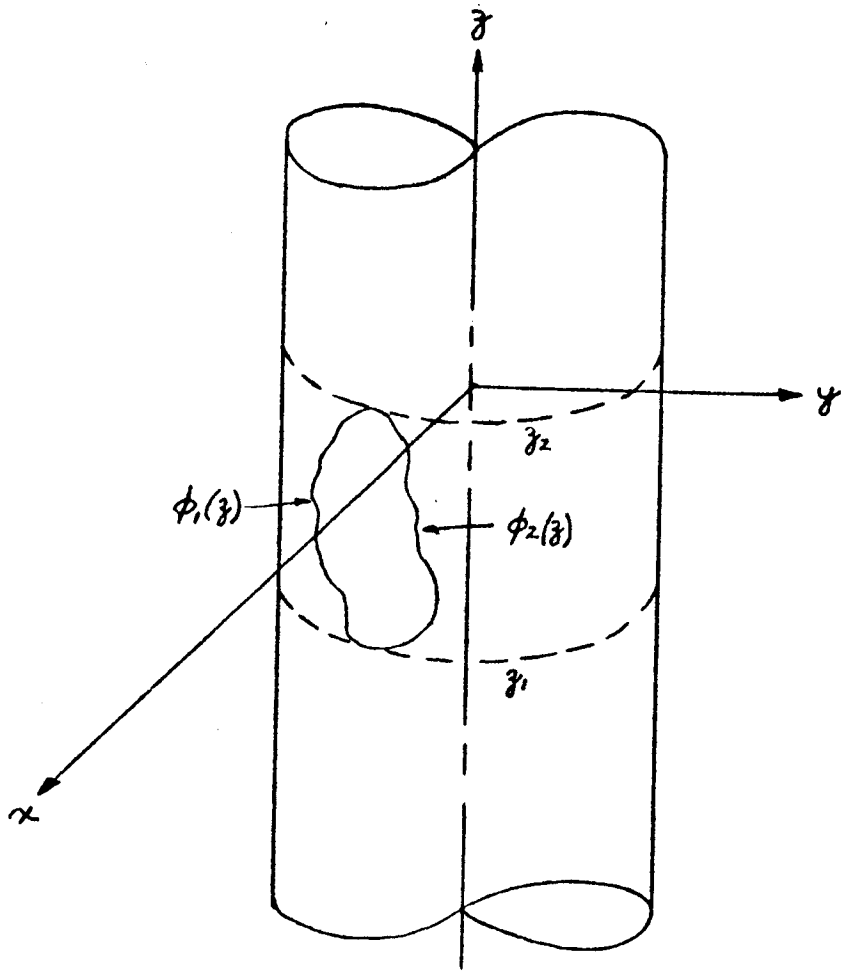

FIGURE V-4

APERTURE GEOMETRY ON CYLINDER

have published very good results for a transverse slot. We will obtain results for crossed slots, holes, and a ring array of crossed slots which also agree very well with experiment. (However, the experiments for a ring array element are difficult by comparison because of the omni-directivity of the pattern and the non-infinite cylinder.) None of these specific computations have been performed before this time.

Silver and Saunders[18] have shown if $E_\phi = f_1(\phi, z)$ and $E_z = f_2(\phi, z)$ are tangential electrical field distributions over the aperture shown in Figure V-4, then the resultant far electric field components E_θ and E_ϕ are given by (at distance R)

$$E_\theta = \left(\frac{e^{-jkR}}{2\pi^2 R}\right) \sum_{n=-\infty}^{\infty} \left\{ \frac{j^{n+1} e^{-jn\phi}}{\sin\theta \, H_n^{(2)}(ka\sin\theta)} \right.$$

$$\left. \times \int_{z_1}^{z_2} d\xi \, e^{jk\xi\cos\theta} \int_{\phi_1(\xi)}^{\phi_2(\xi)} f_2(\beta, \xi) e^{jn\beta} d\beta \right\}$$

and

$$E_\phi = \left(\frac{e^{-jkR}}{2\pi^2 R}\right) \sum_{n=-\infty}^{\infty} \left\{ \frac{j^{n} e^{-jn\phi}}{H_n^{(2)'}(ka\sin\theta)} \right.$$

$$\times \left[\int_{z_1}^{z_2} d\xi e^{jk\xi\cos\theta} \int_{\phi_1(\xi)}^{\phi_2(\xi)} f_1(\beta, \xi) e^{jn\beta} d\beta \right.$$

$$\left. \left. + \frac{n\cot\theta}{ka\sin\theta} \int_{z_1}^{z_2} d\xi e^{jk\xi\cos\theta} \int_{\phi_1(\xi)}^{\phi_2(\xi)} f_2(\beta, \xi) e^{jn\beta} d\beta \right] \right\}$$

In this section we will consider the radiation field from rectangular slots such as is illustrated in Figure V-5.

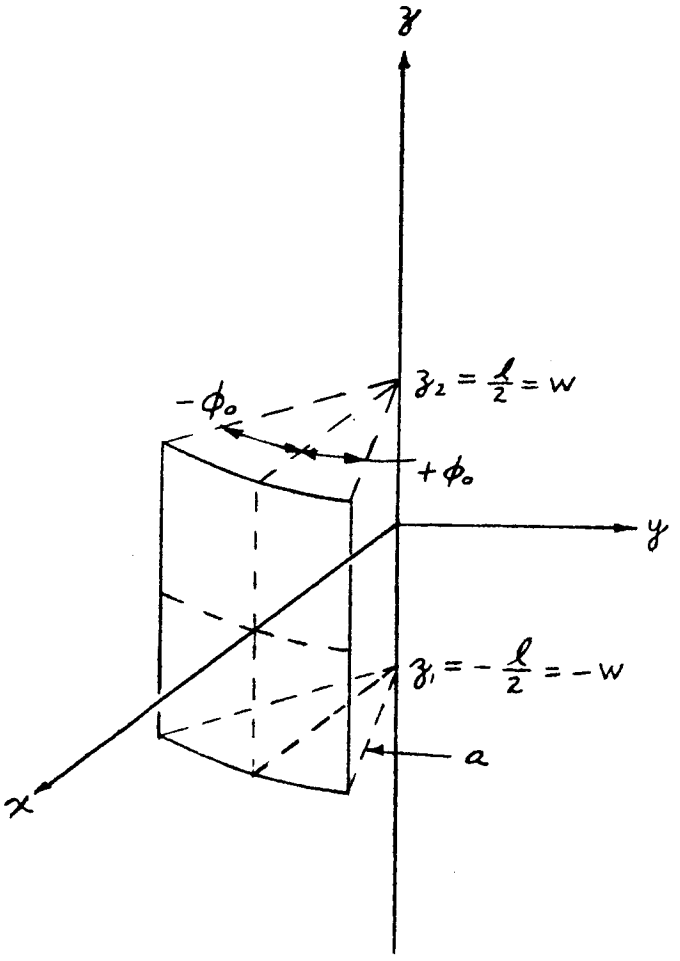

FIGURE V-5

"RECTANGULAR" APERTURE ON CYLINDER WALL

Depending upon whether $(a\phi_o/\lambda) \ll 1$ or $(\lambda/a\phi_o) \ll 1$, the slot is respectively axial or circumferential. A combination of the axial and circumferential slots will give us the basic crossed slot. Experimentally, a crossed slot rotated 45° was used. By comparing the results of a circular hole aperture (next section) with those obtained for the crossed slot oriented vertically or circumferentially, we can show that no significant difference exists. Hence, a crossed slot that is rotated by 45° from the theoretical crossed slot should give no significantly different results either.

2) The Circumferential Half-Wavelength Slot

In this case we assume $(2W/a\phi_o) \ll 1$. The tangential electrical field in the ϕ direction in the aperture is therefore equal to zero. That is

$$E_\phi^a = 0 \Rightarrow F_1 = G_1 = 0,$$

where F and G are defined by

$$f(\beta, \xi) = F(\beta)\ G(\xi)$$

for both f_1 and f_2. That is, we assume separable tangential field distributions.

The z-component field is given by

$$E_z^a = F_2(\phi)\ G_2(z) = \frac{V_c}{2W} \cos\frac{\pi\phi}{2\phi_o}\ e^{-j\phi}$$

for $(-\phi_o \leq \phi \leq \phi_o)$ and $(-W \leq z \leq W)$. Outside of this latter range for ϕ and z we have both E_z^a and E_ϕ^a equal to zero.

The $e^{-j\phi}$ dependence for E_z^a is due to the mode phase variation discussed earlier. It has been found that the effect on the radiation field due to this $e^{-j\phi}$ factor is fairly insignificant. Mathematically it does introduce a reasonably significant complication. Nevertheless, the factor is retained in the calculations since the effect of the factor on the radiation pattern is difficult to ascertain before calculation.

The equation for E_θ becomes, for this case,

$$E_\theta = -\left(\frac{-jkR}{2\pi^2 R}\right) \sum_{n=-\infty}^{\infty} \left\{ \frac{j^{n+1} e^{-jn\phi}}{\sin\theta \, H_n^{(2)}(ka\sin\theta)} \right.$$

$$\left. \times \int_{-w}^{w} \frac{V_c}{2w} e^{-jk\xi\cos\theta} d\xi \int_{-\phi_o}^{\phi_o} \cos\left(\frac{\pi\beta}{2\phi_o}\right) e^{j\rho\beta} d\beta \right\}$$

where $\rho = n - 1$, or

$$E_\theta = -\left(\frac{e^{-jkR}}{2\pi^2 R}\right) \sum_{n=-\infty}^{\infty} \left\{ \frac{j^{n+1} e^{-jn\phi}}{\sin\theta \, H_n^{(2)}(ka\sin\theta)} \right\} I_\xi \, I_\beta$$

where for I_ξ we get

$$I_\xi = \int_{-w}^{w} \frac{V_c}{2w} e^{jk\xi\cos\theta} d\xi = V_c \frac{\sin(kw\cos\theta)}{(kw\cos\theta)}$$

and for I_β we get

$$I_\beta = \int_{-\phi_o}^{\phi_o} \cos\left(\frac{\pi}{2\phi_o}\beta\right) e^{j\rho\beta} d\beta = \left(\frac{\pi}{2\phi_o}\right) \left[\frac{\cos\rho\phi_o}{\left(\frac{\pi}{2\phi_o}\right)^2 - \rho^2}\right]$$

Note that V_c is an arbitrary complex constant coefficient which will ultimately be adjusted in relation to a similar constant for the axial slot in order to achieve a circularly polarized slot excitation from the exciting modal currents discussed earlier.

Collecting the above terms for E_θ and writing E_θ^c for E_θ we have finally that

$$E_\theta^c = -j\left(\frac{e^{-jkR}}{2\pi^2 R}\right) V_c \left[\frac{\sin(kw\cos\theta)}{(kw\cos\theta)}\right] \left(\frac{\pi}{2\phi_o}\right)$$

$$\times \ (1/2) \sum_{n=0} \left\{ \frac{j^n \ \epsilon_n}{\sin\theta \ H_n^{(2)} \ (k a \sin\theta)} \left[\frac{e^{-jn\phi} \cos (n-1)\phi_o}{\left[\left(\frac{\pi}{2\phi_o}\right)^2 - (n-1)^2\right]} \right.\right.$$

$$\left.\left. + \ \frac{e^{+jn\phi} \cos (n+1)\phi_o}{\left[\left(\frac{\pi}{2\phi_o}\right)^2 - (n+1)^2\right]} \right] \right\}$$

where ϵ_n = Newmann constant (= 1 for $n = 0$ and 2 for $n \neq 0$) When the factor $e^{-j\phi}$ is not used for E_z^a we obtain

$$E_\theta^c = -j \left(\frac{e^{-jkR}}{2\pi^2 R}\right) V_c \left[\frac{\sin (k w \cos\theta)}{(k w \cos\theta)}\right] \left(\frac{\pi}{2\phi_o}\right)$$

$$\times \sum_{n=0}^{\infty} \frac{j^n \ \epsilon_n}{\sin\theta \ H_n^{(2)}(k a \sin\theta)} \left[\frac{\cos n\phi}{\left(\frac{\pi}{2\phi_o}\right)^2 - n^2}\right]$$

We have retained the factor $e^{-j\phi}$ despite the fact that we have found the above two equations (for our range of input parameters) yield little difference in the radiation fields.

Another possible approximation, made by Silver and Saunders, is

$$\frac{\sin (k w \cos\theta)}{(k w \cos\theta)} \approx 1$$

since w is very small. Our computations will not include this approximation, although it is a good one. Although these approximations are valid, their usefulness is limited when high speed machine computations are made.

The equation for E_ϕ becomes

$$E_\phi = \left(\frac{e^{-jkR}}{2\pi^2 R}\right) \sum_{n=-\infty}^{\infty} \left[\frac{j^n \ e^{-jn\phi}}{H_n^{(2)'}(k a \sin\theta)}\right] \left(\frac{n \cot\theta}{k a \sin\theta}\right)$$

$$x \int_{-w}^{w} \frac{V_c}{2w} e^{-jk\xi \cos\theta} d\xi \; x \int_{-\phi_o}^{\phi_o} \cos\left(\frac{\pi\beta}{2\phi_o}\right) j\rho\beta_d\beta \Bigg]$$

$$= \left(\frac{e^{-jkR}}{2\pi^2 R}\right) \left(\frac{\cot\theta}{ka\sin\theta}\right) \sum_{n=-\infty}^{\infty} \left[\frac{n\, j^n\, e^{-jn\phi}}{H_n^{(2)\prime}(ka\sin\theta)} I_\xi \; I_\beta\right]$$

Letting $E_\phi \rightarrow E_\phi^c$ as a new notation and inserting the values for I_ξ and I_β given earlier, we have finally

$$E_\phi^c = \left(\frac{e^{-jkR}}{2\pi^2 R}\right) V_c \left[\frac{\sin(kw\cos\theta)}{(kw\cos\theta)}\right] \left(\frac{\pi}{2\phi_o}\right) \left(\frac{\cot\theta}{ka\sin\theta}\right)$$

$$x \sum_{n=-\infty}^{\infty} \left[\frac{n\, j^n\, e^{-jn\phi}}{H_n^{(2)\prime}(ka\sin\theta)} \quad \frac{\cos(\rho\phi_o)}{\left[\left(\frac{\pi}{2\phi_o}\right)^2 - \rho^2\right]}\right]$$

Since it is generally useful to have a summation extend from 0 to ∞ rather than $-\infty$ to ∞ we may make several manipulations to find

$$E_\phi^c = \left(\frac{e^{-jkR}}{2\pi^2 R}\right) V_c \left[\frac{\sin(kw\cos\theta)}{(kw\cos\theta)}\right] \left(\frac{\pi}{2\phi_o}\right)$$

$$x \left(\frac{\cot\theta}{ka\sin\theta}\right) \sum_{n=0}^{\infty} \frac{n\, j^n\, \epsilon_n}{\left[H_{n-1}^{(2)}(ka\sin\theta) - H_{n+1}^{(2)}(ka\sin\theta)\right]}$$

$$x \left[\frac{e^{-jn\phi}\cos(n-1)\phi_o}{\left[\left(\frac{\pi}{2\phi_o}\right)^2 - (n-1)^2\right]} - \frac{e^{jn\phi}\cos(n+1)\phi_o}{\left[\left(\frac{\pi}{2\phi_o}\right)^2 - (n+1)^2\right]}\right]$$

3) The Axial Half-Wavelength Slot

In this case, referring to Figure V-5, we assume $a\phi_o'/2w = a\phi_o'/\ell << 1$. Hence we find that the tangential electric z-component in the aperture is zero, that is

$$E_z^a = 0 \Rightarrow F_2 = G_2 = 0$$

The ϕ component in the aperture is given by

$$E_\phi^a = F_1(\phi)\ G_1(z) = \frac{V_A}{2a\phi_o'} \cos(\pi/\ell\ z)$$

Note that we use ϕ_o' in place of ϕ_o since both these quantities will exist in the crossed slot and we must distinguish their values. Note also that V_A is the complex excitation constant for the axial slot.

This slot gives rise to no θ - component in the radiation field. That is

$$E_\theta^A = 0$$

The ϕ component is readily found (see Silver and Saunders[12]) for the case

$$\ell = \lambda/2$$

Actually, the radiation field changes very little for small changes of ℓ around $\lambda/2$, so this assumption is valid. We obtain,

$$E_\phi^A = \left(\frac{e^{-jkR}}{2\pi^2 R}\right) V_A \left[\frac{\cos(\pi/2 \cos\theta)}{\sin\theta}\right](1/a)$$

$$\times\ 2 \sum_{n=0}^{\infty} \left[\frac{j^n \epsilon_n \cos n\phi}{(\sin\theta)\left[H_{n-1}^{(2)}(ka\sin\theta) - H_{n+1}^{(2)}(ka\sin\theta)\right]}\right]\left(\frac{\sin n\phi_o'}{n\phi_o'}\right)$$

where ϵ_n = Neumann constant. When ϕ_o' is small and the series converges rapidly we may assume

$$\frac{\sin n \phi_o'}{n \phi_o'} \sim 1$$

Although these assumptions are valid for the numerical calculations performed in this report, the above approximation was not used in these calculations.

We will, in a later section, adjust V_A and V_e so that at $\theta = 90°$ and $\phi = 0°$, in line with the slots centers and the cylinder center, the radiated field is circularly polarized when the circumferential and axial slots are radiating simultaneously. The total field is, of course, simple the sum field in this case:

$$E_\theta = E_\theta^c + E_\theta^A = E_\theta^c$$

and

$$E_\phi = E_\phi^c + E_\phi^A$$

d. The Field of a Hole Aperture in the Cylinder

The computation of the radiation field of a circular hole in wall of the cylindrical waveguide is of interest for several reasons.

As explained earlier, if a computation of the radiation field due to the hole aperture is very little different than the field due to a crossed slot aperture, then a rotation of the slots will make little difference in the radiated fields. Rotating the slots may be valuable for mechanical or space saving reasons. Actual computed results do in fact verify the above reasoning when compared with experimental results.

In general, the hole is very simple to construct in the waveguide in comparison to the slots. Furthermore, the hole provides only one variable parameter, the radius, whereas two slot lengths exist for the crossed-slot. Variation of these parameters, radius or lengths, has little effect on the radiation field, however, although they very significantly affect the admittance, the aperture presents to the waveguide mode system. We will not attempt to compute that effect.

Strictly speaking, an elliptic hole would allow two variable parameters to be adjusted. The hole that we shall consider

will not be exactly circular either, but rather it shall be that shape which would occur if it were drilled with a circular drill. Hence, referring to Figure V-6, the projection of the aperture on the y-z plane is a circle, but the aperture is somewhat more complicated.

The radius of the projected circle is α and the equation of this circle is

$$y^2 + z^2 = \alpha^2$$

The radius of the cylinder is a. Expressed analytically as a surface we have

$$\rho = \sqrt{x^2 + y^2} = a$$

for the cylinder. In effect, the intersection of the hole cylinder

$$y^2 + z^2 = \alpha^2$$

and the waveguide cylinder

$$\rho = a$$

defines the aperture hole. We must solve these equations simultaneously to find

$$\phi_1(z),\ \phi_2(z),\ z_1(\phi),\ \text{and}\ z_2(\phi)\ \text{(see Figure V-6)}$$

so that we may ultimately evaluate

$$I = \int_{z_1}^{z_2} G(\xi) e^{ik\xi\cos\theta} d\xi \int_{\phi_1(z)}^{\phi_2(z)} F(\beta) e^{jn\beta} d\beta$$

$$= \int_{\phi_1}^{\phi_2} F(\beta) e^{jn\beta} d\beta \int_{z_1(\beta)}^{z_2(\beta)} G(\xi) e^{ik\xi\cos\theta} d\xi$$

for the radiated field (see Section c.). (Either $\phi_1(\xi)$ and $\phi_2(\xi)$ or $z_1(\beta)$ and $z_2(\beta)$ is necessary).

Solving for the intersection of the two cylinders gives for the aperture hole, the equations:

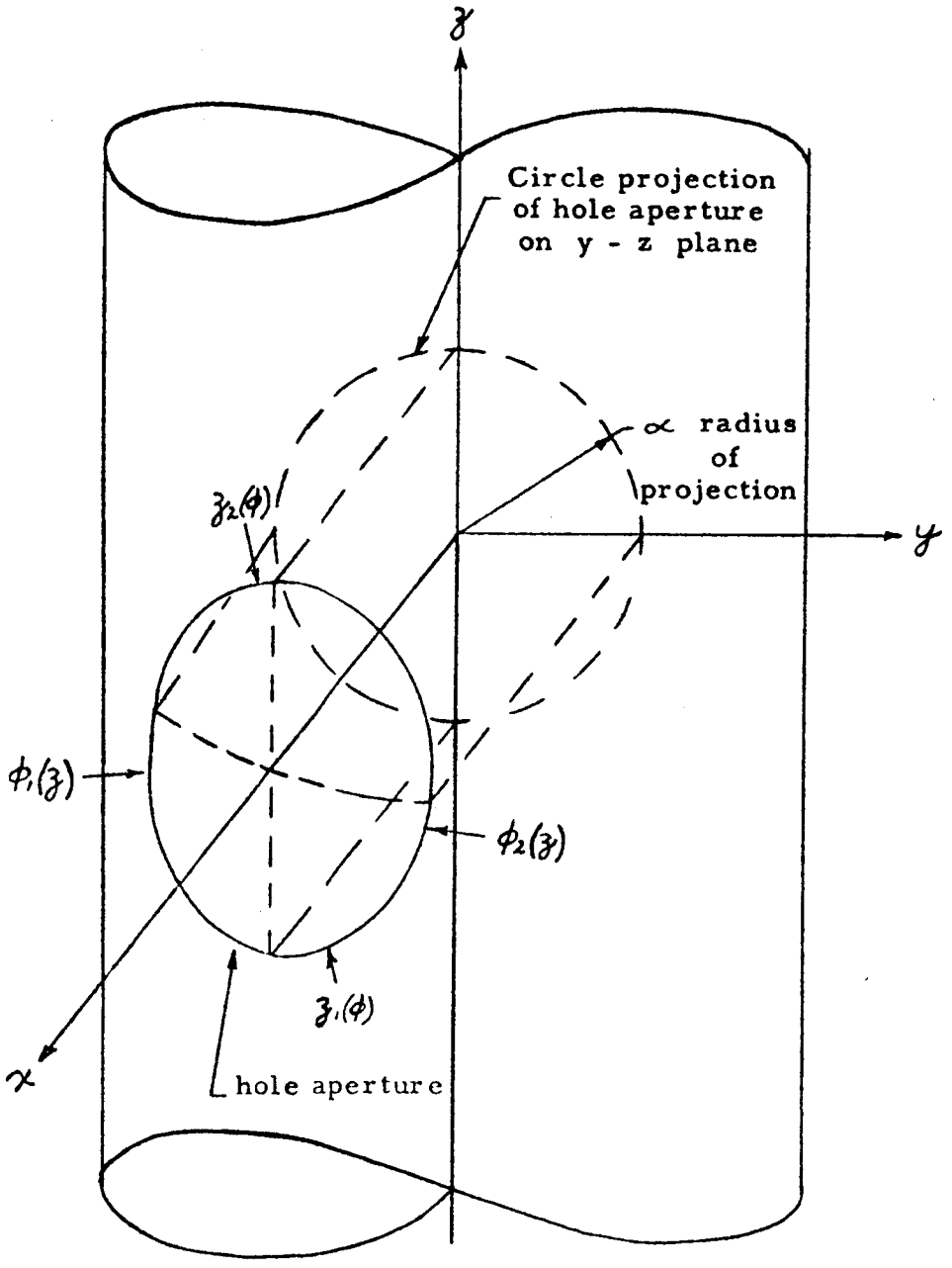

FIGURE V-6

HOLE IN CYLINDER WALL

$$z = \pm \sqrt{\alpha^2 - a^2 \sin^2 \phi}$$

and

$$\phi = \pm \arcsin \sqrt{\frac{\alpha^2 - z^2}{a^2}}$$

From this point on, a number of assumptions and approximations will be made in determining the field radiated by the hole. Ultimately, the computed results will be shown to agree very well with the experimental results so that the assumptions and approximations are indeed good ones.

The first assumption is that for the tangential field in the aperture we will assume a uniform amplitude distribution with a phase variation $e^{-j\phi}$. For a small hole, this assumption is clearly good. However, it does give good results for holes with $2\pi\alpha \approx \lambda$. We assume, therefore, that for a z-directed current excitation

$$E_\phi^a = 0$$

and

$$E_z^a = \left[V_z/2\alpha\right] e^{-j\phi} = F_2(\phi) = G_2(z)$$

when the hole is excited with a z-directed wall current inside the waveguide. The quantity V_z is an arbitrary complex excitation coefficient for the hole. This is similar to the circumferential slot.

We find, in this case, that

$$I = \frac{V_z}{2\alpha} \int_{z_1}^{z_2} e^{ik\xi\cos\theta} d\xi \int_{-\arcsin\sqrt{\frac{\alpha^2 - \xi^2}{a^2}}}^{+\arcsin\sqrt{\frac{\alpha^2 - \xi^2}{a^2}}} e^{j(n-1)\beta} d\beta$$

The right hand integral (the first integration) gives

$$\int_{-\mathcal{L}}^{+\mathcal{L}} e^{+j(n-1)\beta} d\beta = \frac{2\sin\left[(n-1)\arcsin\sqrt{\frac{\alpha^2 - z^2}{a^2}}\right]}{\left[(n-1)\arcsin\sqrt{\frac{\alpha^2 - z^2}{a^2}}\right]} \arcsin\sqrt{\frac{\alpha^2 - z^2}{a^2}}$$

We now make two approximations. We assume that the series will converge rapidly so that n is not large, and we require that $\alpha << a$. With these approximations we find

$$\int_{-\mathcal{L}}^{+\mathcal{L}} e^{j(n-1)\beta} d\beta \approx 2 \sqrt{\frac{\alpha^2 - z^2}{a^2}}$$

and

$$I \approx \frac{2 V_z}{2 \alpha a} \int_{-\alpha}^{+\alpha} \sqrt{\alpha^2 - z^2}\; e^{ik z \cos\theta}\, dz$$

With $\eta = \xi / \alpha$ we obtain the convenient form

$$I \approx (\alpha/a)\, V_z \int_{-1}^{1} \sqrt{1 - \eta^2}\; e^{j(\alpha k \cos\theta)\eta} d\eta$$

$$= (\alpha/a)\, V_z\, (I_1 + j\, I_2)$$

where

$$I_1 = \int_{-1}^{1} \sqrt{1 - \eta^2}\; \cos b\eta\, d\eta,$$

$$I_2 = \int_{-1}^{1} \sqrt{1 - \eta^2}\; \sin b\eta\, d\eta,$$

and

$$b = \alpha k \cos\theta$$

We see by symmetry that

$$I_2 = 0$$

In order to evaluate I_1 we must make an additional approximation. Note that

$$b_{max} = \alpha/\lambda\; 2\pi$$

and $$\cos b_{max} \eta_{max} = \cos (\alpha/\lambda\; 2\pi).$$

If $\alpha \lesssim 1/10\ \lambda$ then $\cos b_{max}\ \eta_{max} \sim 0.8$.

If we assume therefore that

$$\cos b\eta \approx 1 - b^2 \eta^2/2$$

we will have a very good approximation. This gives

$$I_1 \approx \pi/2 - \pi/16\ b^2$$

and

$$I = (\alpha/a)\ V_z\ (\pi/2)\left(1 - \frac{\alpha^2 k^2 \cos^2\theta}{8}\right)$$

For the z-directed wall current excitation we obtain for the radiation field therefore that

$$E_\theta^z \quad -j\left(\frac{e^{-jkR}}{2\pi^2 R}\right) V_z \left[(\alpha/a)\,\pi/2 \quad \left(1 - \frac{\alpha^2 k^2 \cos^2\theta}{8}\right)\right]$$

$$x \sum_{n=0}^{\infty} \left(\frac{j^n \epsilon_n \cos n\phi}{\sin\theta\ H_n^{(2)}(ka\sin\theta)}\right) ,$$

and

$$E_\phi^z \approx \left(\frac{e^{-jkR}}{2\pi^2 R}\right) V_z \left[\left(\frac{\alpha}{a}\right)\pi/2\left(1 - \frac{\alpha^2 k^2 \cos^2\theta}{8}\right)\right]\left(\frac{\cot\theta}{ka\sin\theta}\right)$$

$$x\ 2 \sum_{n=0}^{\infty} \left[\frac{n\, j^n \epsilon_n \cos n\phi}{\left[H_{n-1}^{(2)}(ka\sin\theta) - H_{n+1}^{(2)}(ka\sin\theta)\right]}\right]$$

When the waveguide wall currents are purely circumferential or ϕ-directed we assume that the tangential aperture distribution is

$$E_z^a = 0$$

and

$$E_\phi^a = F_1(\phi)\ G_1(z) = \frac{V_\phi}{2\alpha}\ e^{-j\phi}$$

where V_ϕ is an arbitrary complex excitation coefficient. This case is similar to that of the axial slot. In this case we make the same approximations that were made earlier and find for the radiation field that

$$E_\theta^\phi = 0 = (E_\theta \text{ due to } \phi\text{-directed current})$$

and

$$E_\phi^\phi \approx \left(\frac{e^{-jkR}}{2\pi^2 R}\right) I \sum_{n=-\infty}^{\infty} \left(\frac{j^n e^{-jn\phi}}{H_n^{(2)'}(ka\sin\theta)}\right)$$

where I is the same double integral evaluated earlier. Hence we obtain finally that

$$E_\phi^\phi \approx \left(\frac{e^{-jkR}}{2\pi^2 R}\right) V_\phi \left(\frac{\alpha}{a}\right) \pi/2 \left[\left(1 - \frac{\alpha^2 k^2 \cos^2\theta}{8}\right)\right]$$

$$\times \; 2 \sum_{n=0}^{\infty} \left[\frac{j^n \epsilon_n \cos n\phi}{\left[H_{n-1}^{(2)}(ka\sin\theta) - H_{n+1}^{(2)}(ka\sin\theta)\right]}\right]$$

When the hole is excited by a circularly polarized current we merely add the ϕ and z-directed current excitations with appropriate values for V_ϕ and V_z to get the total field components

$$E_\theta = E_\theta^\phi + E_\theta^z = E_\theta^z$$

and

$$E_\phi = E_\phi^\phi + E_\phi^z$$

We will actually combine the total E_θ and E_ϕ components to compute the total circularly polarized components directly. In addition we will compute the total field of a ring array of holes or crossed slots arranged around the circumference of the waveguide cylinder. This will be done in the next section.

e. Arrays of Radiators on a Cylinder

1) Axial and Circular Array of Radiators

In the previous sections we have derived the radiation fields due to an axial slot, a circumferential slot, and a hole that is excited by the waveguide mode in either the z or ϕ directions. In this section we shall derive the field due to a rather arbitrary array of such radiators on a right circular cylinder. The array may consist of any combination of holes and slots with the exception that at a given value of z on the cylinder (axial position) the ring array in the circumferential direction is equispaced and consists entirely of crossed slots or holes. Such a generalized array is shown in Figure V-7. In practice the array would probably consist of identical elements in the z-direction except for their conductance values and the pattern effect of the z-arraying would then be accounted for most readily by a linear array factor.

For a circumferential slot that is symmetrically located at $\phi = 0$ and $z = 0$ on the cylinder (see Figure V-8a) we have found the radiation field as

$$E_\theta^c = V_c \, f_\theta^c(\theta, \phi)$$

and

$$E_\phi^c = V_c \, f_\phi^c(\theta, \phi)$$

The functions f_θ^c and f_ϕ^c are those actually found in Section c. The excitation coefficient V_c is generally complex and depends on the excitation and the geometry (resonance or admittance characteristics) of the slot. We will assign values to V_c and the excitation coefficients of other radiators in the array later.

The axial slot (Figure V-8b) that is symmetrically oriented along the x-axis at $z = 0$ has a radiation field

$$E_\theta^A = 0$$

and

$$E_\phi^A = V_A \, f_\phi^A(\theta, \phi)$$

where f_ϕ^A is derived in Section c and V_A is the complex excitation coefficient for this slot.

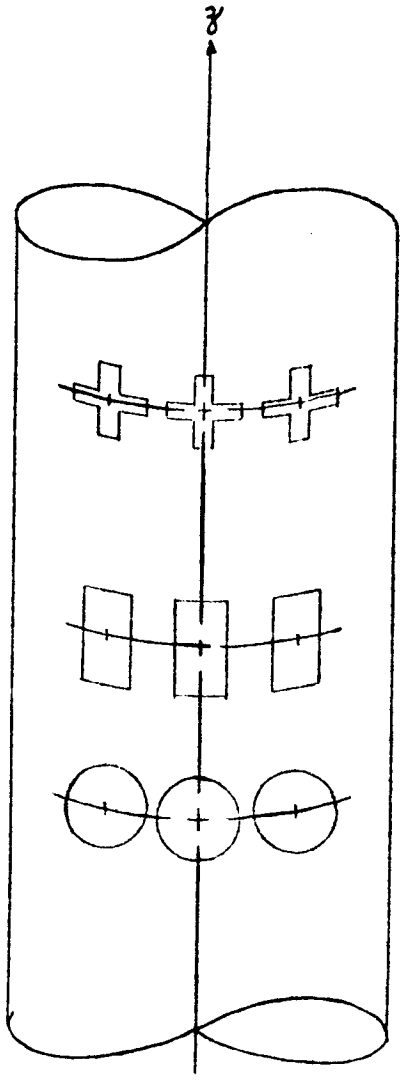

FIGURE V-7

"ARBITRARY" ARRAY ON THE CYLINDER

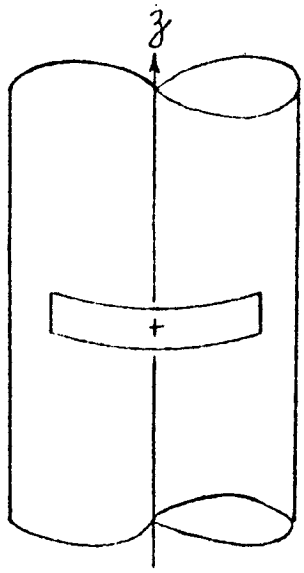

FIGURE V-8a. CIRCUMFERENTIAL SLOT

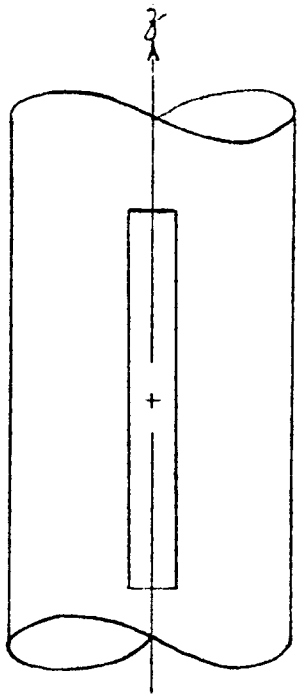

FIGURE V-8b. AXIAL SLOT

and the rotated field is given by

$$\mathcal{E}^{c}_{\phi m_p} = \mathcal{E}^{c}_{\phi m_p}(\theta, \phi - m_p \phi_{sp})$$

In the above formula the following notation is used:

For a given axial position we designate the z coordinate by

$$z = +p\, z_s$$

The value of z_s will be fixed and p will be generally, but not necessarily, an integer. A given value of p therefore designates a given element "ring" of slots or holes as illustrated in Figure V-7. For any given ring (given p) the elements are spaced at angular intervals ϕ_{sp}, and $m_p \phi_{sp}$ from $\phi = 0$. The constants m_p are integers varying from $m_p = 0$ to M_p where $(M_p + 1)\phi_{sp} = 360°$. Hence the slots (or holes) are equally spaced in ϕ.

For a slot or hole at the axial position $z = p z_s$ we have as the radiation field

$$\mathcal{E}^{c}_{\phi m_p p} = \mathcal{E}^{c}_{\phi m_p}(\theta, \phi - m_p \phi_{sp})\, e^{-jkpz_s \sin\theta}$$

This defines the radiation field for a slot or hole that is located at an arbitrary position on the cylinder with respect to the radiation field for the slot or hole located at $(z = 0, \phi = 0)$ on the cylinder.

The excitation coefficients V_A, V_C, V_z, and V_ϕ are fixed for a given ring element. Hence we designate them by V_{Amp}, V_{Cmp}, etc. For a desired circularity for the radiation field in a direction normal to the slots or holes we can relate V_{Amp} and V_{Cmp} for the crossed slots, or V_{zmp} and $V_{\phi mp}$ for the holes. If the circularity of radiation in this direction is defined by a constant $\mathcal{R}_p$ then either V_{Amp} or V_{Cmp} need be specified, the remaining coefficient being defined by the first and $\mathcal{R}_p$. The same situation holds for V_{zmp} and $V_{\phi mp}$.

For a symmetrically located hole in the guide we obtain similar results for the z-oriented excitation:

$$E_\theta^z = V_z \, f_\theta^z \, (\theta, \phi)$$

and

$$E_\phi^z = V_z \, f_\phi^z \, (\theta, \phi)$$

and for the ϕ-oriented excitation:

$$E_\theta^\phi = 0$$

and

$$E_\phi^\phi = V_\phi \, f_\phi^\phi \, (\theta, \phi)$$

where f_θ^z, f_ϕ^z and f_ϕ^ϕ are derived in Section d.

In what follows we will show how V_A and V_c are related for a given far field circularity. Similarly we will also show how V_ϕ and V_z are related so as to achieve a specified circularity in the far field normal to the hole. In addition we will show how the conductance of a given hole or crossed slot may be entered into the formulation for the radiation field.

First of all we may eliminate the R variable from our formulas since R will be a constant in our field calculations. We designate

$$f_\phi^c (\phi, \theta) = \left(\frac{e^{-jkR}}{2\pi^2 R} \right) \mathcal{E}_\phi^c \, (\theta, \phi)$$

Similar substitutions may be made for f_θ^A, f_θ^z, f_ϕ^ϕ, etc., to obtain

$$\mathcal{E}_\theta^A, \; \mathcal{E}_\theta^z, \; \mathcal{E}_\phi^\phi, \text{ etc.}$$

When the z coordinate of a slot is held fixed and the slot (or hole) is rotated in the $+\phi$ direction, the radiation field is also rotated with respect to the coordinate system

We will define the constant $\mathcal{R}_p$ with reference to the waveguide wall currents which were derived in Section b. We recall that wall currents were given by

$$J_{\phi}^{T} = j\ A\ e^{-j\phi}\ \sin\ K_i''\ z$$

and

$$J_z^T = -B\ e^{-j\phi}\ \cos\ K_i''\ z$$

The ratio of the z- directed excitation to the ϕ-directed excitation of either the slots or holes is therefore given by

$$\mathcal{R}_p = -(B/A)\ \text{ctn}\left[K_i''\ p\ z_s\right] = j\left(\frac{J_z^T}{J_{\phi}^T}\right)$$

Hence the circularity of the slots or holes depends upon the z position (with respect to the short). $\mathcal{R}_p$ represents the circularity and we find

$\mathcal{R}_p$ = 1 for right circular polarization

$\mathcal{R}_p$ = -1 for left circular polarization

$\mathcal{R}_p$ = 0 for ϕ polarization

$\mathcal{R}_p$ = ∞ for θ polarization.

The above polarizations are in a direction normal to the hole or slots.

The relationship between $V_{A_{mp\,p}}$ and $V_{C_{mpp}}$ is now readily found. By the above definition for $\mathcal{R}_p$ we have

$$\mathcal{R}_p = E_{\theta}\ (\pi/2,\ 0) \Big/ j\ E_{\phi}(\pi/2,\ 0)$$

where E_{θ} and E_{ϕ} are the total field components for the slots or hole. We find therefore that

$$\mathcal{R}_p = \frac{E_{\theta}^{C} + E_{\theta}^{A}}{j\ (E_{\phi}^{C} + E_{\phi}^{A})}$$

where the superscripts C and A designate the fields due to a circumferential or axial slot on the cylinder. Substituting further we find

$$\mathcal{R}_p = \frac{E_\theta^C}{j\, E_\phi^A} = -j \frac{V_{Cmpp}}{V_{Ampp}} \frac{\mathcal{E}_\theta^C(\pi/2, 0)}{\mathcal{E}_\phi^A(\pi/2, 0)}$$

and finally

$$\frac{V_{Ampp}}{V_{Cmpp}} = -j \frac{\mathcal{E}_\theta^C(\pi/2, 0)}{\mathcal{R}_p \mathcal{E}_\phi^A(\pi/2, 0)}$$

We should note that by $(\pi/2, 0)$ we mean $(\theta = \pi/2, [\phi - m_p \phi_{sp}] = 0)$. Hence $(\pi/2, 0)$ is normal to the slot or hole or alternatively expressed, it is normal to the cylinder axis in the direction of the slot or hole.

The relationship between $V_{\phi mpp}$ and V_{zmpp} in terms of $\mathcal{R}_p$ is similarly defined and found as

$$\frac{V_{\phi mpp}}{V_{zmpp}} = -j \frac{\mathcal{E}_\theta^z(\pi/2, 0)}{\mathcal{R}_p \mathcal{E}_\phi^\phi(\pi/2, 0)}$$

We have now expressed V_{Ampp} and $V_{\phi mpp}$ in terms of V_{Cmpp} and V_{zmpp} respectively. We must now define the amplitude phase of either V_{Cmpp} or V_{Ampp} and $V_{\phi mpp}$ or V_{zmpp} in terms of the slot conductances and rotational position. The phase excitations of the slots or holes will vary as $\exp(j\phi)$ around the cylinder. We will assume that the power radiated by an element ring is given by the conductance defined in the usual way and designated by g_p^s or g_p^h for all the slots or holes in the ring element, respectively. The values that g_p^s or g_p^h should be given is determined by an appropriate array synthesis theory (see next section) if more than one ring element is used. As the computed and experimental results show,

one ring element gives excellent omni-coverage so that an array will not be necessary for most applications.

The voltage excitation coefficients, normalized, for the cross-slot rings are given by

$$V_{C_{mpp}} = \frac{1}{\left|\mathcal{E}_{\theta}^{C}(\pi/2, 0)\right|} \sqrt{\frac{g_p^s}{M_p}}\, e^{-j m_p \phi_{sp}}\, \text{sign}\left\{-\cos K_i'' p z_s\right\}$$

or

$$V_{A_{mpp}} = \frac{1}{\left|\mathcal{E}_{\phi}^{A}(\pi/2, 0)\right|} \sqrt{\frac{g_p^h}{M_p}}\, e^{-j m_p \phi_{sp}}\, \text{sign}\left\{+\sin K_i'' p z_s\right\}$$

$V_{A_{mpp}}$ is found from $V_{C_{mpp}}$ or vice-versa as discussed earlier. The factors signs ( ) are either +1 or -1 as indicated. They are necessary to account for the alternation in sign as the slot or hole position varies by a half guide wavelength in the z-direction. The normalization is arbitrary and chosen by the division of the normally directed $(\pi/2, 0)$ field magnitude. In general all the radiators on a given circle (i.e., a given value of p) are assumed identical. If they are not then $\sqrt{g_p/M_p}$ will be a function of m_p and must be adjusted accordingly. This will ordinarily not be the case for omni antennas.

The phase and amplitude of $V_{\phi_{mpp}}$ and $V_{z_{mpp}}$ is defined and found similarly as

$$V_{\phi_{mpp}} = \frac{1}{\left|\mathcal{E}_{\phi}^{\phi}(\pi/2, 0)\right|} \sqrt{g_p^h/M_p}\, e^{-j m_p \phi_{sp}}\, \text{sign}\,(\mathcal{R}_p')$$

and

$$V_{z_{mpp}} = \frac{1}{\left|\mathcal{E}_{\theta}^{z}(\pi/2, 0)\right|} \sqrt{g_p^h/M_p}\, e^{-j m_p \phi_{sp}}\, \text{sign}\,(\mathcal{R}_p''),$$

where we designate

$$\mathcal{R}_p' = \sin K_i'' p z_s$$

and

$$\mathcal{R}_p'' = -\cos K_i'' p z_s$$

The total field for any one crossed slot or hole is now easily found as

$$F^{C}_{\theta m_{pp}} = (2\pi^2 R e^{jkR})\, E^{C}_{\theta m_{pp}} = V_{C m_{pp}}\, \mathcal{E}^{C}_{\theta m_p}(\theta, \phi - m_p \phi_{sp}) e^{-jkpz_s \cos\theta}$$

$$F^{C}_{\phi m_{pp}} = (2\pi^2 R e^{jkR})\, E^{C}_{\phi m_{pp}} = V_{C m_{pp}}\, \mathcal{E}^{C}_{\phi m_p}(\theta, \phi - m_p \phi_{sp}) e^{-jkpz_s \cos\theta}$$

$$F^{A}_{\theta m_{pp}} = (2\pi^2 R e^{jkR})\, E^{A}_{\theta m_{pp}} = 0$$

$$F^{A}_{\phi m_{pp}} = (2\pi^2 R e^{jkR})\, E^{A}_{\phi m_{pp}} = V_{A m_{pp}}\, \mathcal{E}^{A}_{\phi m_p}(\theta, \phi - m_p \phi_{sp}) e^{-jkpz_s \cos\theta}$$

$$F^{z}_{\theta m_{pp}} = (2\pi^2 R e^{jkR})\, E^{z}_{\theta m_{pp}} = V_{z m_{pp}}\, \mathcal{E}^{z}_{\theta m_p}(\theta, \phi - m_p \phi_{sp}) e^{-jkpz_s \cos\theta}$$

$$F^{z}_{\phi m_{pp}} = (2\pi^2 R e^{jkR})\, E^{z}_{\theta m_{pp}} = V_{z m_{pp}}\, \mathcal{E}^{z}_{\phi m_p}(\theta, \phi - m_p \phi_{sp}) e^{-jkz_s \cos\theta}$$

$$F^{\phi}_{\theta m_{pp}} = (2\pi^2 R e^{jkR})\, E^{\phi}_{\theta m_{pp}} = 0$$

$$F^{\phi}_{\phi m_{pp}} = (2\pi^2 R e^{jkR})\, E^{\phi}_{\phi m_{pp}} = V_{\phi m_{pp}}\, \mathcal{E}^{\phi}_{\phi m_p}(\theta, \phi - m_p \phi_{sp}) e^{-jkpz_s \cos\theta}$$

The total field for an arbitrary array of slots and holes on the cylinder is then given by

$$E^{T}_{\phi}(\theta, \phi) = \sum_{p} \sum_{m_p = 0}^{M_p} \left(F^{C}_{\phi m_{pp}} + F^{A}_{\phi m_{pp}} + F^{z}_{\phi m_{pp}} + F^{\phi}_{\phi m_{pp}} \right)$$

and

$$E_\theta^T(\theta, \phi) = \sum_p \sum_{m_p=0}^{M_p} \left(F^C_{\theta m_{pp}} + F^z_{\theta m_{pp}} \right)$$

For a given ring element (a given value of p), if the radiators are all slots then $F^z_{\phi m_{pp}}$, $F^{\phi}_{\phi m_{pp}}$, and $F^z_{\theta m_{pp}}$ are zero. Similarly, if the elements were all holes in a given ring, then $F^C_{\phi m_{pp}}$, $F^A_{\phi m_{pp}}$, and $F^C_{\theta m_{pp}}$ are zero.

If we designate the total right circularly polarized field as F_R^T and the total left circularly polarized field as F_L^T we find:

$$F_R^T(\theta, \phi) = E_\phi^T - j\, E_\theta^T$$

and

$$F_L^T(\theta, \phi) = E_\theta^T - j\, E_\phi^T$$

If we normalize these fields to the value at

$$(\theta, \phi) = (\pi/2, 0)$$

we have as the total right and left circular polarized fields:

$$E_R^T(\theta, \phi) = F_R^T(\theta, \phi) \Big/ \left| F_R^T(\pi/2, 0) \right|$$

and

$$E_L^T(\theta, \phi) = F_L^T(\theta, \phi) \Big/ \left| F_L^T(\pi/2, 0) \right|$$

2) Array Synthesis Techniques for Omni-Patterns

a) General Discussion

In order to define the general type of pattern which we seek, refer to Figure V-9. We seek a circularly polarized pattern which is omni directional in ϕ and a sector beam in θ. Ideally, the sector is uniform from $-\theta_o$ to $+\theta_o$ with a sharp cutoff or skirt at $\theta = \pm\theta_o$.

In order to obtain an approximation to this pattern we will array a group of elements, $2N + 2$ elements along the z - axis of the system. There will be $2N + 1$ elements with identical patterns, the element pattern, which was essentially as shown in Figure V-10, assumed nearly independent in ϕ.

It can be seen that a single element will actually provide a fair approximation to the desired pattern (element pattern synthesis and analysis as discussed elsewhere in this report).

The $2N + 1$ elements to be arrayed will provide a much sharper skirt than the single element. However, this will be possible only with some sacrifice to the flatness of the sector $|\theta| < \theta_o$. This is a consequence of the fact that the array factor must be symmetrical about $|\theta| = \pi/2$. In other words, a possible array factor will appear as shown in Figure V-11a, with symmetry about $\psi = 0$ ($\psi = \theta - \pi/2$). Figure V-11b illustrates a sector beam with this limitation, the hole at $\theta = 0$. For the waveguide feed system to be used, this array factor symmetry is essentially inherent in the system.

With an array factor such as is illustrated in Figure V-11a and the element pattern of Figure V-10, we will achieve a sharp skirt, but also obtain a "hole" in the $\theta = 0$ direction of the pattern. In order to "fill in" this hole we could add an additional element at the end of the array, although the element factor of the array elements will "fill" this hole to some extent. The position, amplitude, and the phase of this single end element are left variable. This element could be excited by some other method if the optimum conductance became larger than tolerable here. Since the remaining $2N + 1$ elements require a shorted waveguide, this conductance must be small if excited at the end of the guide. In any case, this element pattern will substantially favor the $\theta = 0$ direction and be expected to "fill up" the "hole" generated by the array factor. It is thus clear that for N large, the power radiated by this end element must be increased.

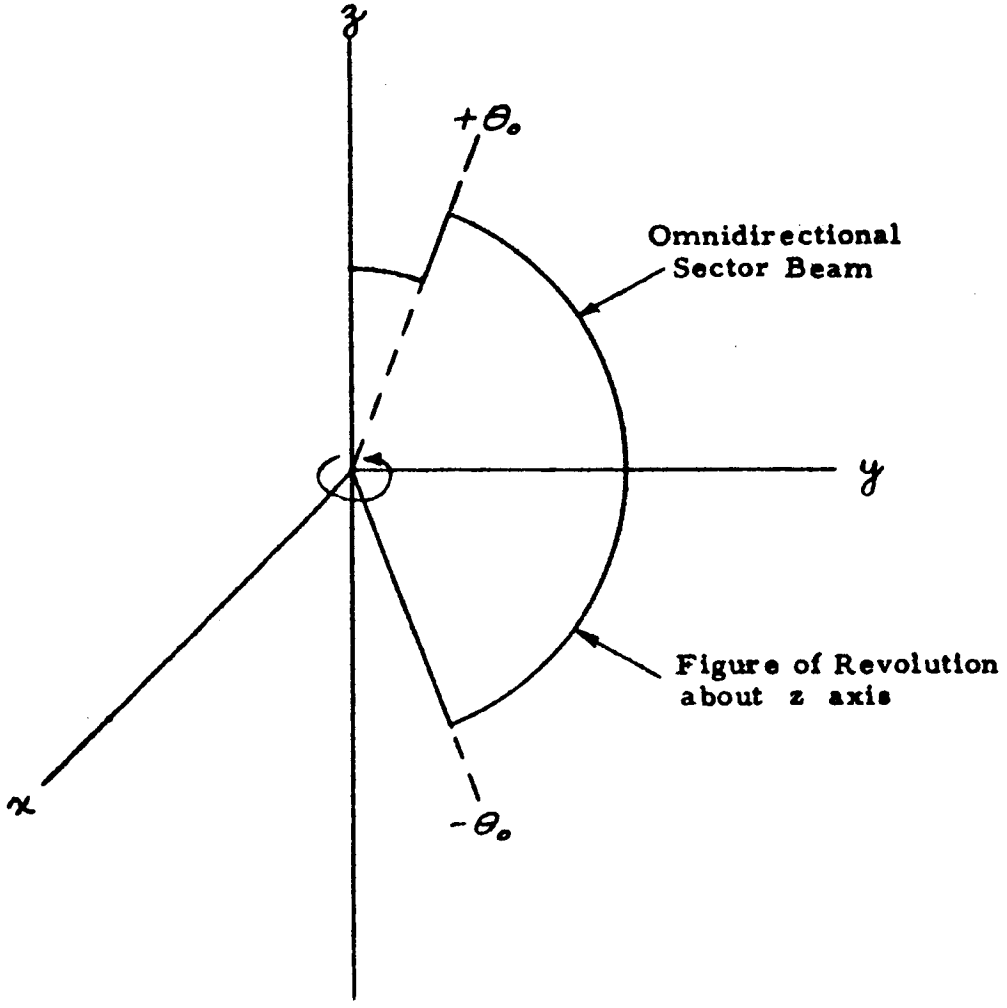

FIGURE V-9

DESIRED PATTERN SHAPE

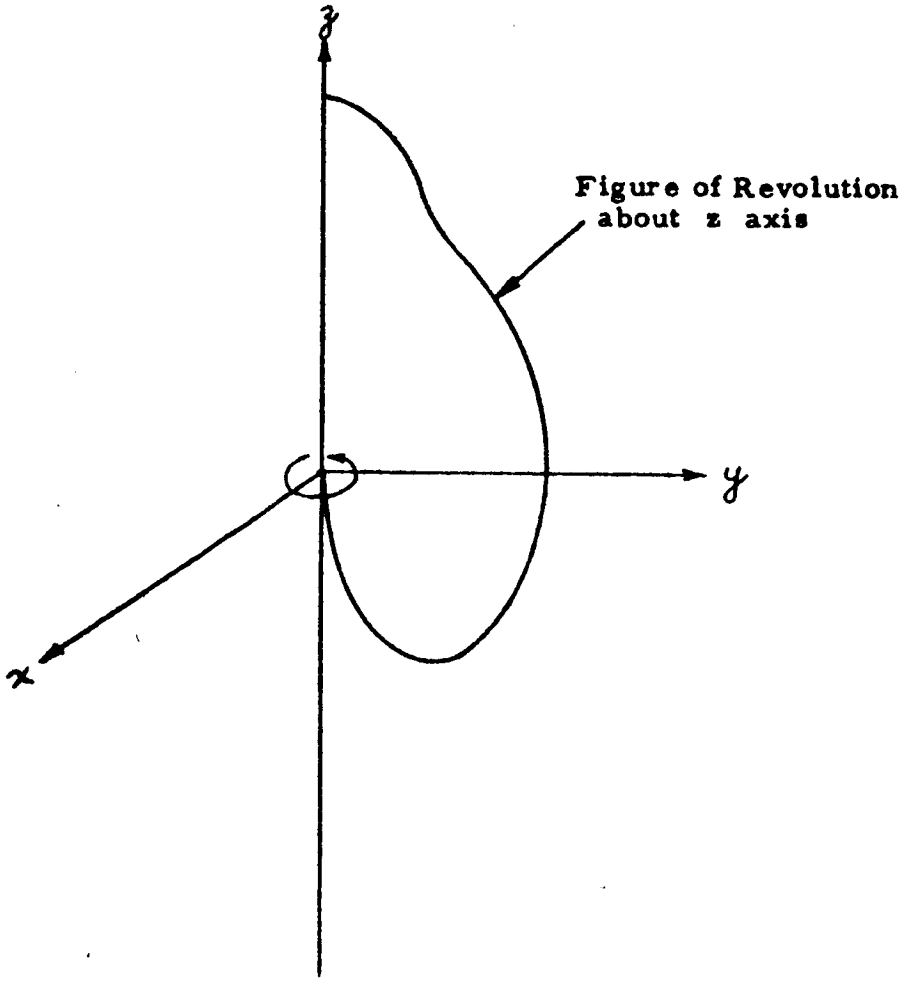

FIGURE V-10

APPROPRIATE ELEMENT PATTERN
SHAPE

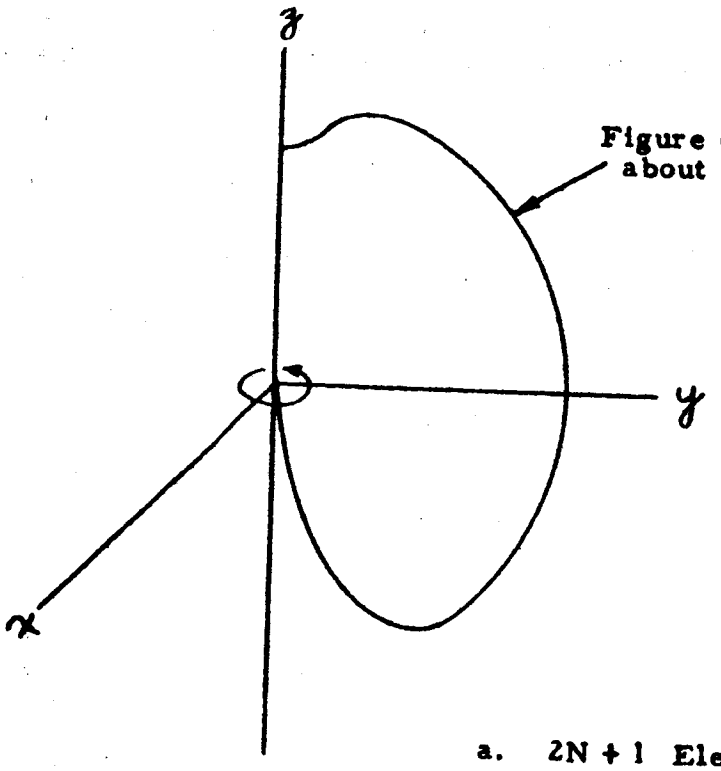

a. 2N + 1 Elements Plus End Element

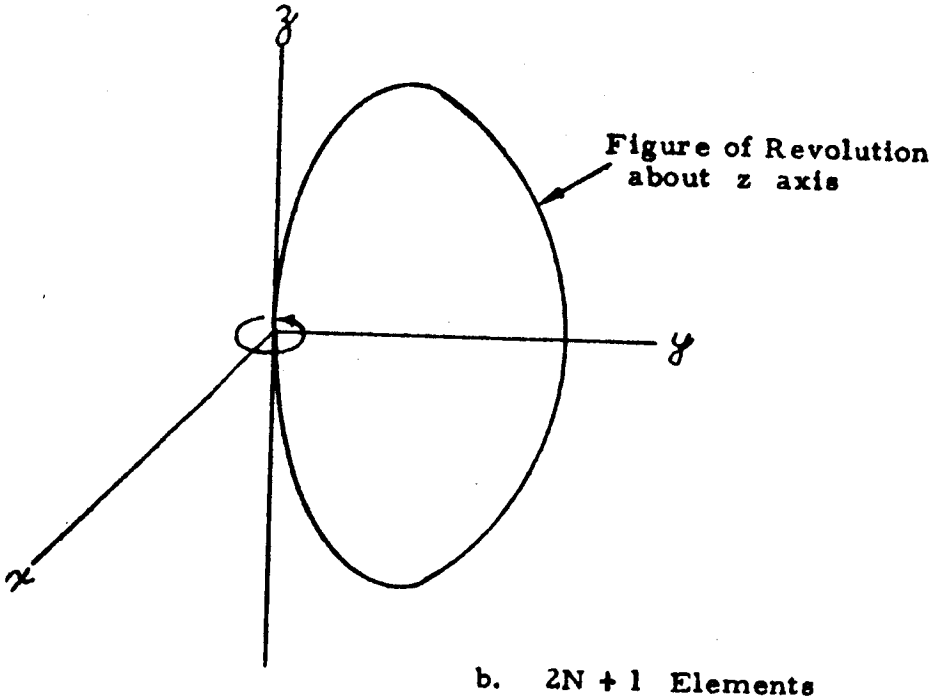

b. 2N + 1 Elements

FIGURE V-11. IDEALIZED ARRAY FACTORS

Hence in general it must be recognized that some alternate excitation (other than suggested above) is necessary.

In the event that the desired sector coverage is that shown in Figure V-11b instead of that in Figure V-9, then only $2N + 1$ elements are used and the problem simplified.

There are four important synthesis methods that are useful for this problem. Each method has certain advantages, depending on the degree of approximation desired in the flat zone ($|\psi| < |\psi_o|$), the skirt sharpness at $\psi = \pm \psi_o$, the number of elements, and the exact element pattern $f_e(\theta)$. (We will assume that $f_e(\theta, \phi) = f_e(\theta)$ for all practical purposes in the synthesis). The methods are the Maximally Flat synthesis (Butterwork circuit analogy), Tchebyscheff Derived synthesis, least square (Fourier) synthesis, and N-point synthesis.

The N-point method makes the approximate pattern go through precisely N points of the desired pattern if N elements are used in the array. That is, N amplitude coefficients of the array are found by the above requirement. A rather simple matrix inversion is all that is required here. The method is not very powerful, since the behavior throughout the rest of the pattern (points other than the N points) are not controlled and no overall behavior is determined.

The maximally flat and quasi-smooth synthesis methods are described in several papers by Ksienski[19, 20]. They are mentioned here because of their suitability to the omnidirectional pattern objectives. In essence this method is an N point synthesis for the pattern derivative as opposed to the pattern itself. This synthesis can lead to a very smooth array factor for $|\psi| < |\psi_o|$, but also leads to a minimum slope at $|\psi| = |\psi_o|$.

A somewhat better compromise between slope and smoothness can be achieved by using a Tchebyscheff derived pattern (see Reference 19 for example). If the desired sector beam is that in Figure V-12a, then the desired derivative pattern is the impulse pair in Figure V-12b. If each impulse is approximated by a Tchebyscheff pencil beam, then the resultant sector beam will not be smooth, but will have an almost equal ripple. The greater the ripple magnitude allowed, the greater the slope at $|\psi| = |\psi_o|$. Hence generally for a given number of elements this synthesis method will give a good compromise between smoothness and cutoff slope. The method has the advantage also of being very easy to apply, since tables of Tchebyscheff polynomials are readily available.

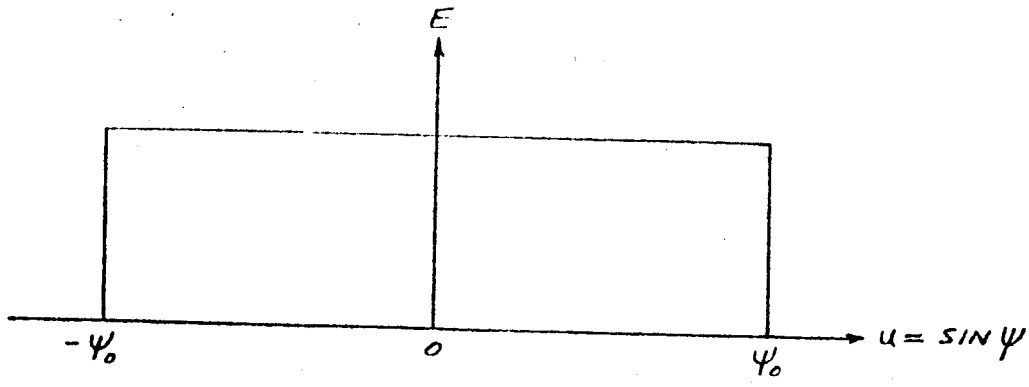

FIGURE V-12a. IDEAL SECTOR BEAM

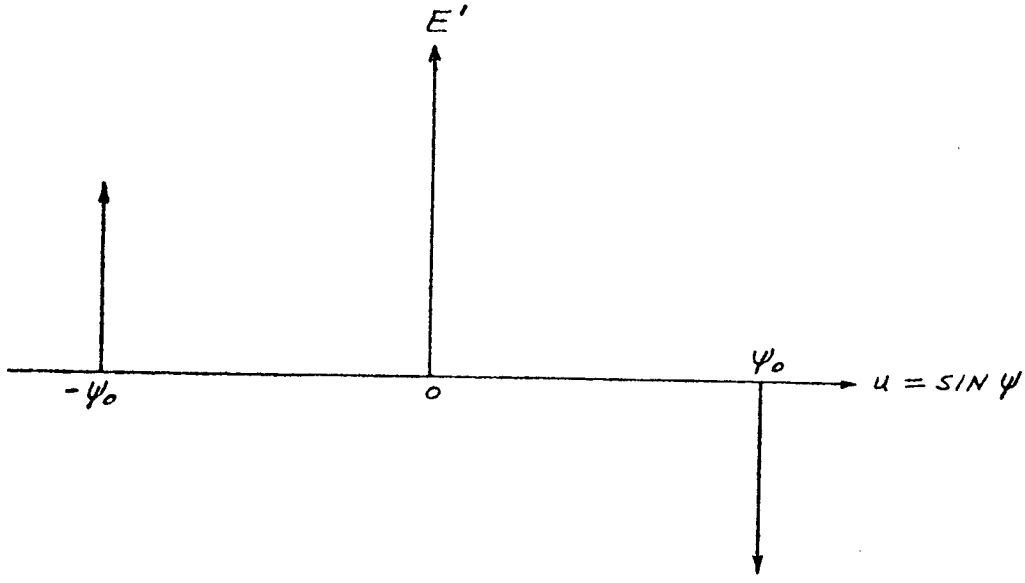

FIGURE V-12b. DERIVATIVE OF IDEAL SECTOR BEAM

The final method which was mentioned, the least square or Fourier synthesis, will be treated in more detail to demonstrate the applicability of all of the methods considered. This method generally yields the sharpest skirt at $|\psi| = \psi_o$, but also has the greatest overshoot away from $|\psi| = \psi_o$. For a very small number of elements (which will probably be the most practical case for the omni-directional application) this synthesis appears to yield the best compromise pattern when considered with the element pattern. The detailed discussion follows.

b) Fourier or Least Square Synthesis

Consider the rectangular pulse shown in Figure V-13. This is a sector beam extended periodically in the variable $u = \pi \sin \psi$.

The Fourier series for this function is

$$f(u) = \left(\frac{u_o}{\pi}\right) \sum_{n=0}^{\infty} \epsilon_n \left(\frac{\sin n u_o}{n u_o}\right) \cos n u$$

where $\epsilon_n = \begin{cases} 1 & n = 0 \\ 2 & n \neq 0 \end{cases}$

Now consider the pattern produced by a (2N + 1) element array symmetrically excited by the real coefficients A_n:

$$f_A(\psi) = \sum_{-N}^{N} A_n \, e^{ikdn \sin \psi}$$

$$= \sum_{n=1}^{N} 2 A_n \left[\frac{e^{ikdn \sin \psi} + e^{-ikd \sin \psi}}{2}\right] + A_o$$

so $$f_A(u) = \sum_{n=0}^{N} \epsilon_n A_n \cos n u$$

where $u = k d \sin \psi = 2\pi/\lambda \; d \sin \psi = \pi \sin \psi$

when $d = \lambda/2$. We will not consider the case when $d = \lambda_g/2$ and $\lambda_g \gtrsim \lambda$ (λ_g only slightly $> \lambda$),

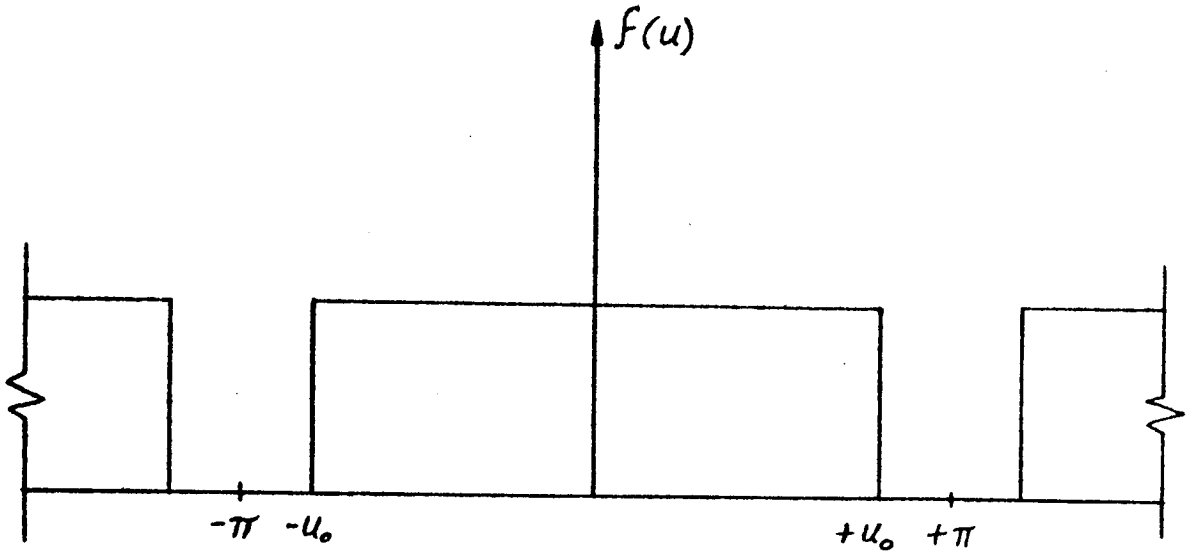

FIGURE V-13

IDEAL SECTOR BEAM

but certain not too serious modifications must be made in the following when d has this value.

It is now immediately clear that if we choose

$$A_n = \frac{u_o}{\pi} \left| \frac{\sin n u_o}{n u_o} \right|$$

we have a least square fit to the sector beam.

We will now demonstrate that for skirt positions which are desired for maximum coverage with the omni antenna and for the particular feeding transmission line (circularly polarized wave in a shorted cylindrical waveguide) these feeding coefficients are readily obtainable. That is, for

$$u_o = \pi (\sin 70°) \approx 0.94\pi$$

the phase of the A_n alternate by 180° with n and this is precisely what occurs in the feeding transmission line. This is true as will be seen up until a maximum n only, but this maximum n is much larger than will be practical for the omni antenna. Figure V-14 demonstrates this effect.

It is clear that the sign of A_n continues to alternate until n is approximately 20. This value is found easily by

$$M = \max n = \frac{\pi}{\pi - u_o} = \frac{1}{0.06} \approx 20$$

That the above result occurs for the other methods of synthesis is easily verified by noting the results in Reference 19. See equation (11) for the Maximally smooth synthesis result, equation (36) for the quasi-smooth synthesis result, and equation (48) for the Tchebyscheff derived result (all in Reference 19). In each case we have the alternating of the signs of the coefficients A_n which lends itself quite readily to realization with the circularly polarized shorted cylindrical waveguide. Finally, note that the closer

$$\psi_o \longrightarrow \pi/2,$$

i.e., the greater the range desired, the greater M, and hence, more elements can be used to achieve the greater coverage. Although the tolerance and design complexity (from a practical point of view) increases with more

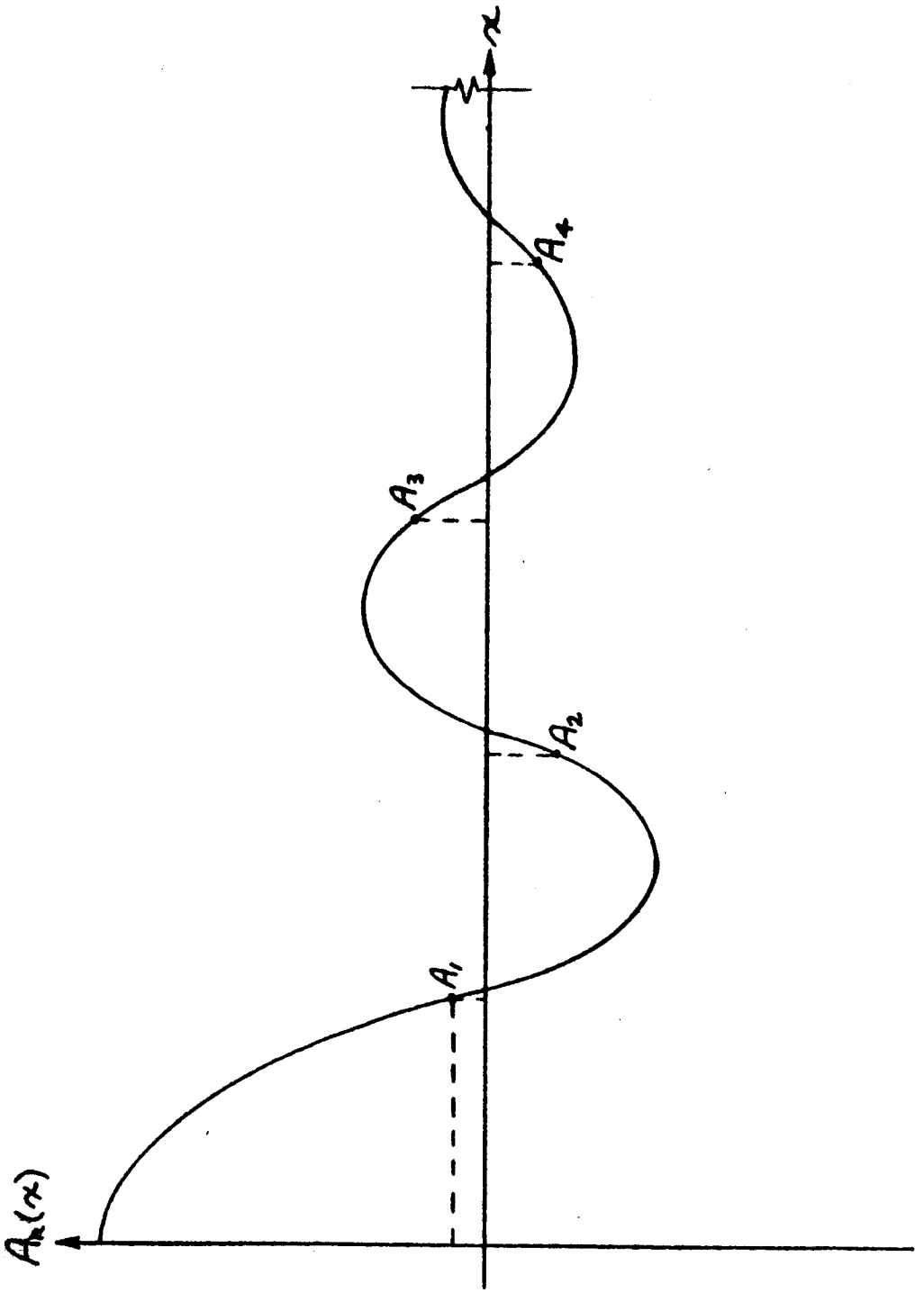

FIGURE V-14

FEEDING COEFFICIENTS

FOR LEAST SQUARE-FOURIER SYNTHESIS

elements, in principle we can achieve as great or complete coverage as desired with as sharp a skirt as desired by increasing the number of elements. (Of course, there is an open end to this limit since complete coverage is theoretically impossible). For a given number of elements, however, some compromise between smoothness and skirt sharpness must be decided upon before a synthesis method is chosen. For any choice or compromise there is a useful easily applied synthesis method to determine the coefficients A_n.

In each case, however, we do require (usually in the Maximally flat synthesis and always in the Fourier synthesis) that the center element and adjacent elements have the same phase. This can be achieved by two antennas operating into each other as illustrated in Figure V-15.

In this case we must use the equivalent even number of elements for the array. We may simply interpolate for excitation coefficients.

f. Theoretical Computations and Some Experimental Results

1) General Discussion

This section presents results of machine computations of the formulas developed in the previous sections. In addition, some experimental results are presented for comparison. A more complete presentation of experimental results is presented elsewhere in the next section. Since the theory for slot radiators on an infinite cylinder is essentially an exact theory, the theoretical results in general represent the "best" or the "ideal" patterns that can be achieved with this type of antenna. A noteworthy exception to this otherwise valid viewpoint will be presented later when the elevation patterns (θ cut) for an eight slot ring are discussed.

Results are presented only for a single ring array of slots. As will be explained in the discussion of the eight slot ring, much of the advantage obtainable with an array of rings can be obtained from a single ring when various diffraction and scattering effects are utilized to advantage.

The calculations were run to determine the omni-pattern ($\theta = 90°$, ϕ varies) and elevation pattern (ϕ fixed, θ varies), as functions of frequency, guide radius, radiator shape (hole or crossed slots), and number of radiators in a given ring.

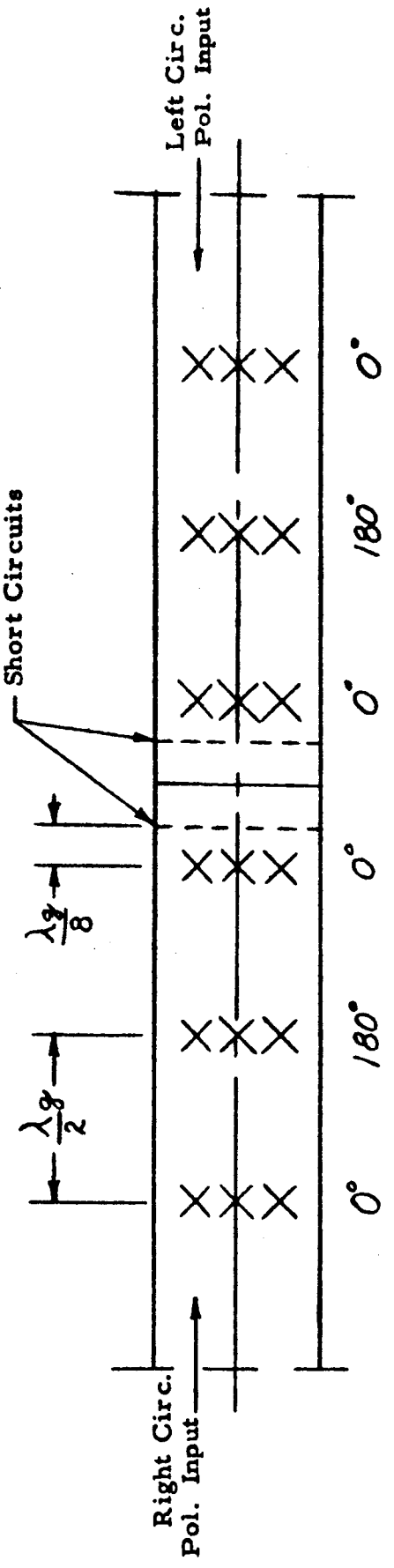

FIGURE V-15

ARRAY IMPLEMENTATION

Results are presented for one and eight elements in a ring. Computations for other numbers of elements, different free space wavelengths and several guide radii were performed to determine the effect of these parameters. Amplitude patterns for right circular and left circular polarization and some phase patterns are also illustrated. Although the illustrations are in general self-explanatory, certain particularly interesting festures will be pointed out in the following sections.

2) Single Crossed Slot and Hole Patterns

We let the single crossed slot or hole be centered at $\phi = 0°$ on the cylinder. Since the pattern variation from $\lambda_1 = 4.92"$ to $\lambda_5 = 5.91"$ is not great only the $\lambda_3 = 5.36"$ wavelength is computed. In all cases we assume a guide radius $a = 2.0"$ and inside guide radius a_i such that $a - a_i = 0.065"$ (wall thickness) unless otherwise specified on the diagrams.

Figures V-16 through V-19 present the single element results. The elevation patterns in Figure V-16 illustrate the effect of the cylinder as compared to a slot on a ground plane. The $\phi = 180°$ pattern would be identically zero if the cylinder radius were infinitely large. The $\phi = 0°$ pattern differs in the two cases mostly in the polar regions. Note the asymmetry about $\theta = 90°$. This is due to the phase variation $e^{-j\phi}$ across the circumferential slot. This asymmetry is evident in the other figures also. (Note especially the θ plane patterns in Figure V-17.) The ground plane pattern in Figure V-16 is given for the infinitesimal crossed dipole which has the elevation pattern

$$P(\theta) = 10 \log_{10} (1 + \sin \theta)^2$$

Figure V-18 shows the $\theta = 90°$ plane (omni) patterns for a single crossed slot at $\phi = 0°$. The differences between $\phi < 0$ and $\phi > 0$ are evident; however, they are not excessive.

The variation in omni plane phase for a crossed slot at $\phi = 0°$ is shown in Figure V-19.

3) Multiple Crossed Slot Results

Computations were run for multiple numbers of crossed slots in a circumferential ring. Equal spacing was always assumed.

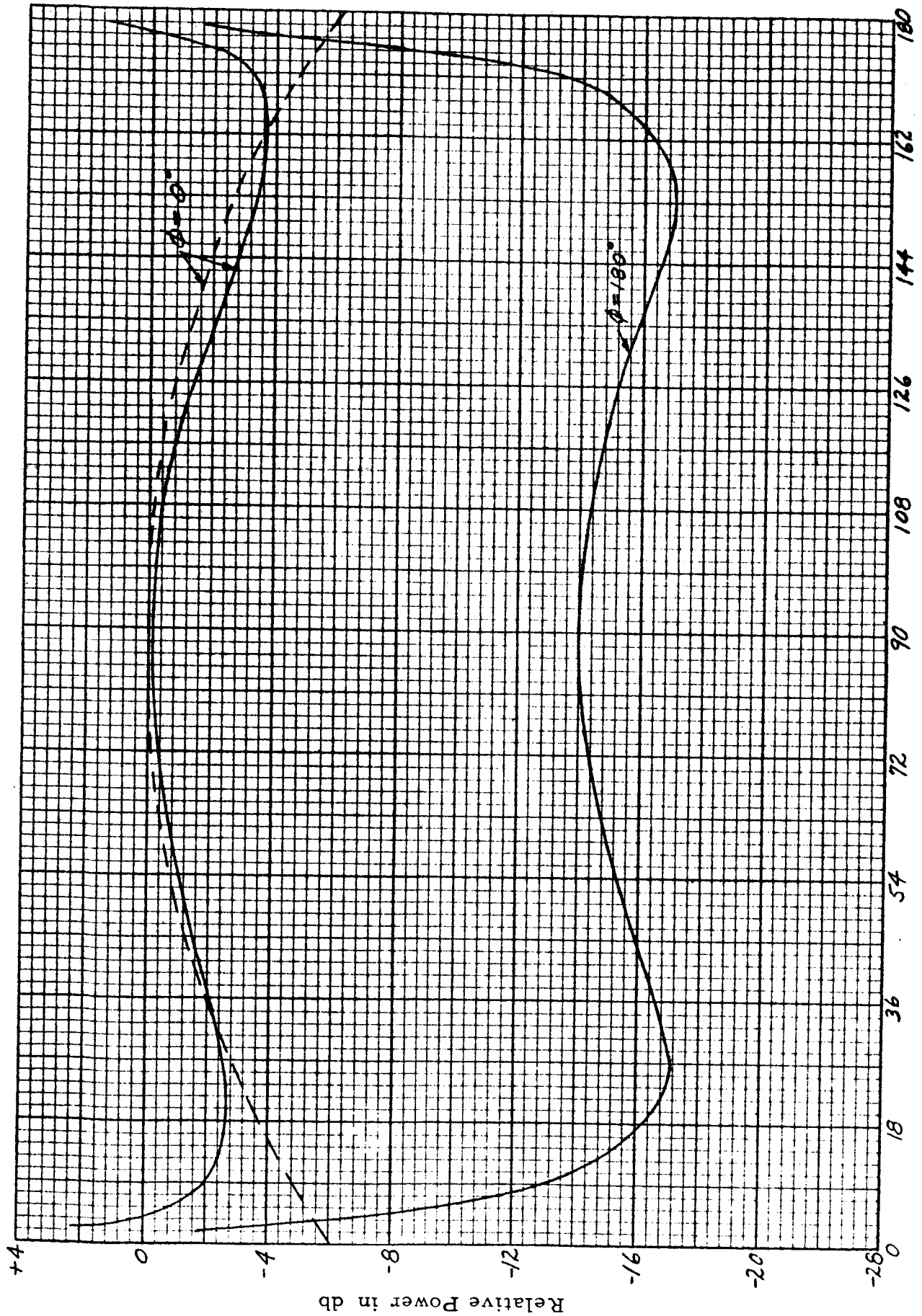

FIGURE V-16

θ PLANE PATTERN FOR A SINGLE CROSSED SLOT AT $\phi = 0°$ and $180°$

65-430

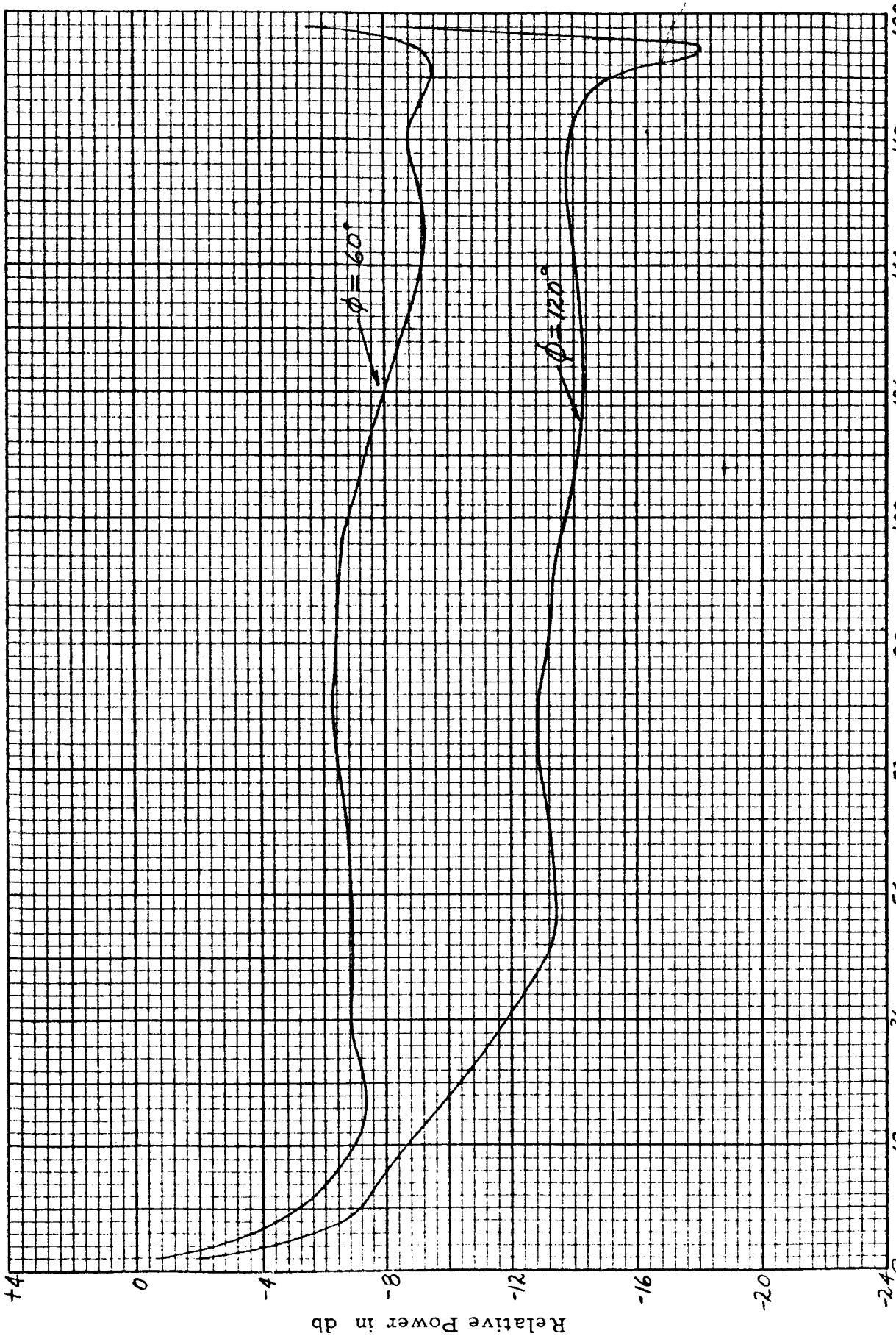

FIGURE V-17

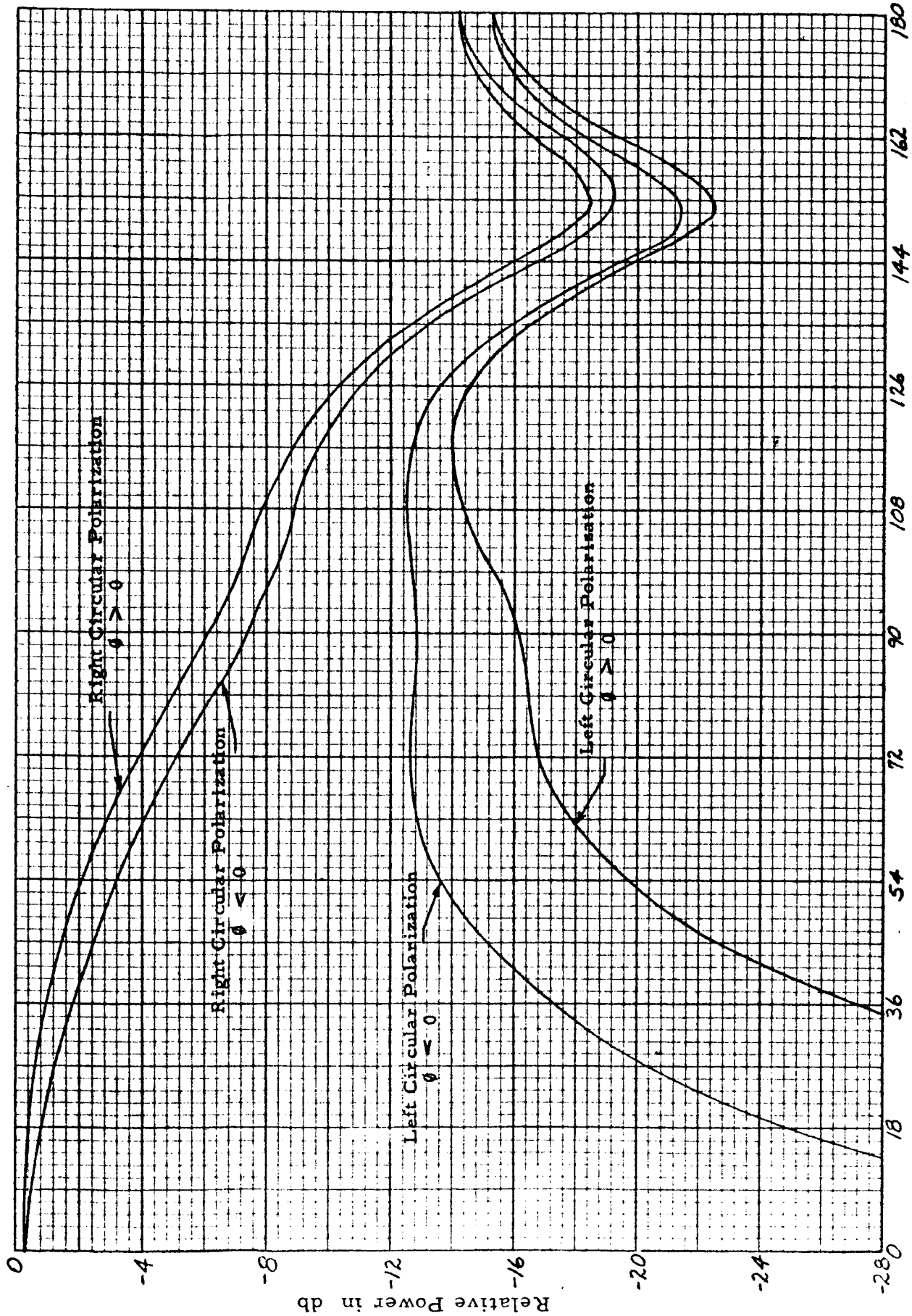

FIGURE V-18

THEORETICAL OMNI PLANE PATTERNS FOR A SINGLE CROSSED SLOT

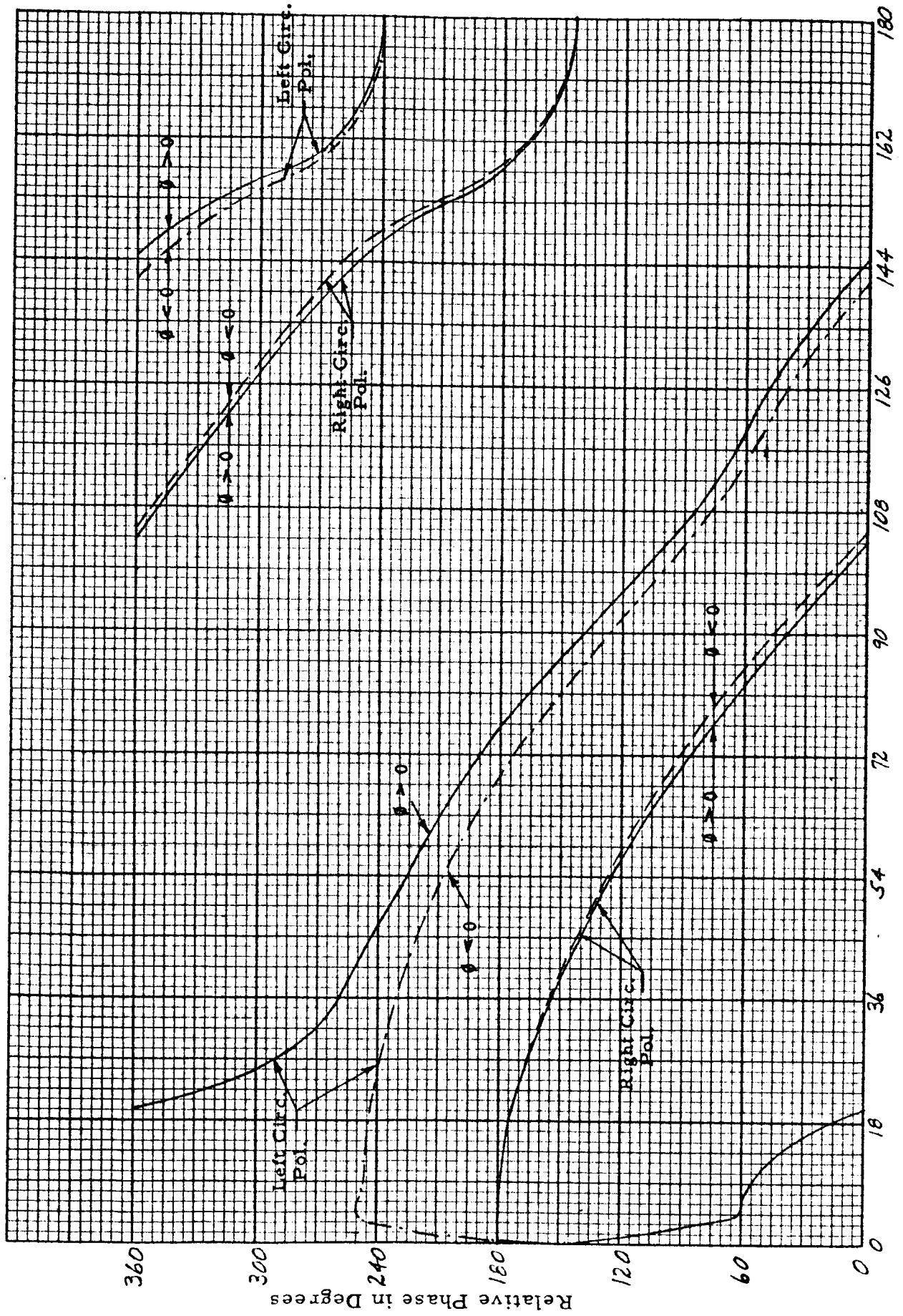

FIGURE V-19

OMNI PLANE RELATIVE PHASE FOR SINGLE CROSSED SLOT

For four crossed slots the computations were compared with experimental results and it was established that good agreement could be obtained. However, the omni plane ($\theta = 90°$) right circular pattern has a maximum to minimum variation of 11 db. Obviously, this case is not acceptable as an omni antenna.

Calculations were run on six and seven sets of crossed slots and the six slot case was experimentally tested. The omni variation was approximately 1 db calculated and 2 db measured. Elevation patterns were also acceptable, but six sets of crossed slots were not sufficient to obtain near 100% coupling from the guide.

It was determined that a maximum of eight sets of resonant length dumbbell slots could be placed in a single ring, so it was decided to restrict further work to this case.

The eight slot ring patterns do not differ in essence with the seven slot ring results with the single exception that now both the right circular polarization and left circular polarization omni patterns are essentially perfectly flat as shown in Figure V-20. The elevation patterns are also illustrated here with no significant changes from previous results. It can be seen here that the left circular polarization omni pattern lies at exactly 20 db below the right circular polarization pattern; this is the "average" difference in level when less elements are used in a ring, but fewer elements allow large variations in the left circular polarization pattern and small variations in the right circular polarization pattern.

Figure V-21 illustrates the omni phase patterns for both the left circular polarization and right circular polarization cases. A perfectly linear variation of ϕ degrees in phase per ϕ degrees in angular position is noted as expected for this case. The right circular polarization and left circular polarization patterns differ in phase by a constant of nearly 30°. Since, of course, the left circular polarization amplitude is at -20 db with respect to the right circular polarization amplitude, the total field is essentially right circularly polarized at the right circular polarization phase.

Figure V-22 compares a typical experimental elevation pattern with the theoretical ideal. The actual experimental antenna model is illustrated in Figure V-23. The experimental pattern, it must be noticed, is very similar to a very long array of ring elements (15 to 20) whose excitation is obtained by a Fourier synthesis method. The oscillations

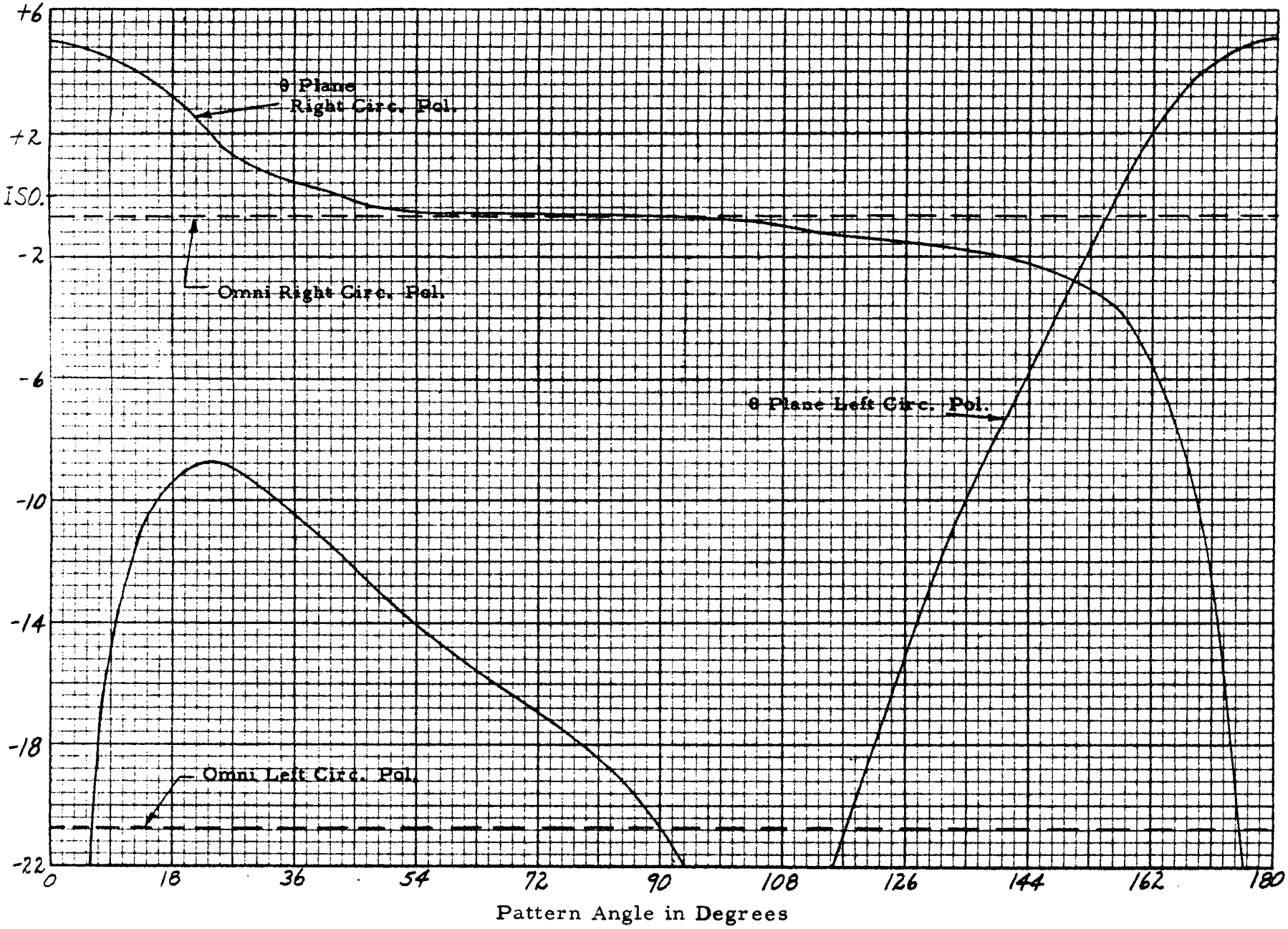

FIGURE V-20. THEORETICAL PATTERNS FOR EIGHT CROSSED SLOTS

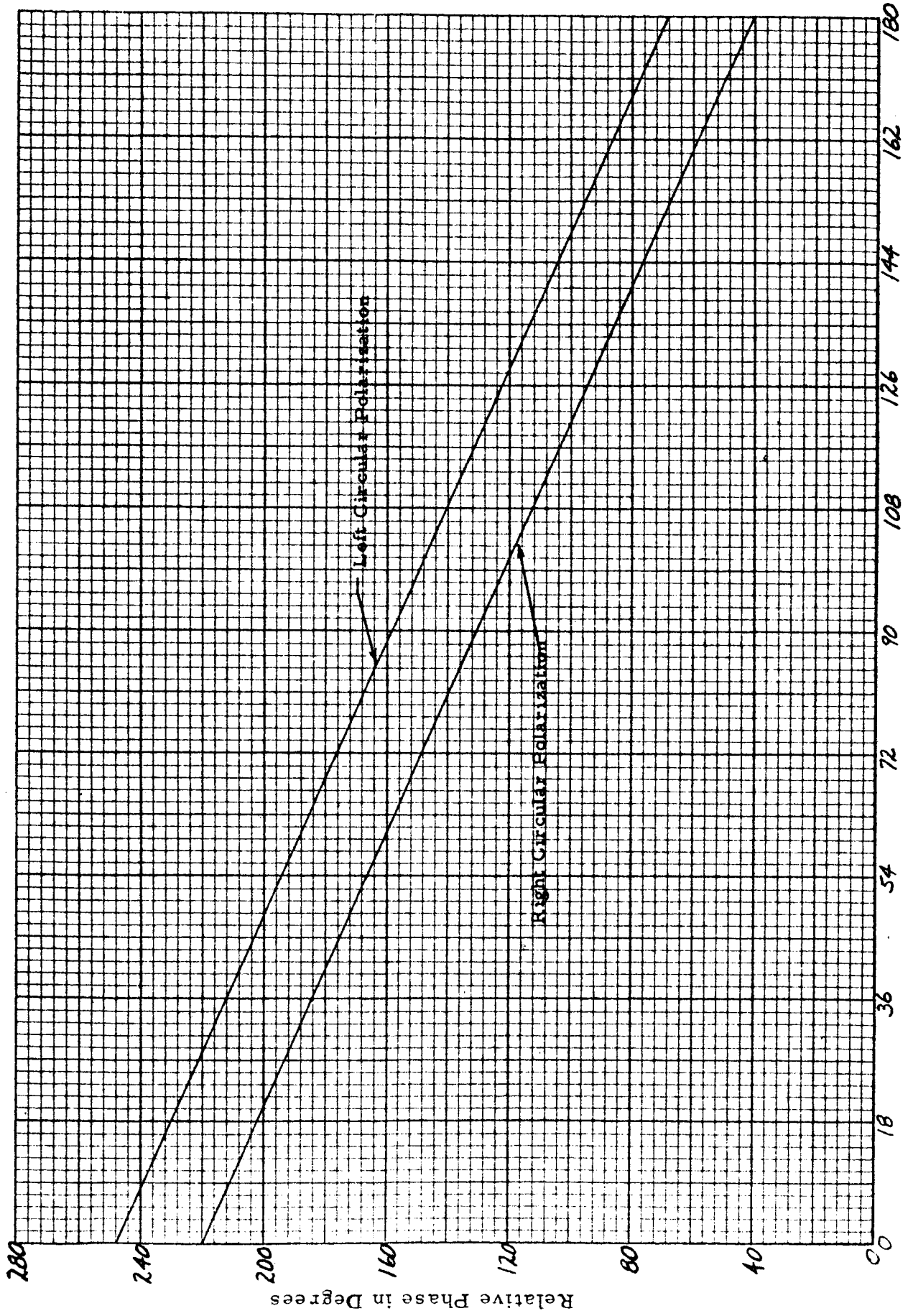

FIGURE V-21. OMNI PLANE PHASE VARIATION FOR EIGHT CROSSED SLOTS

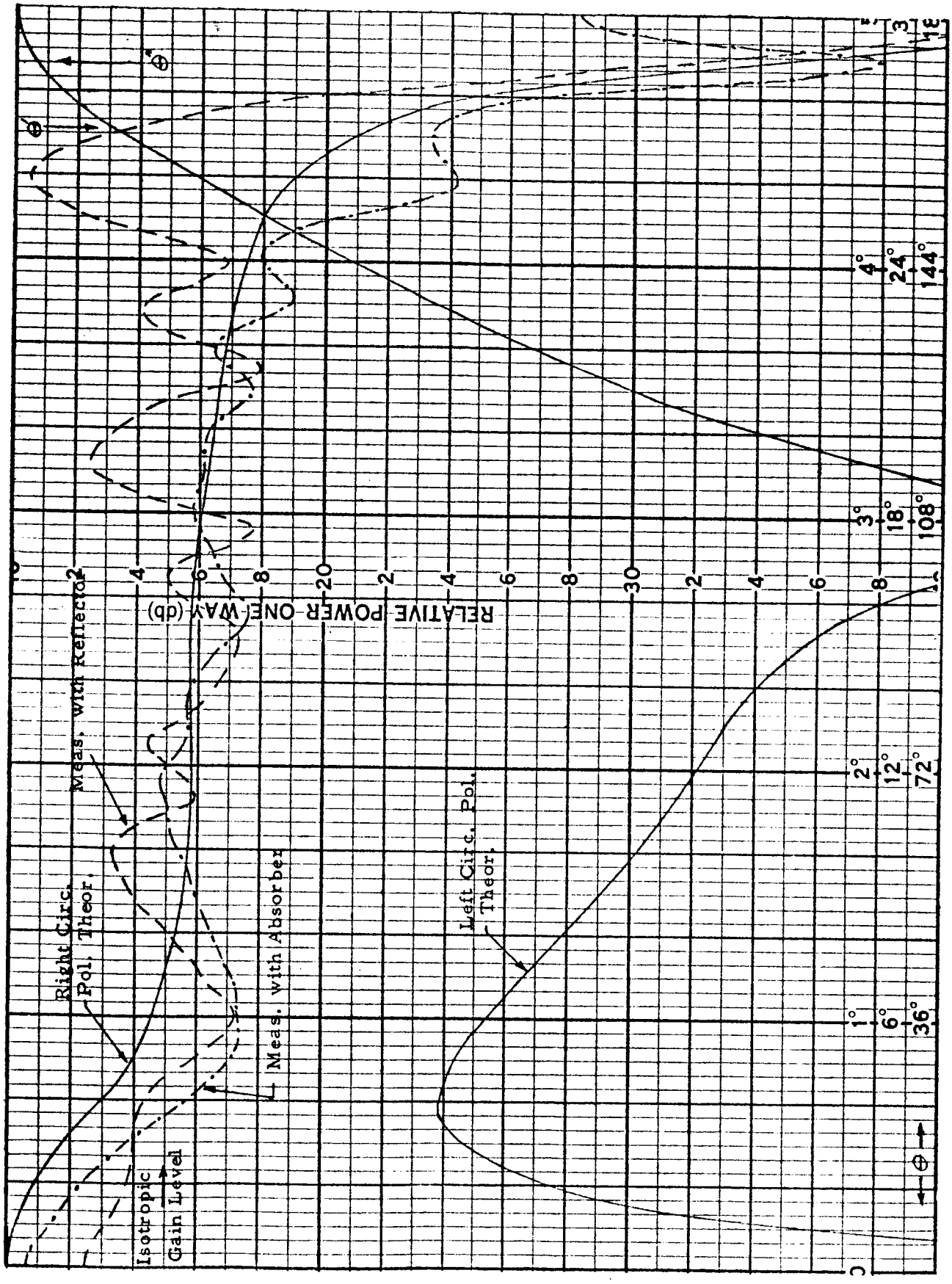

FIGURE V-22. θ PLANE PATTERN COMPARISON

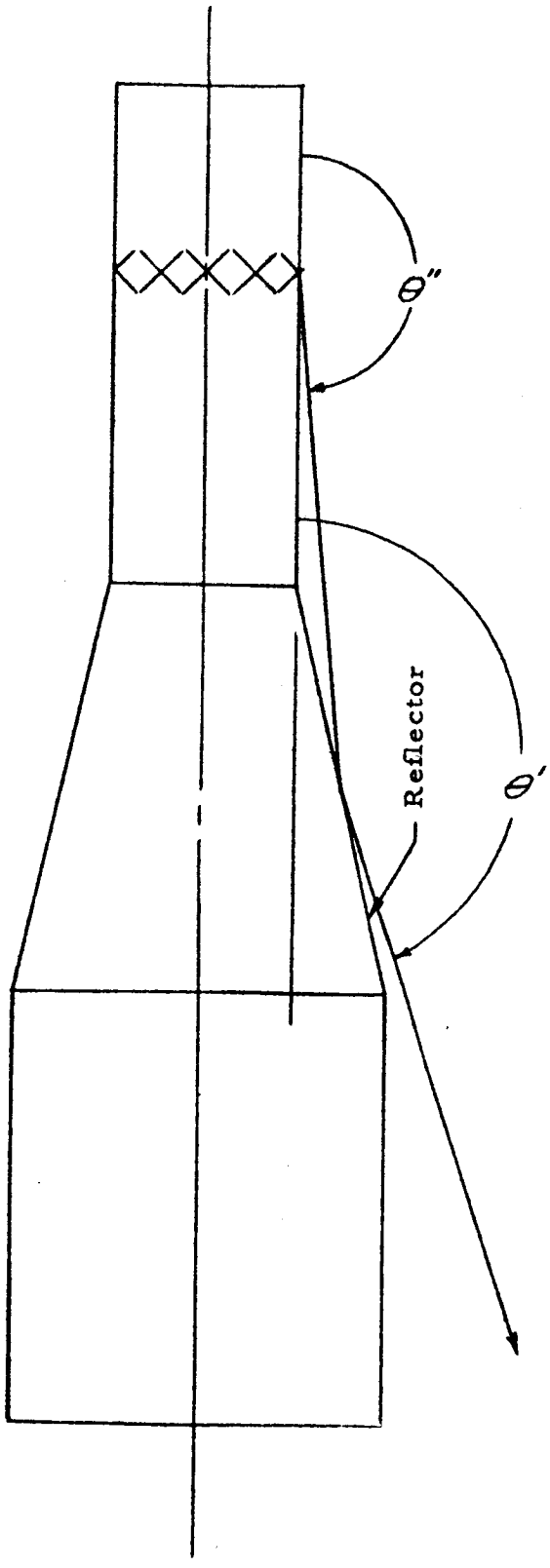

FIGURE V-23

REFLECTED RAY GEOMETRY

are typical of such a synthesis. So is the very sharp skirt and extended range to approximately 168° in θ. Finally, the decrease in the height of the polar lobe at θ = 0° is also a possible result of the Fourier synthesis, although the experimental pattern in Figure V-22 has decreased this lobe to an ideal level that may be very difficult to achieve by an array factor.

A simple illustration of how the diffraction effects have been utilized is shown in Figure V-23. Consider a "central" ray emerging from the ring at an angle θ" with the polar axis. This ray is polarized essentially left circularly polarized if we take θ" as 171.6° as illustrated in Figure V-22. Hence the ray reflected at θ' is essentially right circularly polarized. If we design the conical shield for $\theta' = 162.8°$ to extend the elevation range and sharpen the elevation south polar skirt, we obtain the experimental pattern illustrated in Figure V-22. Hence, the shield serves the dual purpose of providing a transition to the vehicular support for the antenna and also extending the range of the elevation pattern.

The calculated and measured isotropic levels compared nearly identical are shown in the figure. For -4 db gain, the elevation range is experimentally θ = ±167°. The theoretical range is θ = ±156°. At the sacrifice of some ripple and increase in cross polarization, as in the Fourier synthesis for a very long array, we are able to reduce the angle of the null region of the right circular polarization pattern.

The theoretical coverage factor (C. F.) is 95.8% and the diffraction increased C. F. is 98.7% (both for the -4 db gain contour).

Also shown in Figure V-22 is a measured pattern recorded with the conical reflector covered by absorbent material. Much closer agreement with the theoretical is evident. Some ripple is still present and the average gain is slightly less than the theoretical. The -4 db gain coverage extends only to 150°, which is equivalent to a C. F. of 93.3%.

2. Prototype Development

The laboratory test model of the omni antenna has three main sections, as shown in Figure V-24.

1) Mode Launcher
2) Polarizer
3) Radiating Section

a. Mode Launcher

This section describes the unit used to launch the linearly polarized H_{11} mode and absorb the cross polarized reflection.

The mode launcher is a simple probe transition from coax (Type "N") to circular waveguide with an inside diameter of 3.870 inches and a wall thickness of 0.065 inch (4 inches O.D.). This size circular waveguide was chosen for use throughout the antenna because it was readily available commercially and would support the H_{11} mode over the necessary bandwidth without propagating any higher order modes. The probe transition is the simplest type that could be employed, hence, it has reliability and weight advantages. It is a narrow band and low power device, but adequate for this application. Resulting VSWR was 1.15 maximum. Other more sophisticated designs could be substituted if the VSWR less than 1.10 were desired.

The probe transition furthest from the base of the antenna is terminated with a 50 ohm coaxial load obtained from Electronic Standards Corporation of America. This terminal is simply to absorb any reflected signal at the transmit frequency which is cross polarized to the input terminal. Tests discussed later show that the portion of the transmitted power reaching this load will not exceed 5 per cent. For 50 watts of transmitted power, the load should be capable of dissipating 2.5 watts. The septum separating the two probes was used to assure >20 db isolation between them to allow accurate measurements of reflected cross polarized power. Once the entire antenna is designed, the two probes can be placed in the same cross section, resulting in a smaller mode launcher. Also, if the reflected cross polarized energy at the transmit frequency can be held to approximately -15 db or less, or if absorption seems impractical due to heat dissipation, the loaded terminal could be eliminated. The reflected energy will then be retransmitted as left circular polarization, but due to its reduced magnitude, it will have no appreciable effect on the desired right circularly polarized pattern. This fact also shows that a failure of the load will not cause a failure of the antenna. At worst, there will be only a slight degradation in the polarization characteristics of the pattern.

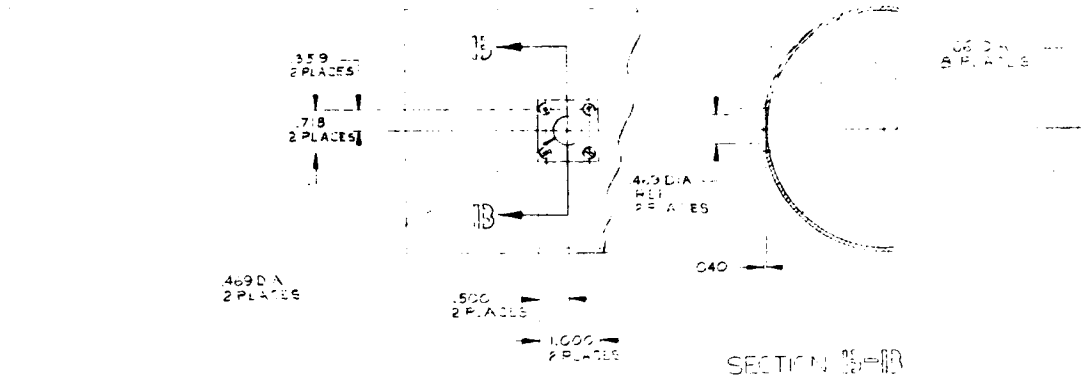

SECTION 15-15

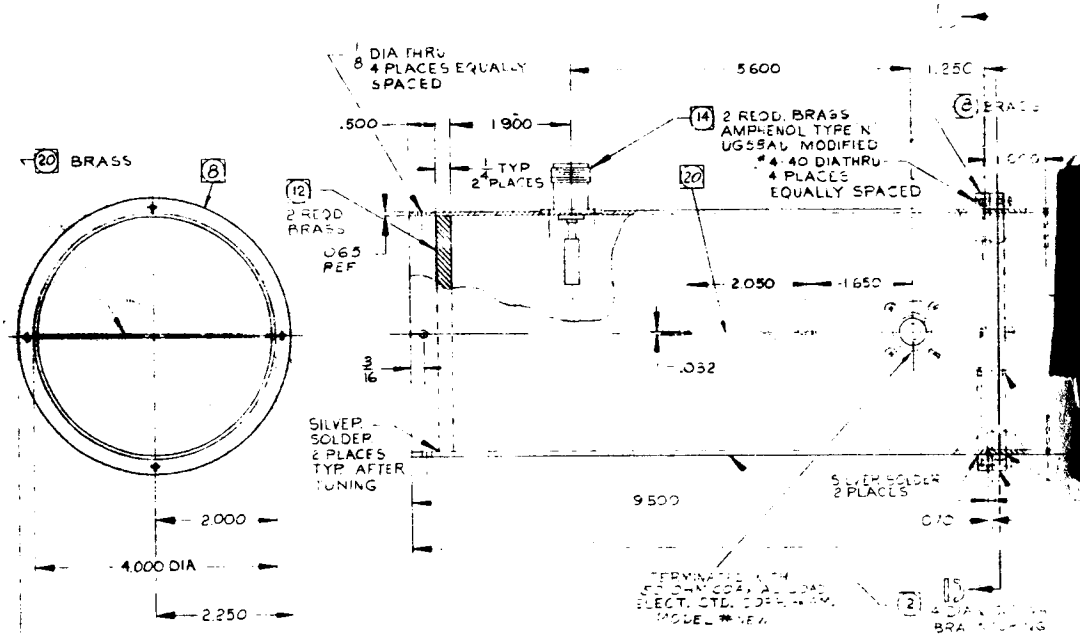

BOND WITH EMSCO CUMMINGS
ECCO BOND EC56C OR EQUIVALENT

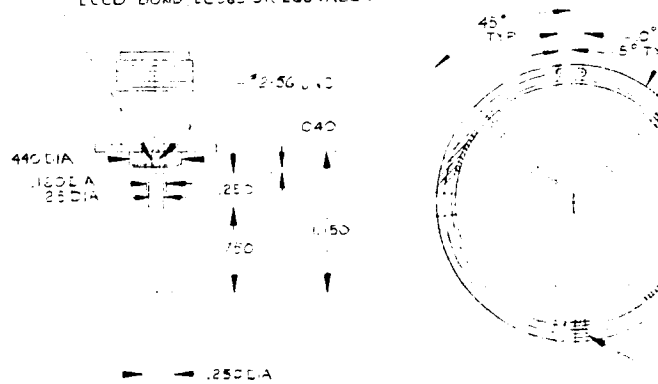

DETAIL OF 14
SCALE 2/1
BRASS

SECTION

#1

NOTES

1. INTERPRET DIMENSIONS, SYMBOLS, ETC., IN ACCORDANCE WITH LISTED DOCUMENTS, AS FOLLOWS:
   - DIMENSIONS AND TOLERANCES MIL-STD-8
   - SURFACE ROUGHNESS MIL-STD-10
   - ABBREVIATIONS MIL-STD-12

(22) SILVER PLATE AND NICKLE FLASH

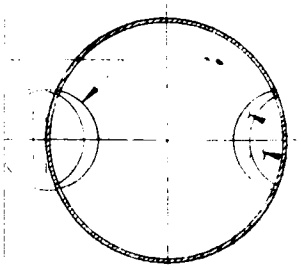

SOLDER AND CUT OFF FLUSH WITH OUTER WALL AFTER TUNING

.560 ± .005 TYP 4 PLACES

.810 ± .005 TYP 4 PLACES

SECTION B-B

(16) 4 REQD BRASS

(4) 4 DIA x .062 WALL BRASS TUBING

SILVER SOLDER

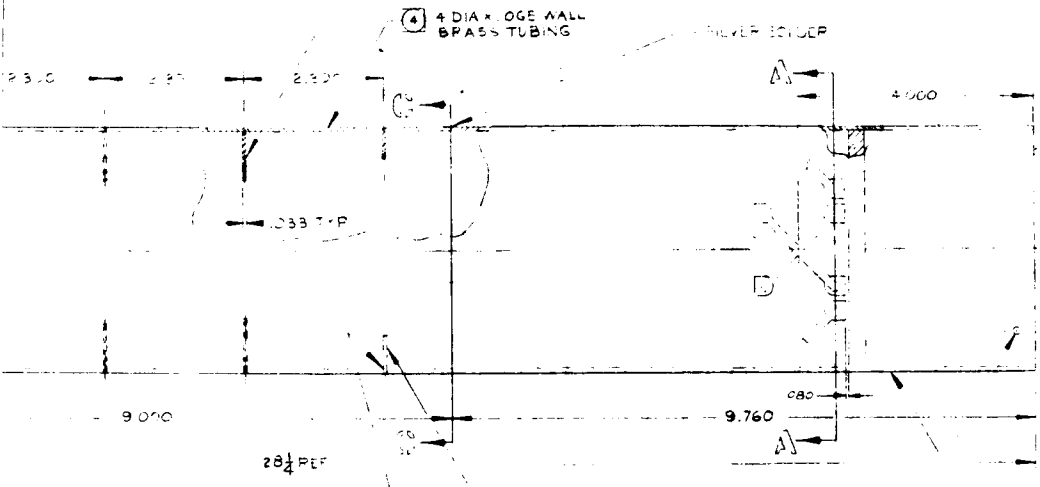

AFTER ELECTRICAL ALIGNMENT PIN FLANGES (8) AND (10) (1) PIN

(18) 4 REQD BRASS

(6) 4 DIA x .065 WALL BRASS TUBING

ALIGNMENT HOLE, ALLOWED ON THIS END

(10) BRASS

TYP 4 PLACES

8 SETS OF SLOTS EQUALLY SPACED 8 PLACES

SILVER SOLDER

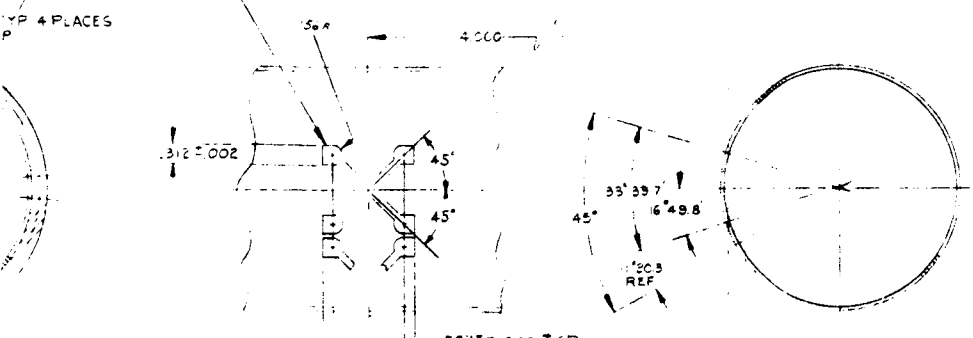

4 SLOTS THRU EQUALLY SPACED 4¼ DIA BOLT CIRCLE

.5875 ± .002 TYP

1.175 ± .002 TYP

.755 ± .002 TYP

1.500 ± .002 TYP

SECTION A-A

SYM	ZONE	REVISIONS DESCRIPTION

NUMBER	SHEET
PROJECT	ISSUE

QTY REQD PER DASH NO	NOMENCLATURE OR DESCRIPTION	CODE IDENT	PROJECT NO	DWG SIZE	PART OR IDENT NO	SPEC	ITEM

LIST OF MATERIAL

DIMENSIONS ARE IN INCHES

UNLESS OTHERWISE SPECIFIED: TOLERANCES ON FRACTIONS ± 1/32 ANGLES ± 1° DECIMALS 2 PLACES ± .1 3 PLACES ± .05 CONCENTRICITY .010 TIR SURFACE ROUGHNESS 125

HEAT TREAT —

MATERIAL —

DRAWN — DATE

CHECKED — DATE

APPROVED — DATE

APPROVED — DATE

APPROVED — DATE

DALMO VICTOR COMPANY
DELIGHT CALIFORNIA A [redacted] DIVISION

TITLE: JPL OMNI ANTENNA

CODE IDENT NO 15788 | SIZE B | FIGURE II-24

SCALE 1/1 | WEIGHT | SHEET 1 OF 1

DASH NO	PROJECT SEE NUMBER / NEXT ASSEMBLY / APPLICATION	EFFECTIVE SERIAL NO	NEXT ASSY USED	KEEP WITH PART OR ASSY	QTY REQD

#2

Figure V-25 is a view looking into the output end of the mode launcher, showing the orthogonal probes, load, and isolation septum.

b. Polarizer

A 90° differential phase shifter is placed at 45° to the excited linear H_{11} mode to transform it to a rotating, or circularly polarized, mode. The design was adapted from the square waveguide polarizer described by Simmons[22].

A short study was performed to determine the iris configuration that would yield susceptance versus frequency curves of equal slope for the two orthogonal components of the input mode. Various radii and straight edged irises were investigated. For the range of susceptances ($\pm j\ B/Y_o$) desired, in 4 inch guide over the 2100 to 2300 Mc band, an iris with a radius of 0.830 inches was found to have the characteristics shown in Figure V-26A. The nearly identical slopes shown for both $+j\ B/Y_o$ and $-j\ B/Y_o$ at various iris depths is necessary to assure a nearly constant 90° differential phase shift across the entire band and to maintain low VSWR.

A three section phase shifter, with ±15° phase shift per section, was designed for 2185 Mc, in accordance with Reference 22. The 2185 Mc was chosen as the design frequency because $|+j\ B/Y_o| \approx |-j\ B/Y_o|$ for a medium depth iris. The following equations were used.

$$\beta = 360° / \lambda_g$$

$$\Delta\theta = 180° - 2\beta\ell$$

$$\text{Cot}\ \beta\ell = B/2Y_o$$

where

$\Delta\theta$ = phase shift per section = ±15°

ℓ = distance between irises

λ_g = guide wavelength

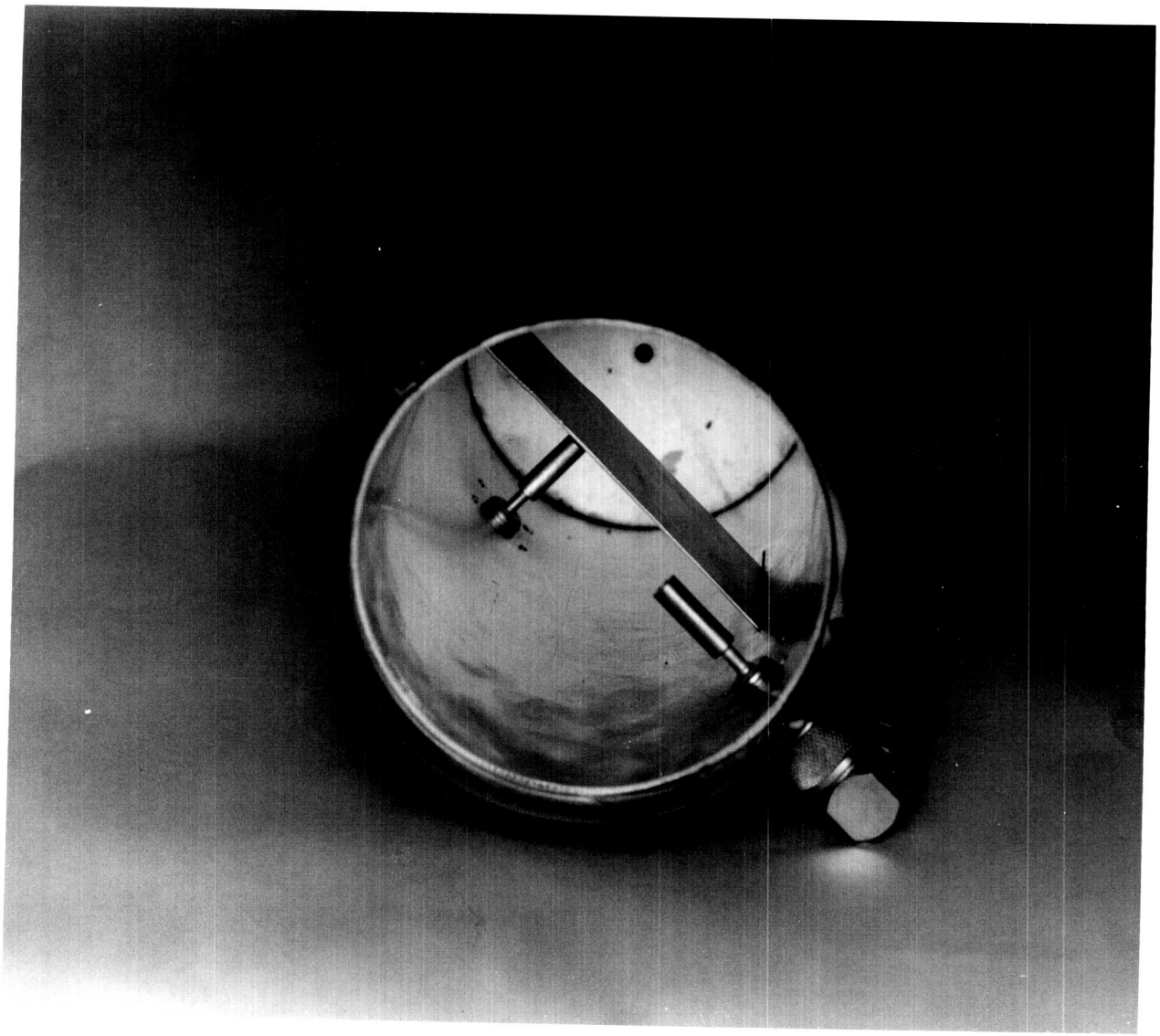

FIGURE V-25. MODE LAUNCHER

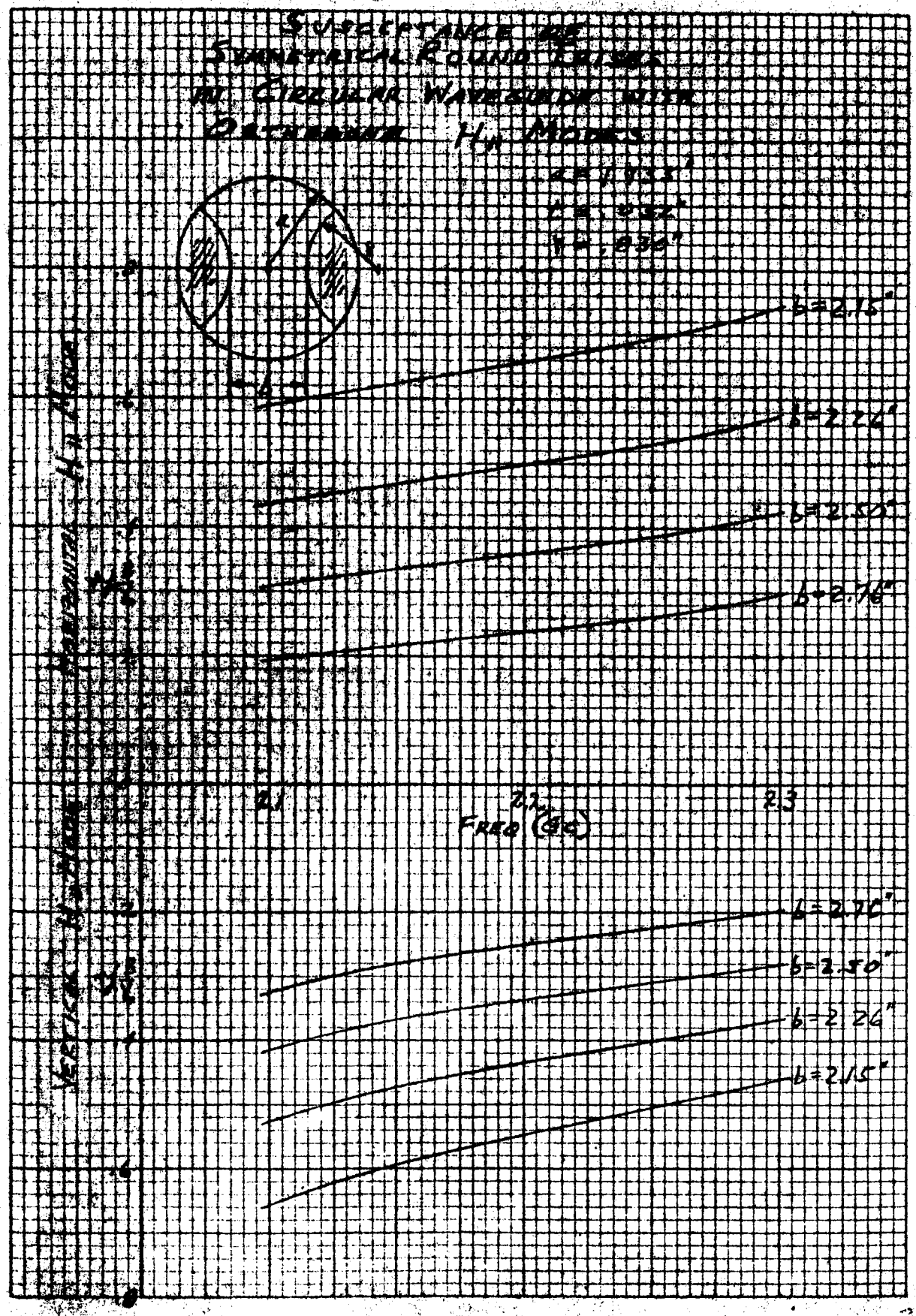

FIGURE V-26A. CIRCULAR IRIS SUSCEPTANCE

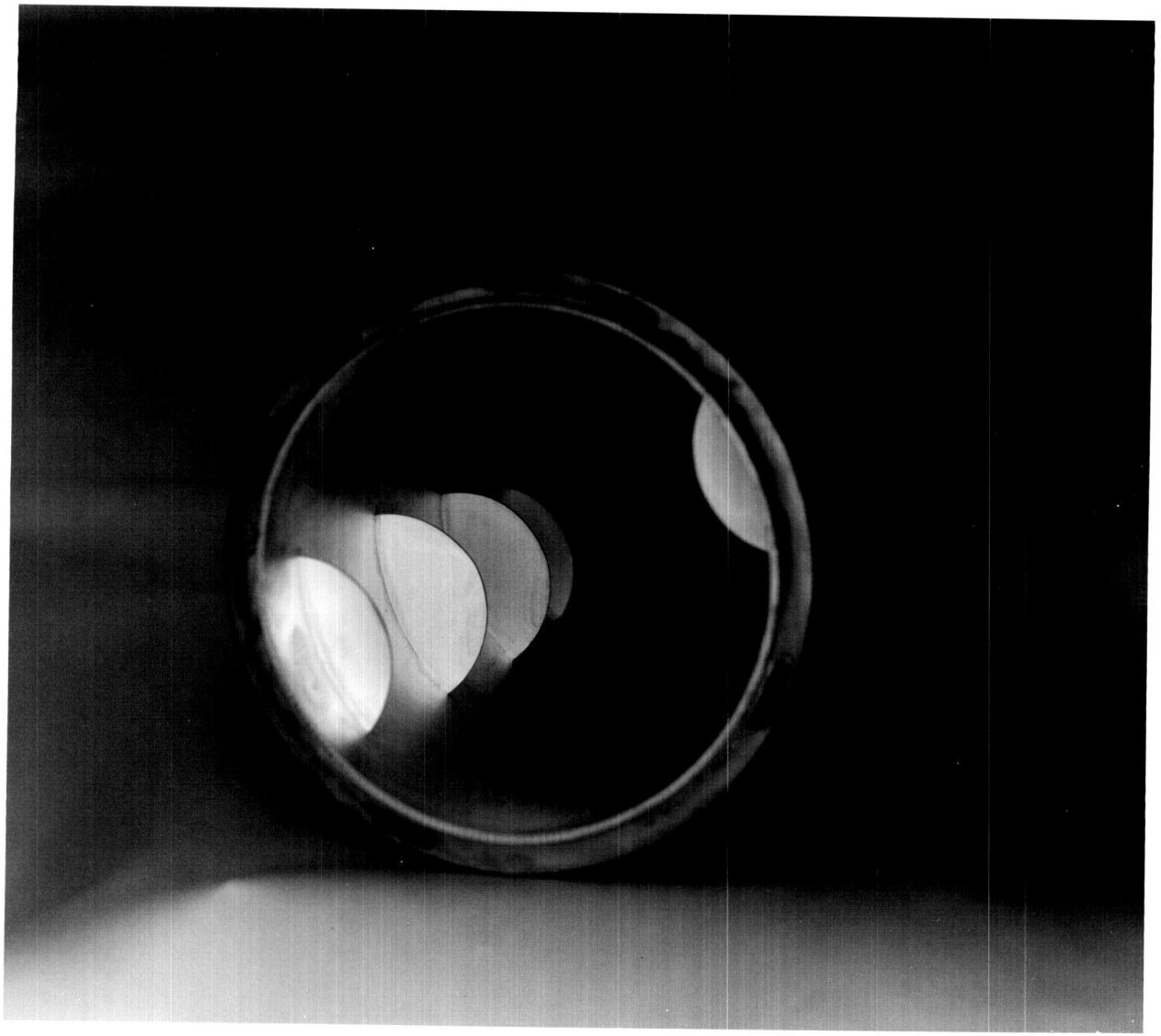

FIGURE 26-B. POLARIZER

Figure V-24 gives the details of the resulting design. The unit was fabricated and tested with the following results:

	Frequency		
	2113	2200	2295
Axial Ratio of Rotating Mode	1.1 db	1.0 db	1.0 db
VSWR - Mode Launcher and Polarizer	1.26	1.17	1.13

The polarizer and mode launcher have been aligned in angle for the best electrical results and pinned together to prevent misalignment. A view of the polarizing irises is shown in Figure V-26B.

c. Radiating Section

The radiating section consists of eight sets of dumbbell loaded[23] crossed slots[24] equally spaced on a circumference of the waveguide. Their distance from the short circuited end of the waveguide (z) has been set so that the requirements for circular polarization are met at the slot centers. (Refer to mode theory section.) Of course, the z distance cannot be exact at both operating frequencies, and the theory assumes that the slots in the waveguide wall do not disturb the internal currents, which they must to produce coupling, so perfect circular polarization cannot be obtained.

Several slot and hole configurations were studied to determine which would best meet the requirements of coupling the maximum circularly polarized energy at the two operating frequencies without appreciably distorting the internal mode.

All hole configurations investigated were unsuccessful for the following reasons:

1) A hole large enough to produce substantial coupling is no longer round when drilled on a cylindrical surface.

2) A resonant hold (diameter = λ / π) only has approximately one-fifth the conductance of a resonant crossed slot, so high efficiency could not be obtained.

3) Holes approaching resonance greatly affect the axial ratio of the internal mode.

Although holes have the advantage of being easier to machine, it was concluded that crossed slots were necessary.

The theory has been developed for slots in axial and circumferential directions. These have two disadvantages:

1) The two slots of a given crossed set are different since one is cut on a flat surface and the other on a curved surface.

2) The resonant length of a circumferential slot limits the number of crossed slots in a ring to six. Measurements of power radiated by a single crossed slot of resonant length indicate that maximum coupling of six crossed slots would be approximately 70 per cent.

To approach 100 per cent coupling from one ring element, it must contain eight crossed slots. The crossed slots can be oriented at ±45° to the waveguide axis without affecting the radiated field, since the theoretical field is essentially the same for holes and crossed slots. However, the maximum slot length that can be obtained with eight sets of ±45° crossed slots on a four inch diameter waveguide is approximately 2.0 inches, allowing a minimum spacing between slots. Since a resonant length is approximately 2.5 inches, some method of loading the slots to increase their effective length is necessary. Dielectric filled slots could be used, and would be desirable if a sealed waveguide were needed, but for space applications, dumbbell slots are superior.

It was also noted that the on-axis axial ratio of the field radiated by a single crossed slot is affected by the slot width and inclination angle. That is, the slot coupling to the two components of the circularly polarized mode are functions of the inclination angle and width as well as distance from the short circuit. Still another factor to be considered when positioning the short circuit for optimum bandwidth is the phase shift that off resonant slots produce in the internal mode. For this reason, the physical location of the short circuit is usually not at the $\lambda_g/8$ position predicted by the theory when the slot lengths are near resonance. Simmons[25] has shown that crossed slots much below resonance have a phase shift characteristic that is nearly zero and constant with frequency. Hence, these short slots were used to study the effects of inclination angle and width.

For slot widths of 0.250 inch and several sizes under 0.100 inch it was found that inclination angles greater than ±45° were necessary to obtain on-axis circular polarization. For widths of 0.100 inch and 0.120 inch, an inclination angle of ±45° yielded nearly circular polarization on-axis. Noting that angles greater than ±45° would restrict the lengths of the slots still further and due to the poor axial ratios obtainable for slot angles less than 45°, it was decided to use slot widths between 0.100 inch and 0.120 inch oriented at ±45°. The longer slots physically possible with less than ±45° inclination might be undesirable anyway due to the proximity of the short circuit.

Eight dumbbell loaded crossed slots were fabricated as shown in Figure V-27. The power radiated was measured by noting the VSWR on the input terminal and decoupling on the cross polarized terminal. Waveguide losses were neglected. The error in this assumption was determined to be approximately 1 per cent by short circuiting the slots and noting that over 98 per cent of the input power was returned to the two terminals. This established the two-way loss at less than 2 per cent. (This is also an excellent method of testing and tuning the polarizer. The better the axial ratio of the polarizer's output, the more energy is returned to the cross polarized terminal when the slots are shorted.)

The eight sets of slots of the type shown in Figure V-27 were loaded in increasing increments by drilling out the holes and the power radiated was measured each time. Figure V-28 shows the results. When the diameter of the holes reached 0.312 inch, the remaining wall thickness was judged to be at a minimum and further increases were made by using square holes. The measurements shown at diameters greater than 0.312 inch are really for the equivalent diameter that would yield the same total slot circumference as the square holes that were actually used. Figure V-29 is a photograph showing the detail of the resulting slot configuration. Dimensions are given in Figure V-24. It must be noted that extreme care must be exercised to maintain identical slots with good symmetry. Also, the short circuit must be perpendicular to the axis.

It can be seen in Figure V-28 that an electrically resonant slot length was approached, but not quite reached. Further lengthening of the slots was not possible because the short circuit had to be moved closer than its theoretical spacing (1.15 inches) to compensate for the slot produced phase shift and maintain circularly polarized radiation. As seen in Figure V-24, the short is nearly flush with the slot ends

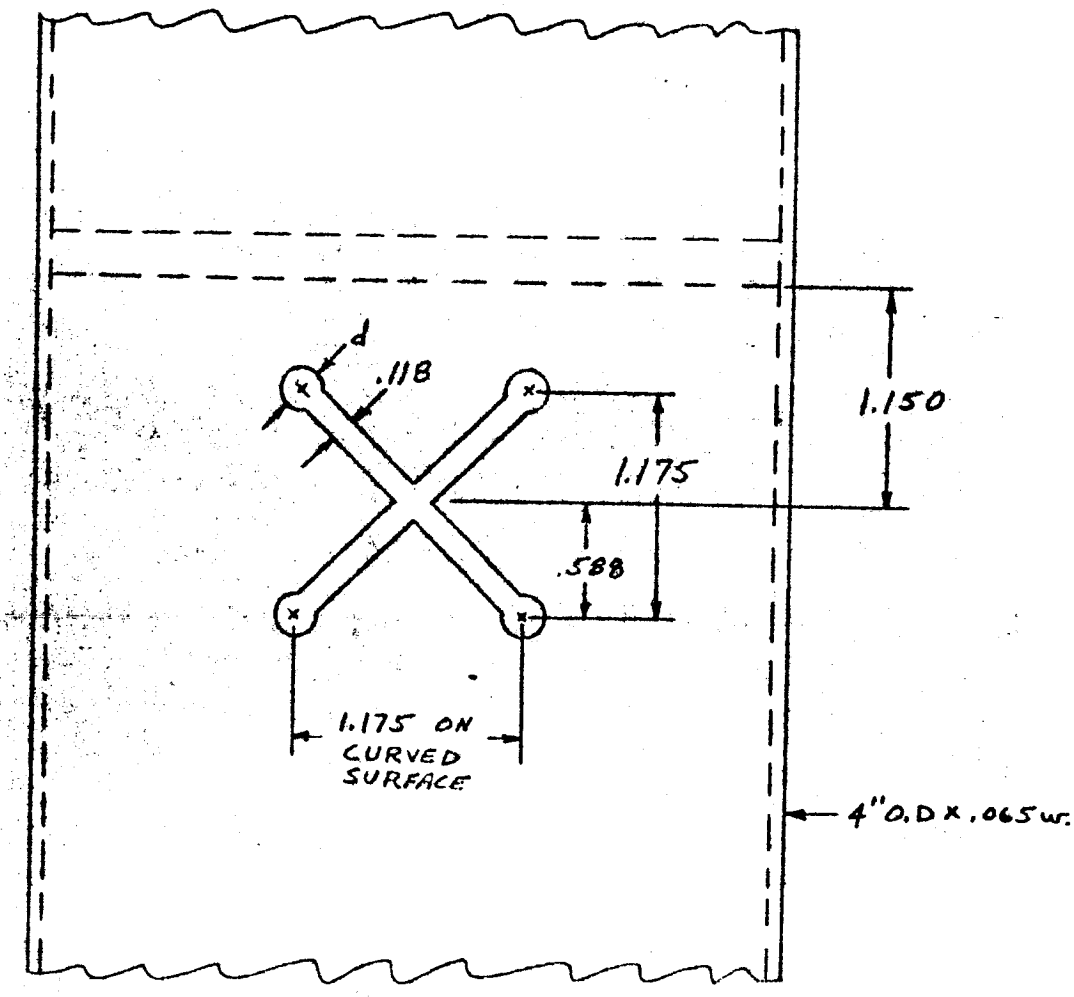

FIGURE V-27

EXPERIMENTAL DUMBBELL LOADED CROSSED SLOT

65-430

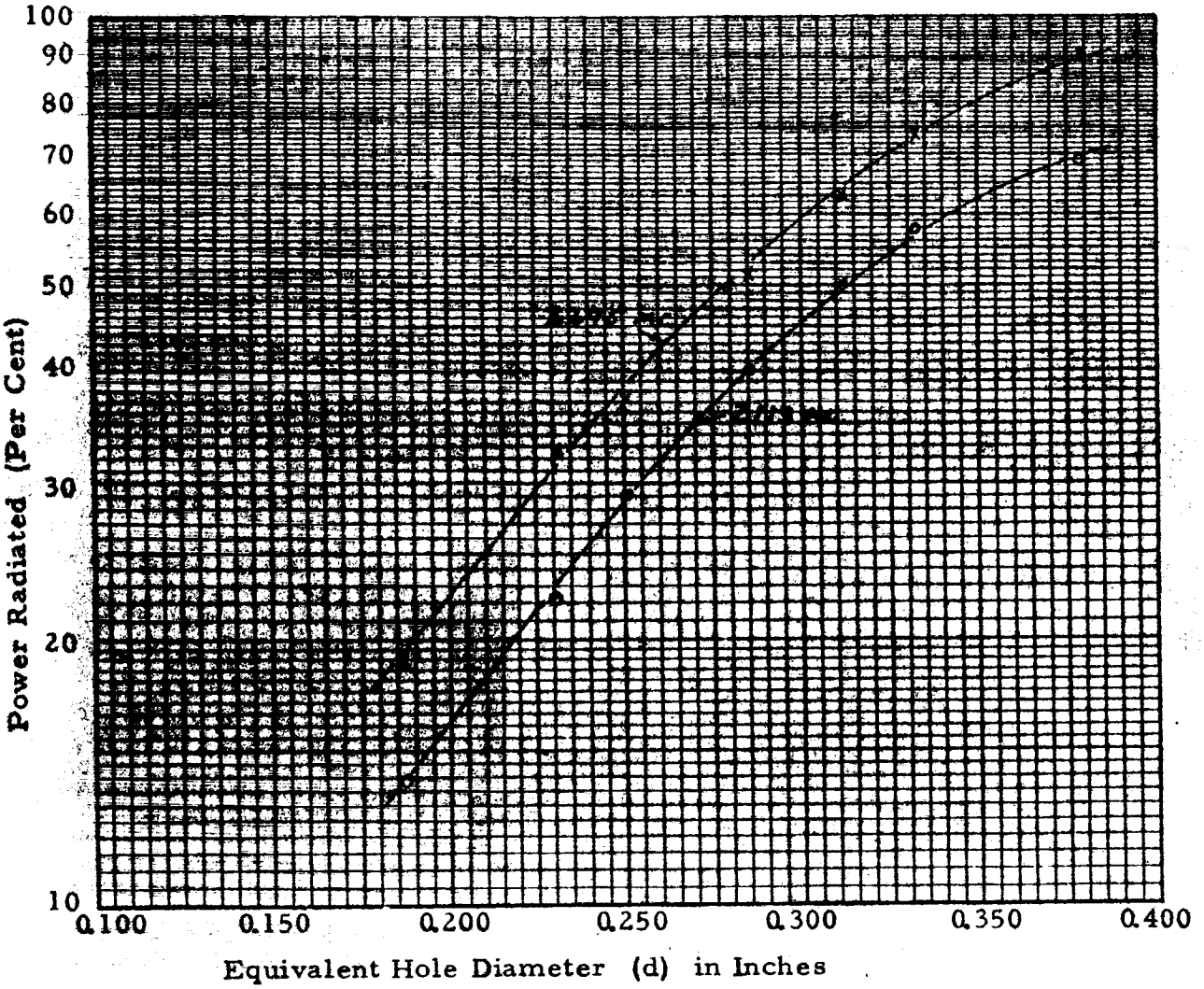

FIGURE V-28

POWER RADIATED VERSUS SLOT LOADING FOR EIGHT CROSSED SLOTS

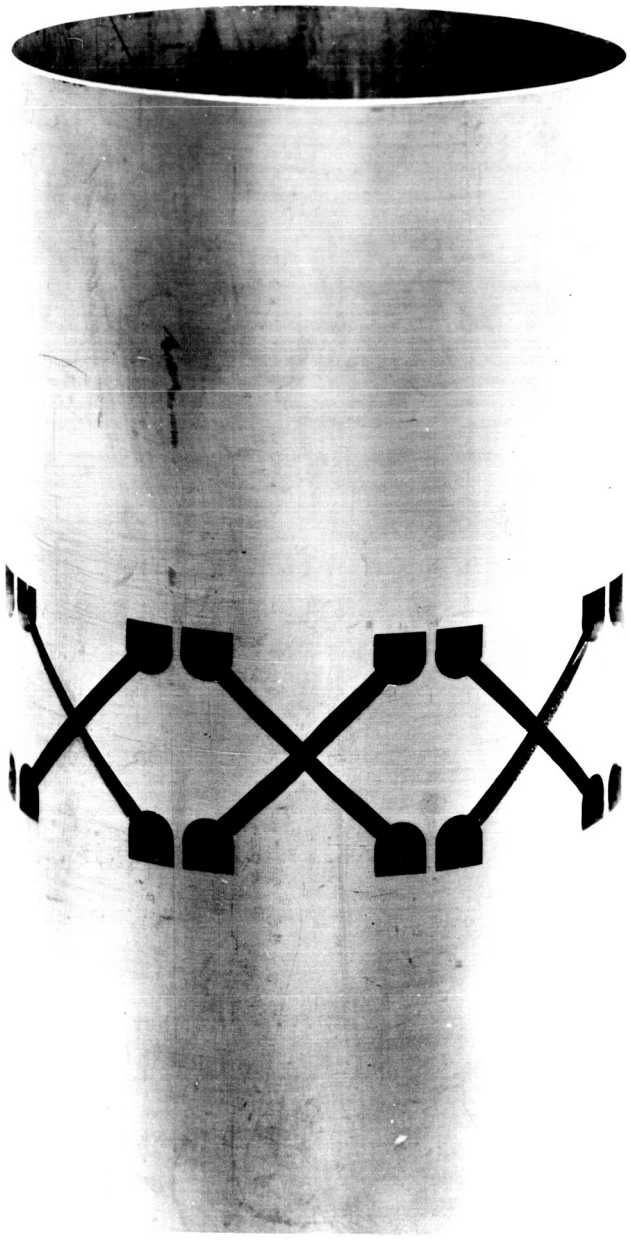

FIGURE V-29

LOADED SLOT CONFIGURATION

at 0.755 inch from the slot center. (This actually increased the coupling by capacitively loading the slot, and will be discussed later.) Also, it is this compromise between slot length and short position that is responsible for the higher then theoretical cross-polarized pattern. It is also evident in Figure V-28 that a perfectly resonant ring element of eight crossed slots at 2295 Mc would still not couple 100 per cent of the power at 2113 Mc. Fortunately, the high power (transmit) is at the higher frequency and the greater coupling can be obtained where it is more important.

Theoretically, introducing a tuning element (susceptance) at the proper point in the guide should enable one to tune the non-resonant slots to obtain an impedance match and assure maximum power radiation. However, the guide wavelengths for the two operating frequencies in this size circular waveguide are substantially different. Hence, no position for a tuning element could be found that would match one frequency without mismatching the other. Also, the magnitude of the mismatch at each frequency is substantially different, so this approach was dropped.

Once slots as near resonant as possible were obtained and the short positioned for circularly polarized radiation in the omni plane, a plot of antenna efficiency versus frequency was made. See Figure V-30. Assuming waveguide losses to be negligible, efficiency can be calculated from

$$\text{Eff.} = \left[1 - (P_{\text{Refl.}} + P_{\text{Load}})\right] \quad 100\%$$

where $P_{\text{Refl.}}$ = power reflected as input VSWR

P_{Load} = power into cross polarized load

It can be seen by comparing Figures V-28 and V-30 that greater coupling was obtained after the short was adjusted for circularly polarized radiation. The drop in efficiency near 2170 Mc is due to an interaction of the impedances (resonance) of the slots and polarizer. It is therefore a function of the length between the slots and polarizer. This length has been chosen to move the null away from 2113 Mc. The resulting input VSWR to the total unit is 1.20 maximum in the receive band (2113 ±5 Mc) and 1.32 maximum in the transmit band (2295 ±5 Mc). The orthogonal terminal minimum decoupling is 8.0 and 13.0 db in the same bands, respectively.

100

65-430

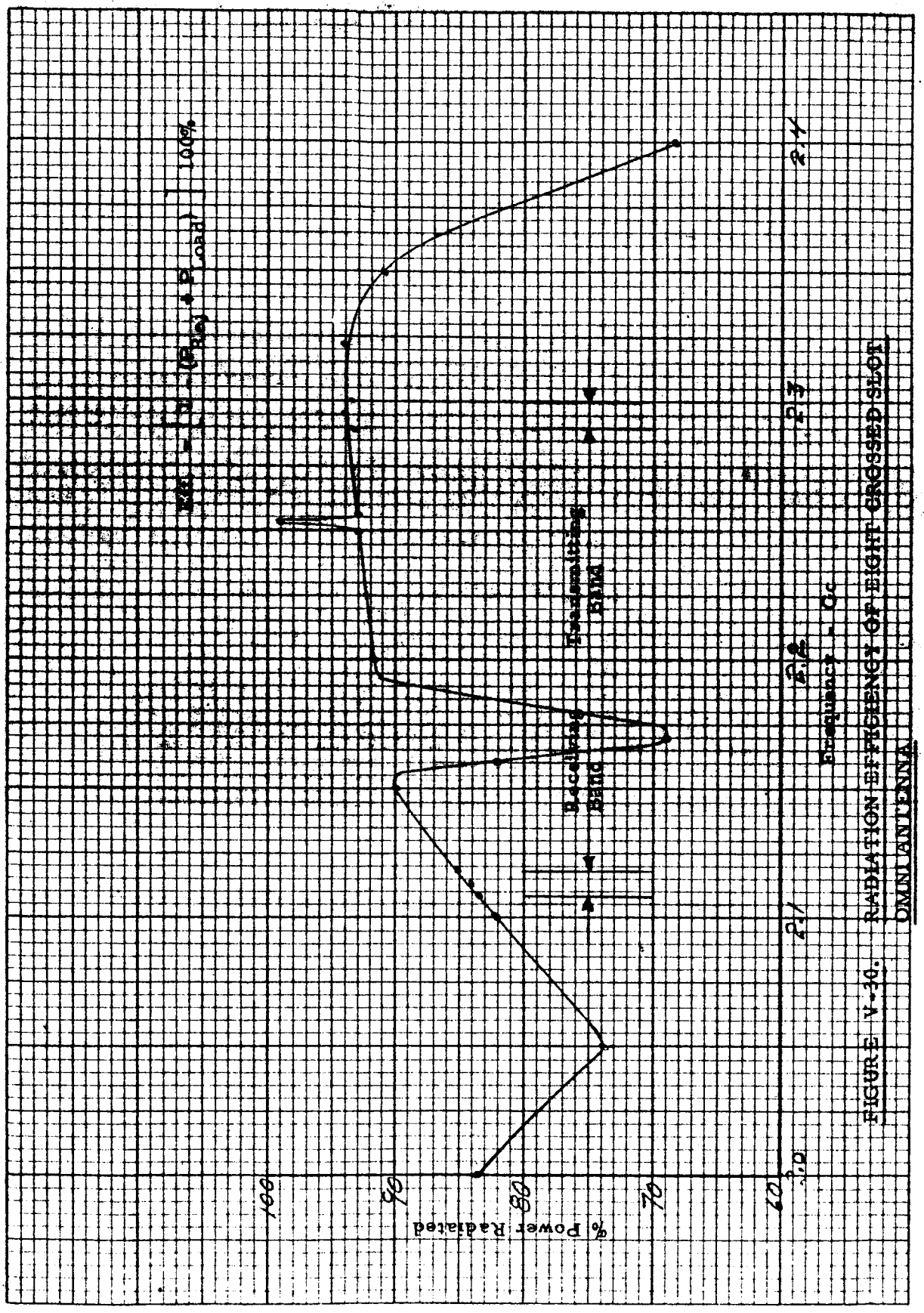

FIGURE V-30. RADIATION EFFICIENCY OF EIGHT CROSSED SLOT OMNIANTENNA

101

Due to the rotating standing wave and the circular symmetry of the eight crossed slots, the angular alignment of the radiating section relative to the polarizer is unimportant.

The length of the truncated waveguide is chosen for optimum pattern performance as discussed in the next section.

d. Assembly Performance

The three main sections of the omni antenna were assembled as shown in Figure V-24. This much of the omni antenna assembly is sufficient for checking input VSWR and orthogonal decoupling. However, when the load and a detector are attached to the terminals, the patterns are affected by the reflections. Hence, the conical housing shown in Figure V-31 must be used to provide a quasi-smooth transition from the 4 inch diameter to approximately 8 inches and to maintain circular symmetry. The 8 inch maximum diameter was chosen to mate with the top of the Ranger spacecraft. For other installations, this size could be changed. The flared section was experimentally positioned to produce an optimum phase for the reflection of the left circular energy and increase the coverage as discussed in the theoretical section of this report. The spacecraft mounting flange detailed in Figure V-32 also serves the dual purpose of supporting the large end of the conical housing, and should be employed even when the antenna is not mounted on the spacecraft. Figure V-33 shows the entire omni antenna assembly. The Type "N" terminal is for test purposes only. Normally, the outer surface is completely smooth.

Figures V-34 thru V-37 are typical measured patterns of the free space omni antenna as shown in Figure V-33. Figures V-34 and V-35 are θ plane patterns for 2113 and 2295 Mc respectively. Right and left circularly polarized patterns are shown and can be compared with the theoretical pattern of Figure V-20. Comparison shows the right circularly polarized pattern to contain an unpredicted ripple and to have an average gain about 2.0 db below isotropic. The ±2 db ripple means the minimum gain will be as low as -4 db from isotropic (exclusive of the null region, when $|\theta| \longrightarrow 180°$). The gain at $\theta = 0°$ is greater than isotropic, but is not as high as theory predicts. Also, the cross polarization (L.C.P.) in the region $35° < |\theta| < 140°$ has higher gain than predicted.

The high cross polarization is due to two effects:

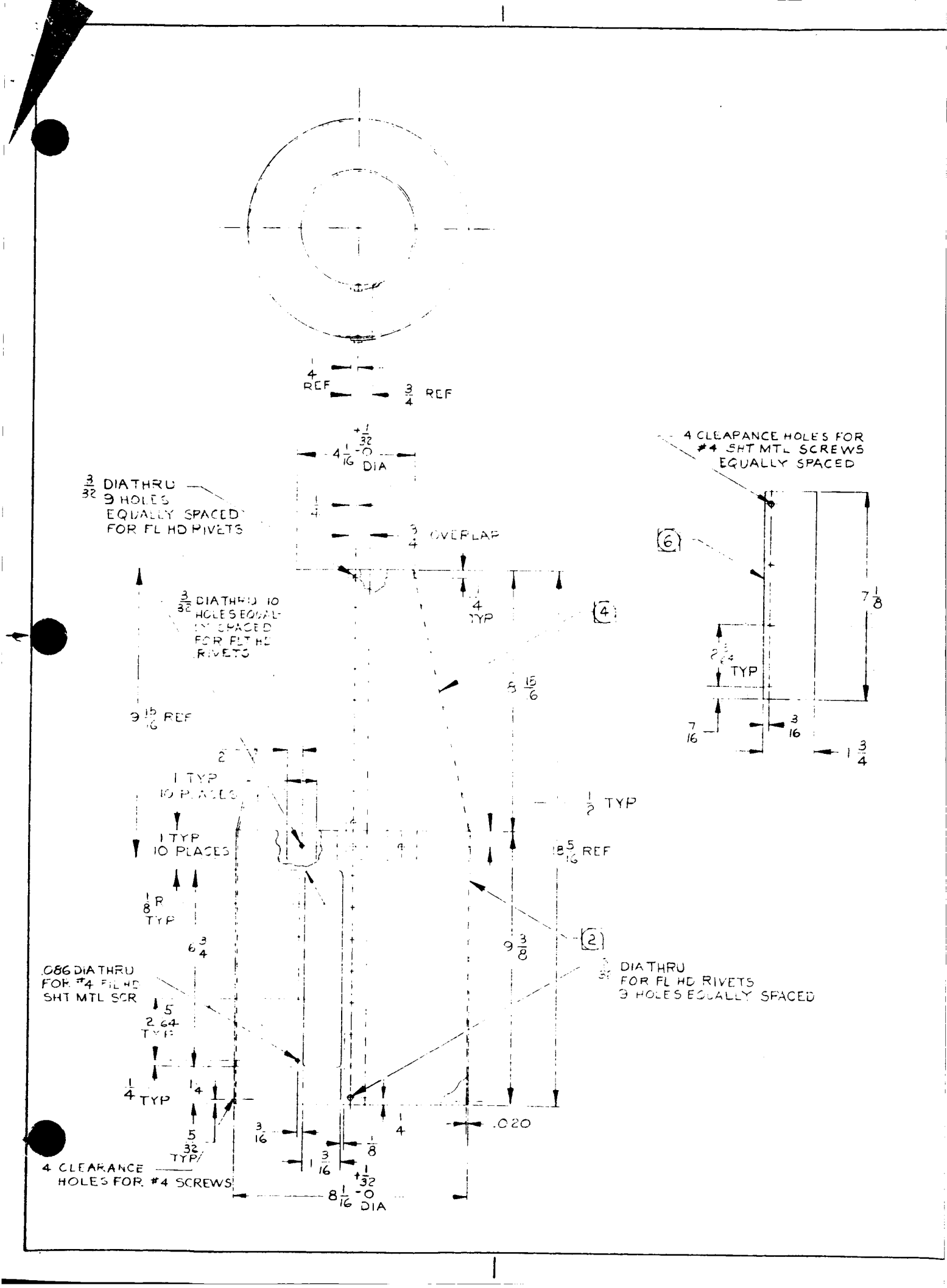
1/4 REF
3/4 REF
+1/32
4 1/16 -0 DIA
3/32 DIA THRU 9 HOLES EQUALLY SPACED FOR FL HD RIVETS
1/4
3/4 OVERLAP
3/32 DIA THRU 10 HOLES EQUALLY SPACED FOR FL HD RIVETS
4 TYP
4
9 15/16 REF
5 15/16
2
1 TYP 10 PLACES
1 TYP 10 PLACES
1/2 TYP
18 5/16 REF
1/8 R TYP
6 3/4
9 3/8
2
.086 DIA THRU FOR #4 FIL HD SHT MTL SCR
5/32 DIA THRU FOR FL HD RIVETS 9 HOLES EQUALLY SPACED
5/64 TYP
1/4 TYP
1/4
5/32 TYP
3/16
1 3/16
1/8
+1/32
8 1/16 -0 DIA
1/4
.020
4 CLEARANCE HOLES FOR #4 SCREWS
4 CLEAPANCE HOLES FOR #4 SHT MTL SCREWS EQUALLY SPACED
6
7 1/8
2 5/64 TYP
7/16
3/16
1 3/4

NOTES

1. INTERPRET DIMENSIONS, SYMBOLS, ETC., IN ACCORDANCE WITH LISTED DOCUMENTS, AS FOLLOWS:
   - DIMENSIONS AND TOLERANCES MIL-STD-8
   - SURFACE ROUGHNESS MIL-STD-10
   - ABBREVIATIONS MIL-STD-12
8. PAINT LIGHT GREY

REVISIONS				
SYM	ZONE	DESCRIPTION	DATE	APPROVED

QTY REQD PER DASH NO	NOMENCLATURE OR DESCRIPTION	CODE IDENT	PROJECT NO	DWG SIZE	PART OR IDENT NO	SPEC	ITEM
-4	-3	-2	-1				
	LIST OF MATERIAL						

DASH NO	PROJECT	SIZE	NUMBER	EFFECTIVE SERIAL NO	NEXT ASSY	ASSY PER UNIT
APPLICATION	NEXT ASSEMBLY				QTY REQD	

DIMENSIONS ARE IN INCHES
UNLESS OTHERWISE SPECIFIED:
TOLERANCES ON
FRACTIONS ± 1/32 ANGLES ± 1°
DECIMALS
2 PLACES ± .__ 3 PLACES ± .___
CONCENTRICITY — TIR
SURFACE ROUGHNESS —√

HEAT TREAT —

MATERIAL: ALUM .020 THK

PROJECT NUMBER

ISSUE — SHEET — OF —

DRAWN [signature] 1-1-64 DATE
CHECKED DATE
APPROVED DATE
APPROVED DATE
APPROVED DATE
APPROVED DATE

DALMO VICTOR COMPANY
BELMONT, CALIFORNIA A [illegible] DIVISION

TITLE
HOUSING, CONICAL
JPL OMNI ANTENNA

CODE IDENT NO	SIZE	
15786	D	FIGURE V-31
SCALE 1/2	WEIGHT —	SHEET 1

R-2870-3582

NOTES:
1 INTERPRET DIMENSIONS, SYMBOLS, ETC. IN ACCORDANCE WITH LISTED DOCUMENTS AS FOLLOWS.
DIMENSIONS AND TOLERANCES MIL-STD-8
SURFACE ROUGHNESS MIL STD-10
ABBREVIATIONS MIL-STD-12

REVISIONS			
SYM	DESCRIPTION	DATE	APPROVED

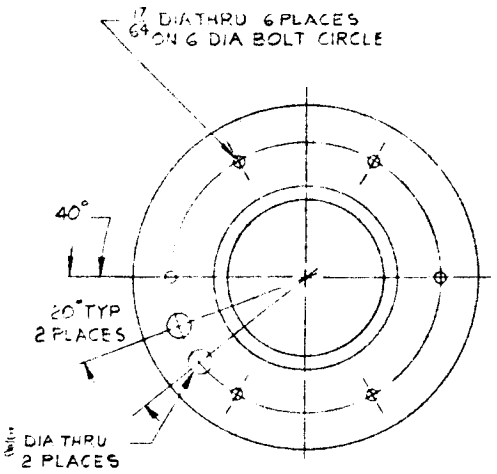

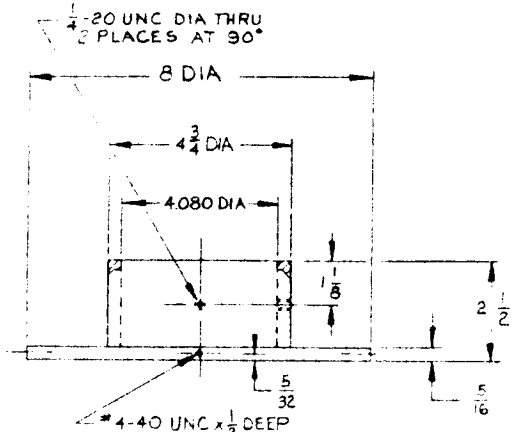

NUMBER	SHEET 1 OF 1
PROJECT	ISSUE

-4	-3	-2	-1	-	NOMENCLATURE OR DESCRIPTION	CODE IDENT	PROJECT NO	DWG SIZE	PART OR IDENT NO	SPEC	ITEM
QTY REQD PER DASH NO											

LIST OF MATERIAL

DASH NO	PROJECT NEXT ASSEMBLY	SIZE NEXT ASSEMBLY	NUMBER NEXT ASSEMBLY	EFFECTIVE SERIAL NO	NEXT ASSY	QTY PER UNIT
APPLICATION						

DIMENSIONS ARE IN INCHES
UNLESS OTHERWISE SPECIFIED
TOLERANCES ON
FRACTIONS ± 1/32 ANGLES ± 2°
DECIMALS
2 PLACES ± .03 3 PLACES ± .010
CONCENTRICITY — TIR
SURFACE ROUGHNESS 125

HEAT TREAT —

MATERIAL ALUM 6061-T6

DRAWN	DATE
CHECKED	DATE
APPROVED	DATE
APPROVED	DATE
APPROVED	DATE
APPROVED	DATE

DALMO VICTOR COMPANY
BELMONT, CALIFORNIA A [illegible] DIVISION

TITLE
FLANGE
ANTENNA BASE MOUNT

CODE IDENT NO	SIZE	
15786	C	FIGURE II-32

SCALE 1/2 WEIGHT SHEET

II-77

V-77

65-430

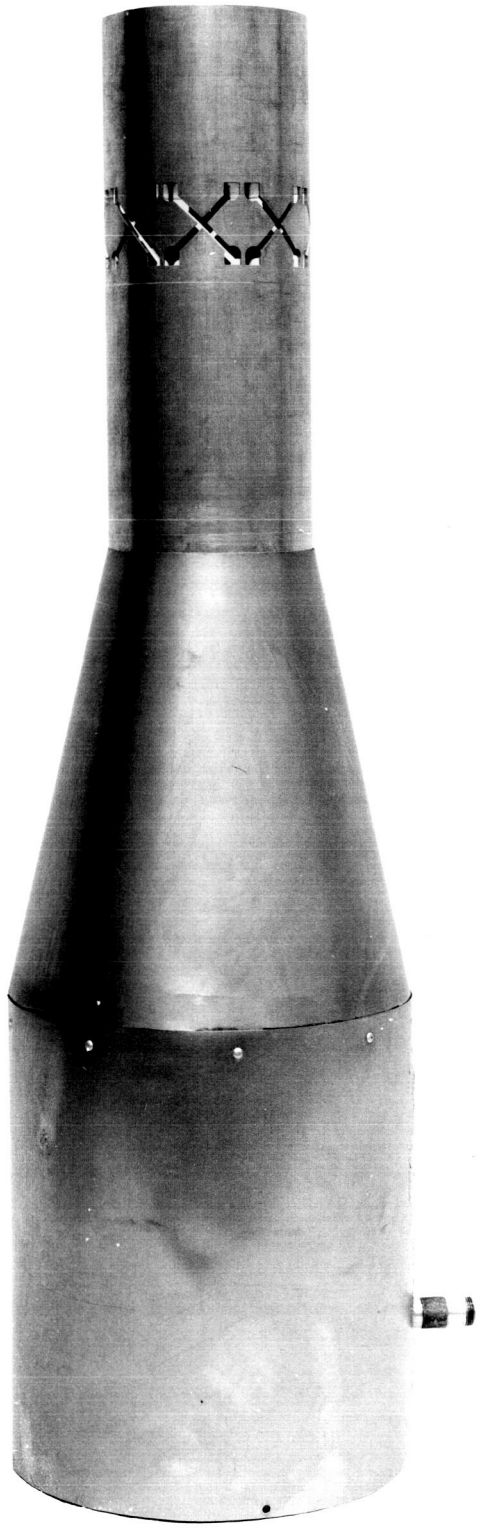

FIGURE V-33. FREE SPACE OMNI ANTENNA

RE-ORDER NO. 65-430

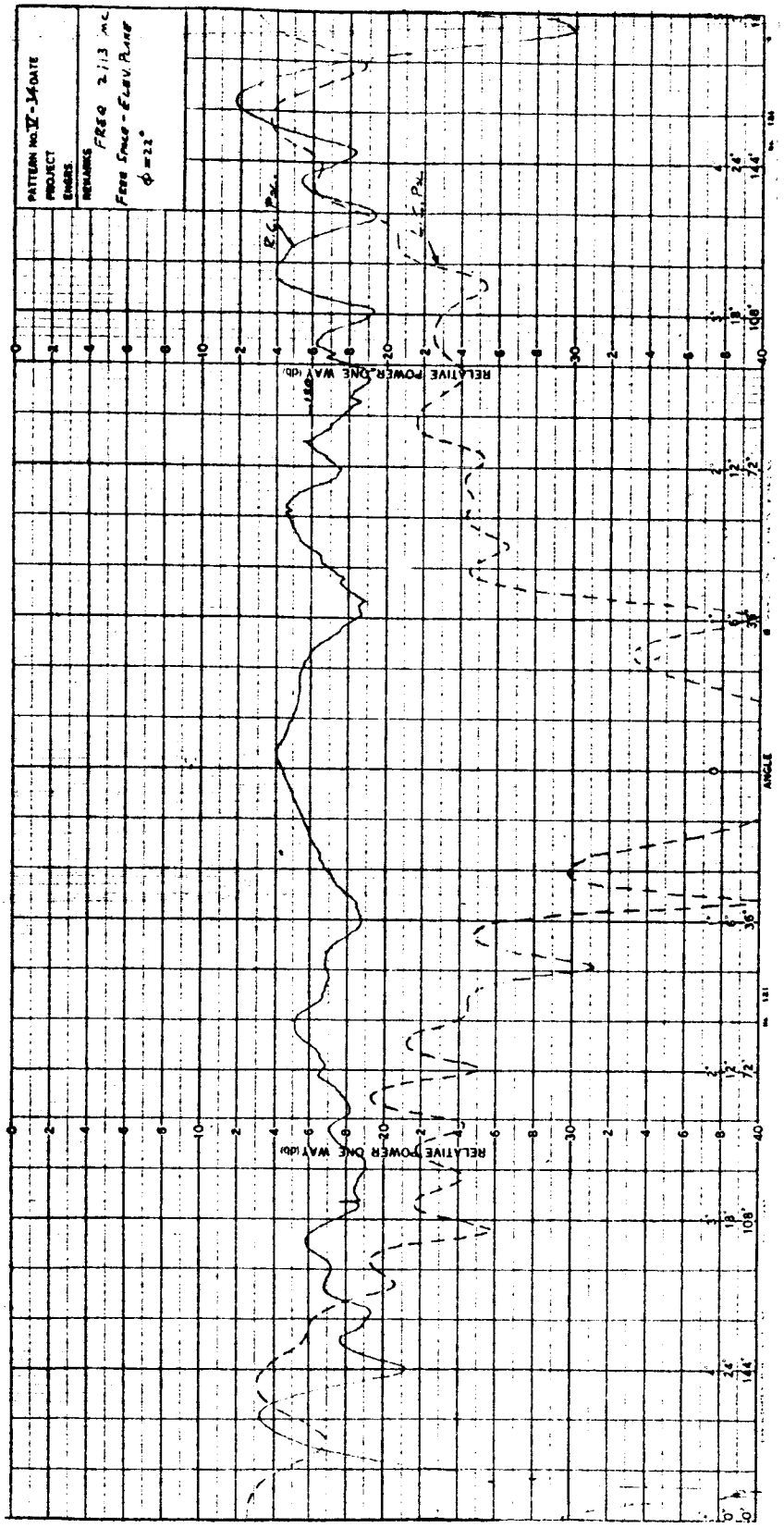

FIGURE V-34

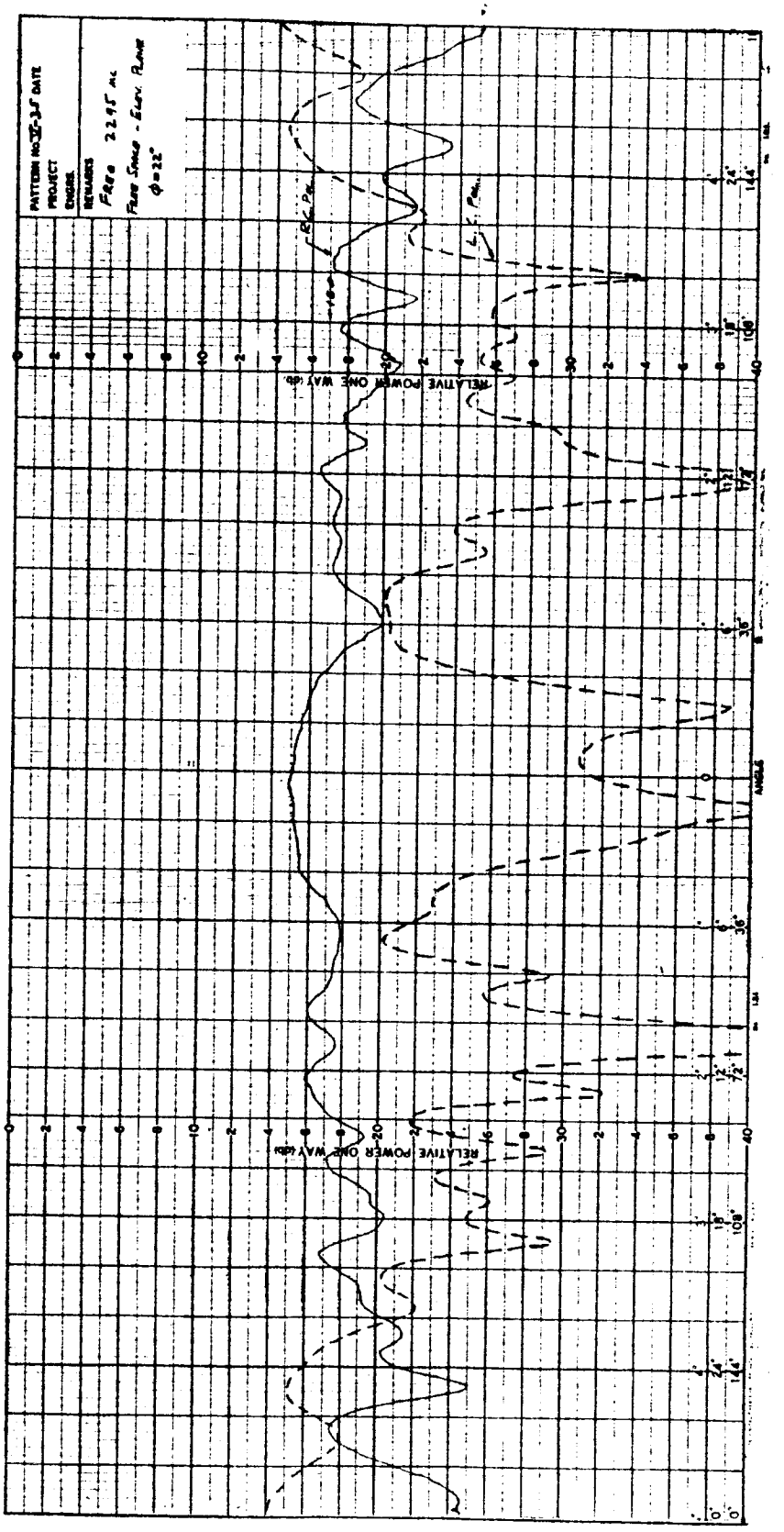
PATTERN NO. 35-3F DATE
PROJECT
ENGR.
REMARKS
Freq 2295 mc
Plane Source - Elev. Plane
φ = 22°
RELATIVE POWER ONE WAY dB
RELATIVE POWER ONE WAY dB
ANGLE

FIGURE V-35

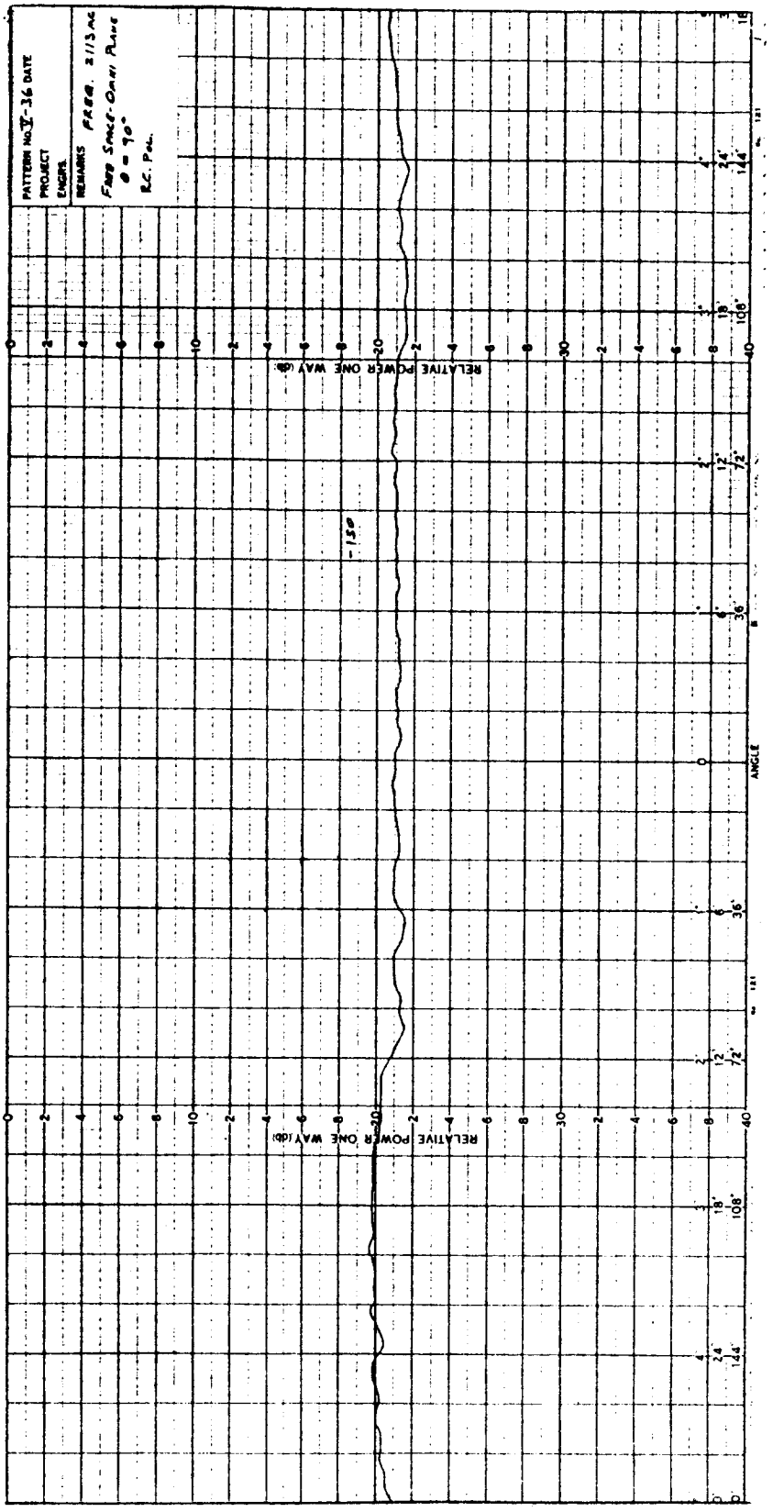
PATTERN NO. V-36 DATE
PROJECT
ENGR.
REMARKS FREQ. 2113 MC
Free Space Omni Plane
θ = 90°
R.C. Pol.
RELATIVE POWER ONE WAY (db)
-15θ
ANGLE

FIGURE V-36

65-430

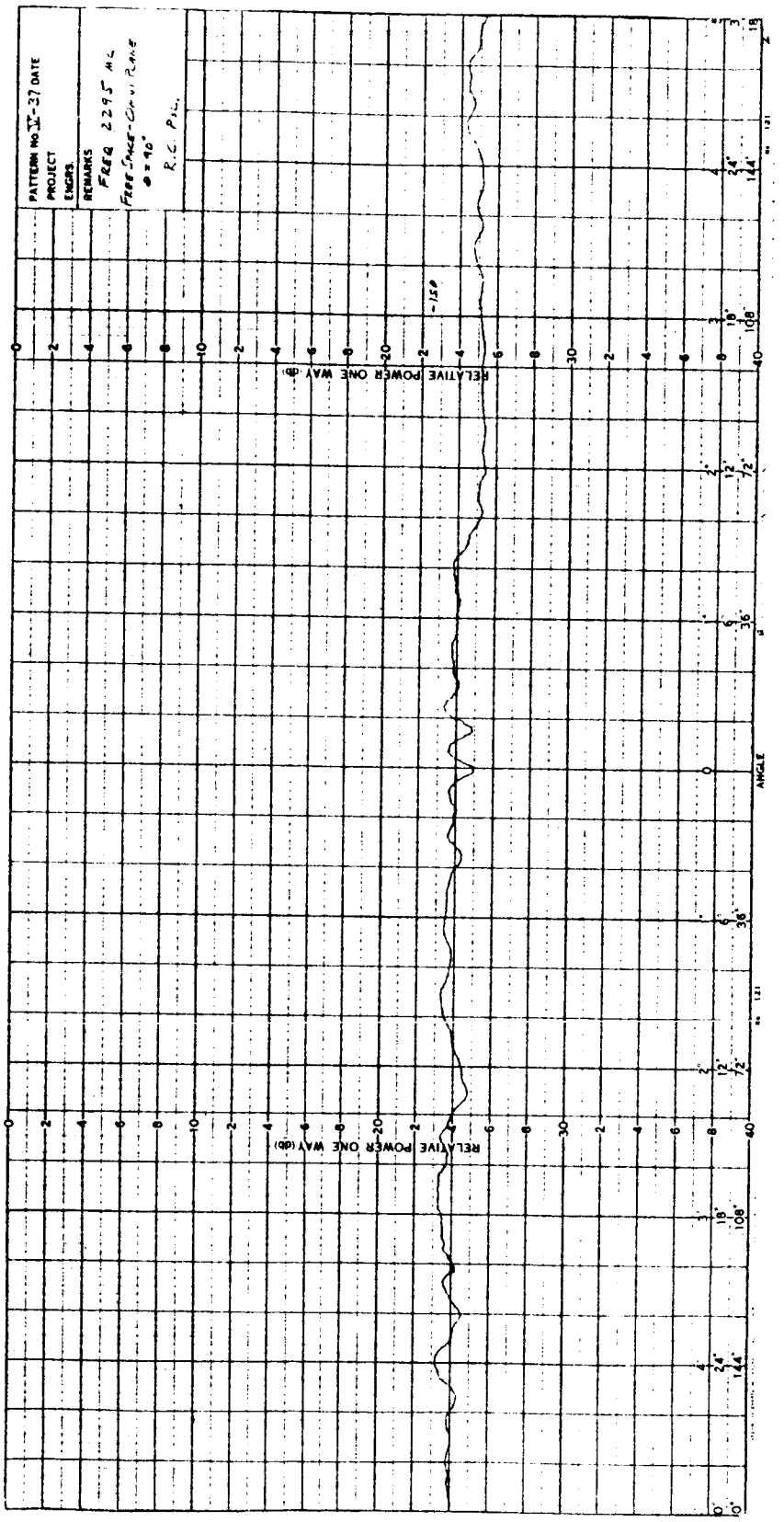

FIGURE V-37

1) The short circuit in the waveguide cannot be perfectly positioned for both frequencies. Due to the compromise short position the crossed slots are excited with slightly elliptical currents. (The short was positioned to favor 2113 Mc, since the slot length favors 2295 Mc.)

2) Diffraction from both ends of the antenna as well as from the conical housing creates some cross polarization. When the antenna is mounted on the spacecraft the smooth transition reduces the end effect from the base of the antenna.

The high cross polarization is the chief reason for the right circular gain being less than the theoretical maximum. The radiation efficiency of 85 to 95 per cent accounts for the remaining loss in gain.

The reduction in gain at $\theta = 0°$ is due to the dummy length of waveguide that extends beyond the short circuit. This length was determined experimentally to be optimum. Theoretically, the waveguide should be infinitely long, but it must be truncated in a reasonable length. Truncation near the short circuit produced higher gain at $\theta = 0°$, but also produced 6 db nulls at $|\theta| = 36°$.

θ plane patterns at other values of ϕ are essentially the same as those presented here, indicating that the expected excellent circular symmetry was achieved.

Figures V-36 and V-37 are omni plane patterns ($\theta = 90°$) at 2113 and 2295 Mc. Theoretically, the minimum obtainable ripple is less than 0.1 db. Practically, the ellipticity of the internal mode and slot asymmetries (tolerances) limit the minimum ripple to about 1 db. Measurement errors, due to range reflections and antenna mounting structure contribute the remainder of the 2 db ripple. These errors are estimated as ±1 db in the isotropic to -4 db absolute range.

The estimate of measurement error was made by comparing several θ plane patterns recorded on various length ranges and also by comparing a pattern with the mirror image of one recorded with the antenna inverted 180°.

The measurement of isotropic level gain is also difficult and is estimated to contain ±0.5 db error. Two horns with different gains were used and the results were compared to the isotropic level obtained through pattern integration, as adjusted by radiation efficiency. Agreement within ±0.5 db was obtained.

A complete set of patterns for both frequencies, both polarizations and several θ plane cuts is presented in Appendix I.

Also included in Appendix I is the results of a pattern study for this antenna mounted on a mockup of a Ranger spacecraft.

e. Conclusions

The hardware development program successfully demonstrates the validity of the theory of this antenna type. Extremely good agreement was obtained between theoretical and measured antenna patterns. By use of diffraction from the antenna mounting structure even greater than theoretical coverage can be obtained. The right circularly polarized pattern exceeds -4 db gain over approximately 98 per cent of space with only one null at both operating frequencies.

Some difficulty was encountered in producing a highly efficient ring element with the necessary bandwidth without destroying the circularly polarized wall currents. This problem was overcome for this application, but a considerably more detailed study should be conducted on the performance of this type of radiator.

This type of omni antenna can be built with similar results over any 10 per cent band between 1 and 10 Gc. Slightly degraded performance can be obtained over a 20 per cent band.

C. Secondary Antenna

1. Choice of Design

The secondary, or null fill in, antenna should be chosen and designed to have its beamwidth at the -4 db from isotropic level, equal to the angular region not covered by the principle antenna. Of course, the free space null of the principal antenna is very narrow, indicating that a rather narrow beam and relatively high gain secondary antenna is desirable. However, in the case of the Ranger Spacecraft, the solar panels shadow the Case I omni antenna and cause a drop in gain for the pattern cut in the plane of the panels. The -4 db gain crossover level for the two antennas must be found for this "worst case" even though it will cause overlapping pattern coverage in planes not containing the panels. Pattern measurements of the omni antenna on the mockup Ranger in the plane of the panels ($\phi = 0°$) show that the gain has dropped to -4 db at approximately $\theta = 130°$. This means the -4 db gain level beamwidth of the secondary antenna should be approximately 100°. Assuming the fillin lobe to be parabolic on a decibel versus

angle plot, the half power beamwidth should be approximately 43°. As noted in Section IV, an axial mode helix is a good selection for a circularly polarized antenna with a half power beamwidth less than 60°. To assure adequate coverage, a design beamwidth of approximately 50° should be chosen.

2. Helix Theory

Reference 9 gives the complete theory of axial mode helices so only the results of the application of the theory will be repeated here.

An axial mode helix should have a circumference (C/λ) of approximately 1.0 ±0.1 in wavelengths.

For 50 degrees half power beamwidth and using $C/\lambda = 1.0$, the axial length should also be 1.0 wavelengths ($L/\lambda = 1.0$). This will require 4.8 turns on the helix ($n = 4.8$).

The axial ratio of the radiated polarization can be calculated, assuming a perfectly wound helix from

$$AR = \frac{2n + 1}{2n}$$

For our case this yields AR = 0.5 db. However, the asymmetrical loop at the feed end of the helix always increases this somewhat. An axial ratio of approximately 1.0 db can be obtained over a 10 per cent bandwidth.

The gain of the helix can also be calculated, neglecting side lobes from

$$G(db) \doteq 11.8 + 10 \log (C/\lambda)^2 (L/\lambda)$$

and for our design, approximately 12 db of gain can be expected.

The input impedance of the helix is given by

$$R \doteq 140\ C/\lambda \pm 20 \quad \text{(ohms)}$$

Again, our case should have a terminal resistance between 115 and 170 ohms. Since we will be feeding the helix with 50 Ω coaxial transmission line, an impedance transformer will be necessary to obtain low VSWR. A quarter wave section of near 80 ohm transmission line will suffice.

3. Prototype Development and Results

Figure V-38 is a photo of the helix that was fabricated and tested to substantiate the preceding theory, and Figure V-39 gives the mechanical details of the design.

Good agreement was obtained between measurements and theory. The following list compares the results:

	Frequency		
	2113	2295	Theory
VSWR	1.17	1.18	1.3 max.
Gain	12.2 db	12.4 db	12 db
Axial Ratio	1 db	1 db	1 db
θ(1/2)	48°	48°	50°
θ(-4 db)	122°	128°	100°

The only discrepancy in the results occurred at the -4 db gain level where shoulders (minor lobes) broadened the beamwidth. This is unpredictable and unavoidable.

Figures V-40 and V-41 are the meaured helix patterns, in free space, at the two operating frequencies. It can be seen that the beam broadening occurred on one side only and must be discounted in the design of the antenna. Helix patterns on the base of the Ranger mockup are essentially the same as in free space.

4. Conclusions

The helix has been found to be a satisfactory fillin antenna. Figure V-42 shows the design of a similar helix wound on a dielectric cylinder for mechanical strength. A dielectric suitable for space environments would have to be selected. This would necessitate using a slightly smaller helix, due to the dielectric constant, and would raise the Q of the antenna, but similar results could easily be obtained over the desired band.

FIGURE V-38. SECONDARY ANTENNA - AXIAL MODE HELIX

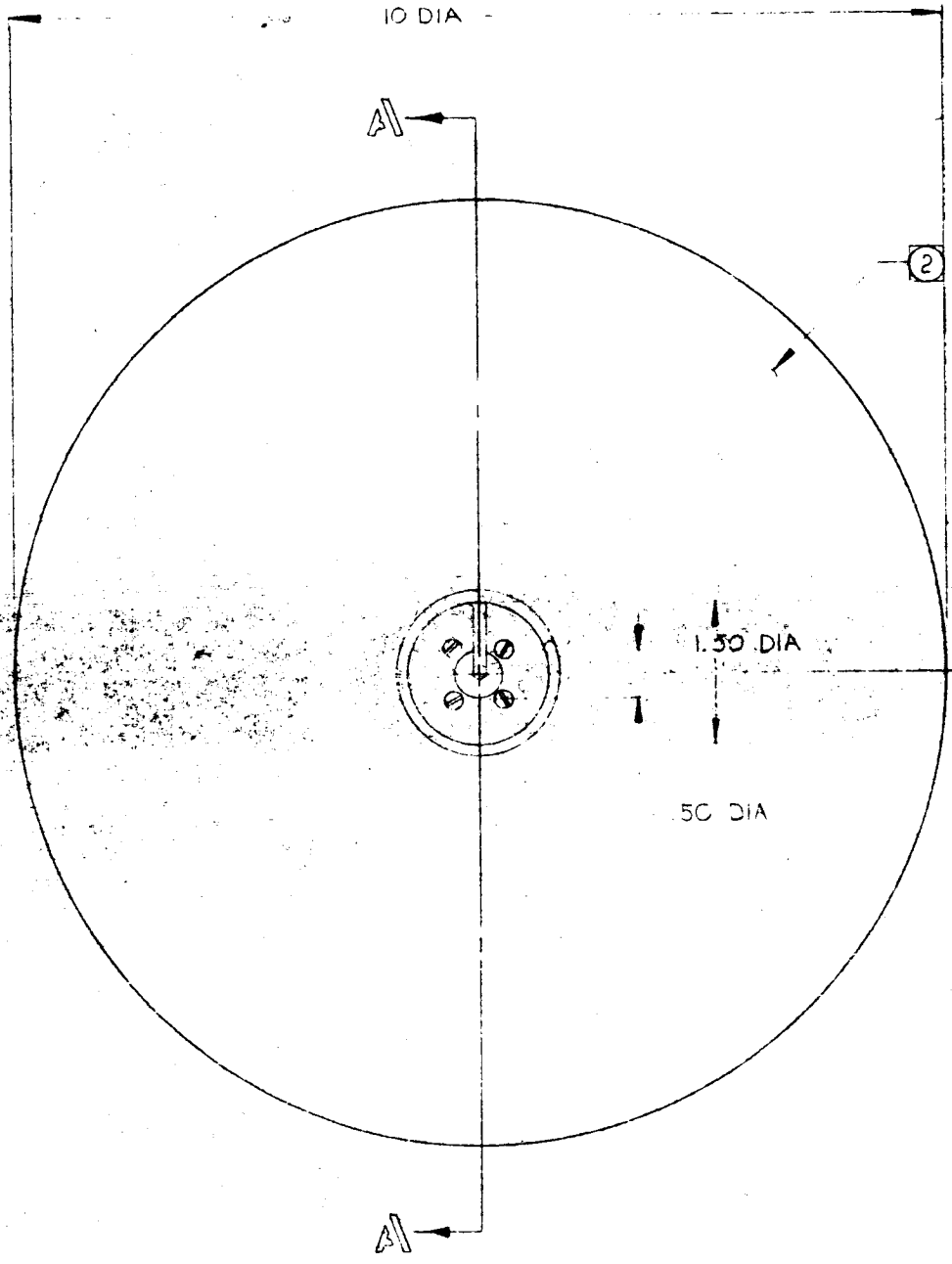

#1

NOTES

1. INTERPRET DIMENSIONS, SYMBOLS, ETC., IN ACCORDANCE WITH LISTED DOCUMENTS, AS FOLLOWS:
   - DIMENSIONS AND TOLERANCES MIL-STD-8
   - SURFACE ROUGHNESS MIL-STD-10
   - ABBREVIATIONS MIL-STD-12
2. ALUMINUM
3. TEFLON
4. COPPER
5. AMPHENOL Nº UG-58A/U (MODIFIED)

REVISIONS				
SYM	ZONE	DESCRIPTION	DATE	APPROVED

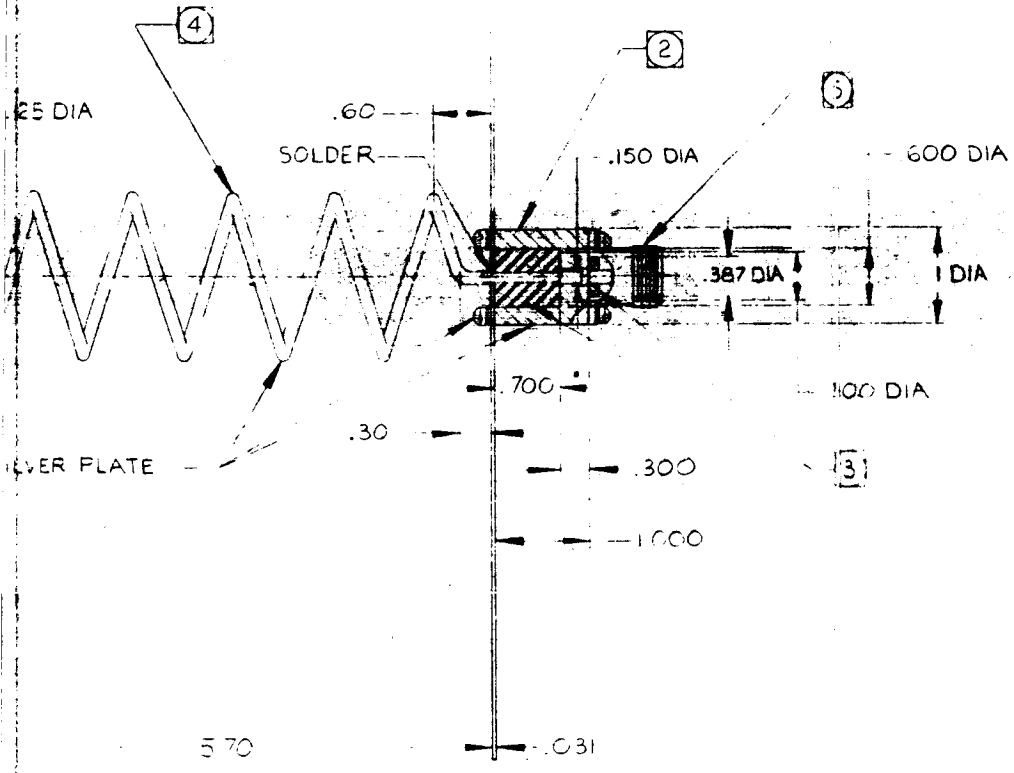

SECTION A-A

DASH NO	PROJECT	SIZE	NUMBER	EFFECTIVE SERIAL NO	NEXT ASSY	ASSY PER UNIT
	NEXT ASSEMBLY					
APPLICATION					ON HAND	

DIMENSIONS ARE IN INCHES
UNLESS OTHERWISE SPECIFIED
TOLERANCES ON FRACTIONS ± 1/32 ANGLES ± —
DECIMALS 2 PLACE ±.020 3 PLACE ±.005
CONCENTRICITY —
SURFACE ROUGHNESS 125
HEAT TREAT
MATERIAL 2 3 4 5

CODE IDENT	PROJECT NO	DWG SIZE	PART OR IDENT NO	SPEC	ITEM

LIST OF MATERIAL

DALMO VICTOR COMPANY
BELMONT, CALIFORNIA A DIVISION

TITLE
SPL SECONDARY ANTENNA
4 6 TURN HELIX

CODE IDENT NO	SIZE	FIGURE NO
15786	D	FIGURE 1-33

SCALE FULL	WEIGHT	SHEET

#2

65-430

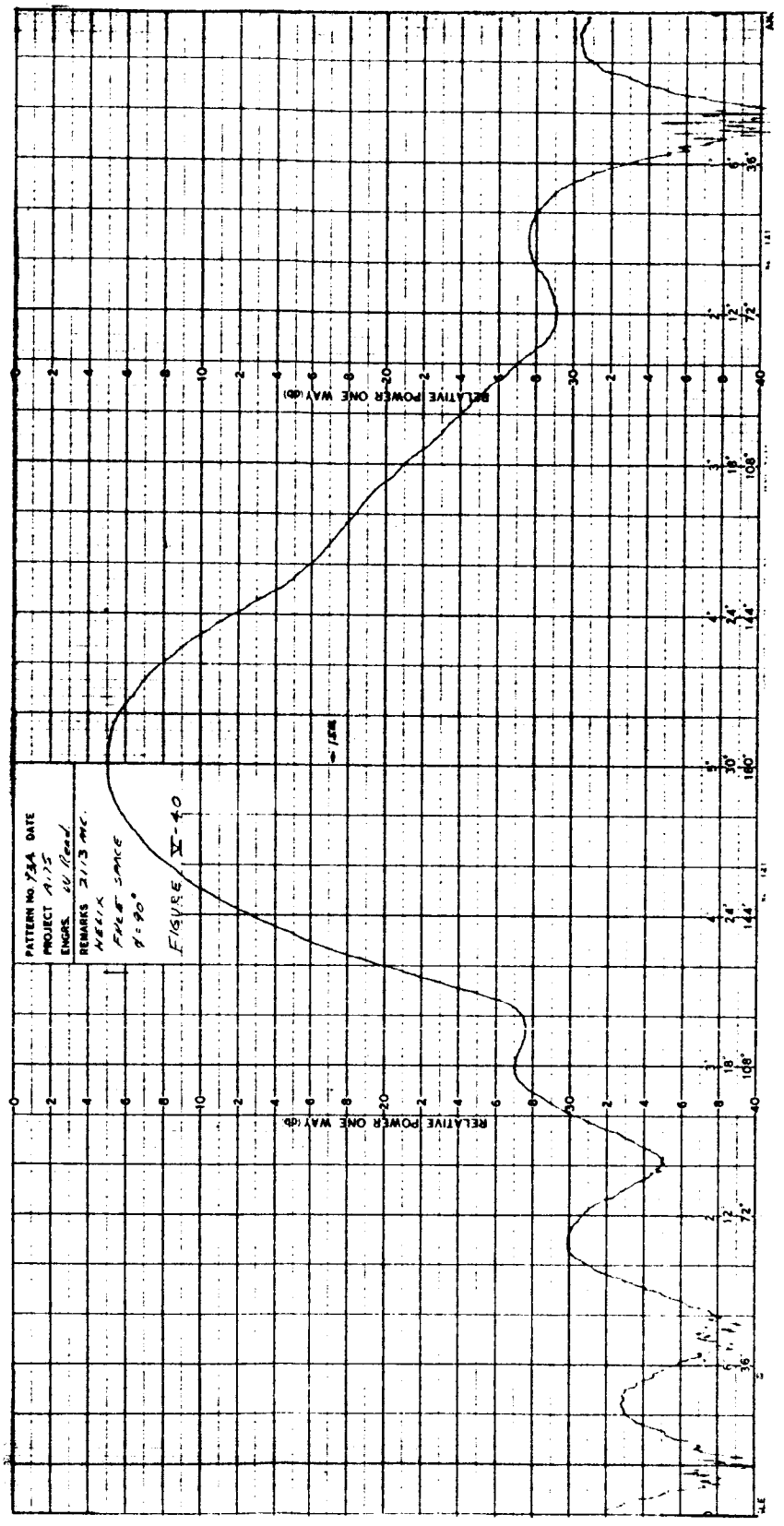

FIGURE V-40

65 +30

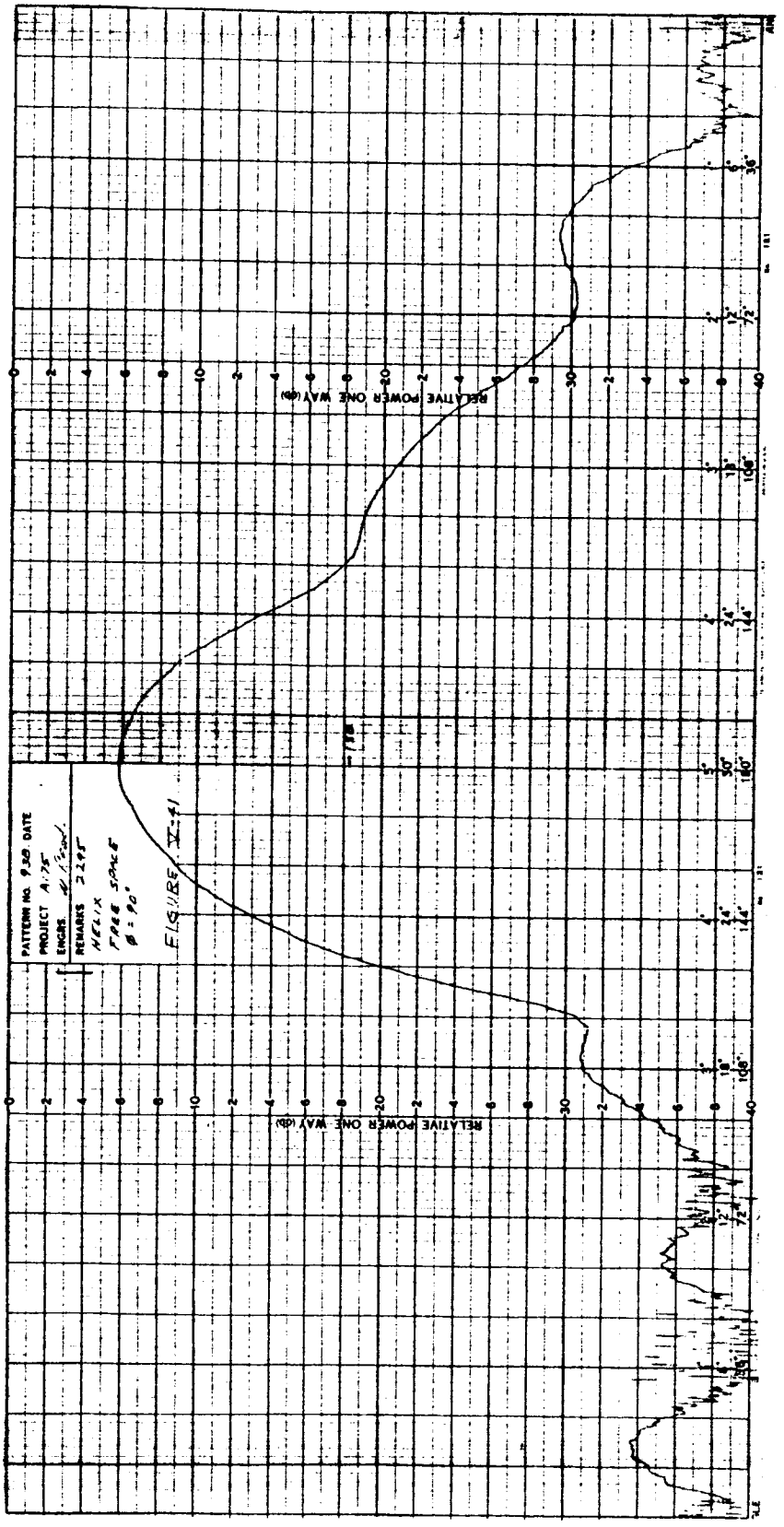

FIGURE V-41

65-43

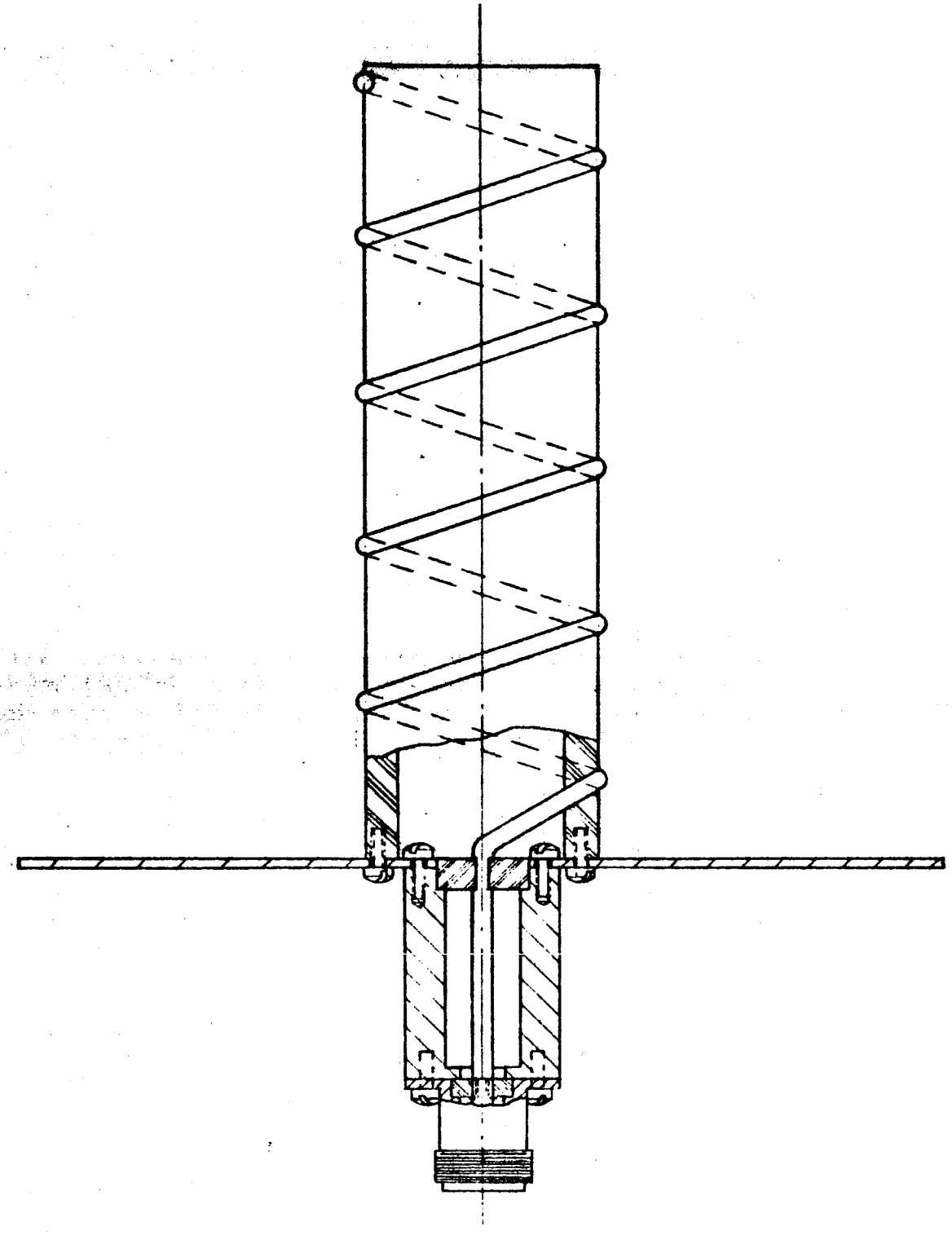

FIGURE V-42

HELIX WOUND ON DIELECTRIC CYLINDER

65-430

VI. ANTENNAS - CASE II

A. Discussion

The pattern requirements of Case II (planetary missions) dictate a primary antenna with less coverage and greater on-axis gain. the coverage could be needed on either end of the spacecraft. Of course, the larger null region for fill-in requires greater beamwidth from the secondary antenna. The logic and switching requirements will be identical to Case I with a possible exception of the best sequence of action in case of lost contact, tumbling or equipment failure.

B. Principal Antenna

The desired pattern shape can be approximated using a modification of the omni antenna of Case I. The theoretical coverage of the ring element on an infinite waveguide can be modified to yield many different pattern shapes as was done to smooth out and extend the coverage in Case I. The end effect from the truncated waveguide can be used to shape the pattern in the axial region. The conical skirt of Case I can be designed to reflect the energy from the lower portion of the pattern to the upper half. Control of the location, flare angle and length of the skirt can result in various degrees of pattern coverage. This effect was noted when the shape of the skirt was being developed to increase the Case I coverage, but no attempt was made to find the optimum design for Case II coverage. A variation of the skirt would be a set of radial monopoles. The truncated end can be constructed in many configurations, also. Hemispherical and conical flares are two methods that have been tried to smooth the pattern of Case I.

This method of employing diffraction can be considered as similar to a three element array with limited control of the "end elements." It must be recognized, however, that the "elements" do not have isotropic or even identical patterns.

The gain that can be realized at various pattern angles cannot be calculated, but this technique of developing the optimum pattern shape will result in the maximum gain that can be achieved for that pattern shape.

The reduced coverage on the lower portion of the pattern (spacecraft side) sould reduce the solar panel reflections also. When the primary antenna is located on the spacecraft apex, deflection screens on the panels should not be necessary. Of course, when the principal antenna is located on the opposite end of the spacecraft it must be mounted sufficiently far from the base and panels to allow coverage at angles greater than 90° from the antenna's axis.

C. Secondary Antenna

The secondary (fill-in) antenna for Case II must have greater coverage than for Case I. A shorter helix (fewer turns) would yield a slightly broader pattern (up to 60° half power beamwidth)[9] and could meet the -6 db gain specification. However, the other types have inherently broader patterns and should cover the entire null region with better than -6 db gain.

One of the more simple and lightweight types is an Archimedian spiral (planar spiral)[11]. This design has a half power beamwidth of 80°. The disadvantage is that it requires a balun feed and should be mounted a quarter wave above a ground plane.

Another design with similar coverage, but lacking the disadvantages of the planar spiral is the conical spiral[10]. A very short, truncated cone could be used for the small bandwidth desired.

D. Conclusions

The principal antenna coverage of Case II can be obtained by modifying the configuration on both ends of the omni antenna of Case I. The exact requirements of a particular mission should be considered when defining the desired coverage and the pattern should be developed on the exact spacecraft to be used. The changes necessary to meet the general shape called out in Section II-B must be developed experimentally.

The fill-in antenna for Case II could be a helix (as in Case I) or a form of planar or conical spiral. The best choice and manner in which the beamwidth is optimized must be determined after the extent of the null region of the principal antenna is measured on the spacecraft.

VII. SWITCHING LOGIC

A. Logic Description and Constraints

The logic selects one antenna and one receiver for use on-line. In Mode II the other antenna is connected to the other receiver; in Mode I no second receiver is available, so alternate antenna is not used. The logic will make no change in the antenna/receiver combination for use for momentary loss of signal. The logic considers any loss of contact for less than two minutes as momentary. For Mode II service, the logic will make no change unless the alternate receiver input is known to be better and remains so for one full minute, and on-line receiver is known to be inadequate. This limits the switching frequency in the case where vehicle orientation results in nearly equal response from the two antennas. In addition, the logic is biased to require about 1 to 5 db preference depending on signal level.

If contact is lost, the logic system selects the alternate antenna/receiver combinations. If no signal is found, the system switches back to the original configuration. The initial search is conducted using a relatively high threshold in an effort to obtain a high quality link. If unsuccessful, the search is repeated using a minimum threshold so as to restore contact if at all possible.

If, during a prolonged period of time, no signal is received, the logic system selects the prime antenna for the transmitter and on-line receiver. Since the logic tends to select the best receiver for use on-line, the on-line receiver remains in service throughout the course of logic-controlled switching unless the on-line receiver fails.

After the prime antenna has been selected, the logic causes the second antenna to be sampled periodically for the presence of an (acceptable) signal.

For tumbling rates of three degrees a second or higher, the timing constraints prevent antenna switching. The communications system will remain connected to the antenna in use prior to start of tumbling. If this were the secondary antenna, transfer to the principal antenna will be accomplished only if the standby receiver AGC is able to override the comparator bias for at least one full minute, and the AGC of the on-line receiver is not adequate. Transfer to the alternate antenna can be assured under tumbling conditions only by removing ground station RF output for about two and one-half minutes.

B. Circuitry Design

1. System Layout

a. General

The recommended logic circuitry differs somewhat from the actual breadboard. The nature of these differences is such that the current breadboard is sufficient to prove feasibility of the recommended circuit. The changes are as follows:

1) Counter should have seven instead of only five binary stages. This allows for an improved switching pattern. The lost-contact mode is thus set at 34 minutes instead of at 6 minutes. The lost-contact cycle is 66 instead of 30 minutes long. In addition the increased counter capacity allows testing the standby antenna at the high and then both antennas at the low threshold, so that the best antenna can be selected as long as contact is maintained at all.

2) The gate group module is simplified by removal of one gate.

The following description applies to the recommended logic circuitry:

b. Mode III Logic

The proposed Mode III logic would be separated from the Mode II and Mode I logic. Figure VII-1A is a block diagram of a Mode III system. The comparator would be utilized as well as the relay control modules. The hardware needed over and above that required for a complete Mode II system is:

1) An additional diplexer
2) Two coaxial relays, K2 and K5
3) Two relay control modules
4) Hi-Gain Steerable Antenna
5) Additional logic gates

Mode III Logic Criteria:

Mode III-A is the acquisition mode wherein the on-line receiver is attached to the high gain steerable antenna

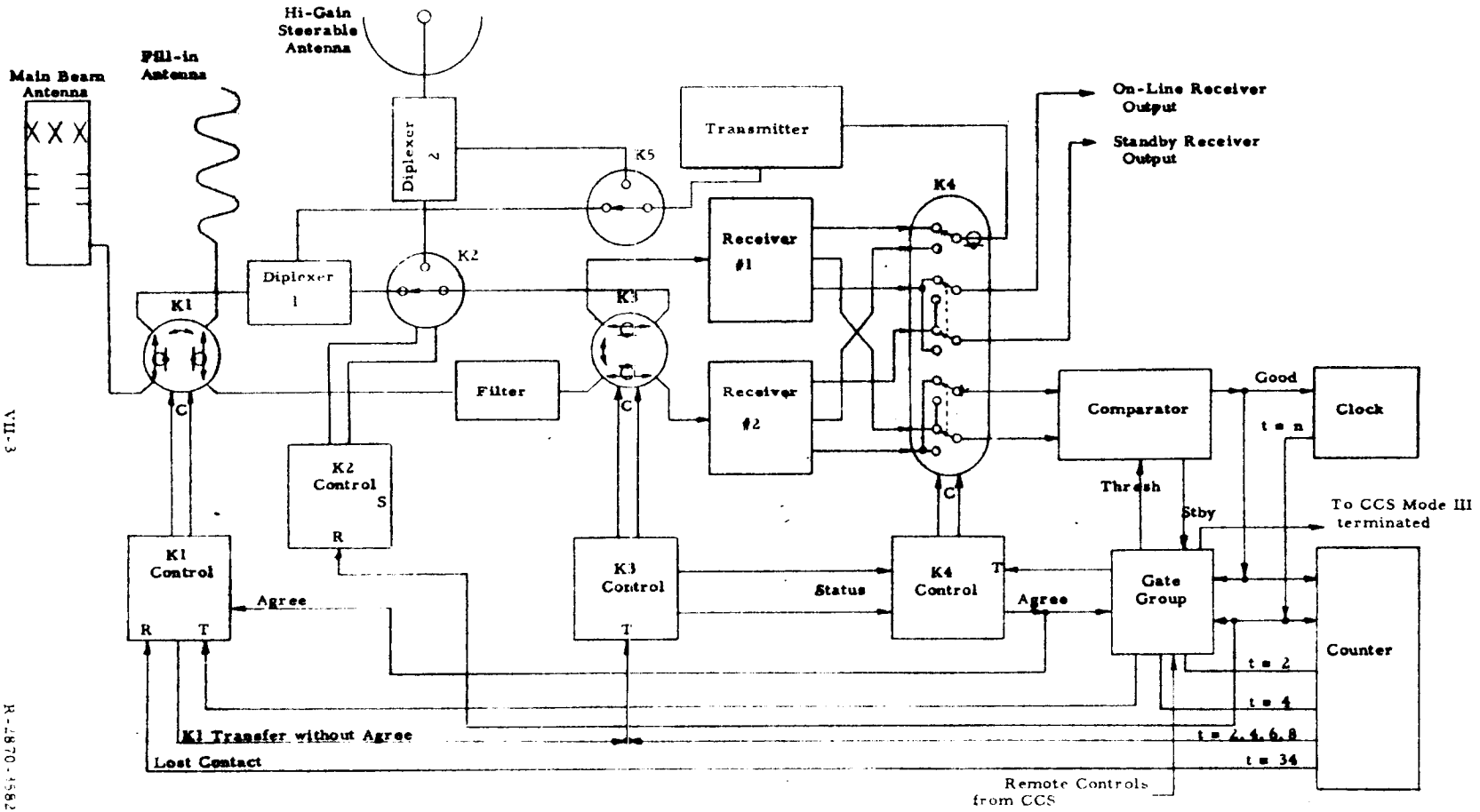

FIGURE VII-1A

BLOCK DIAGRAM OF ANTENNA SWITCHING LOGIC SYSTEM MODE III

by K2 transfers. The transmitter remains attached to the previously selected antenna via diplexer 1. To initiate a Mode III-A acquisition mode, the Control Command Sequencer transmits a ready command to the Mode III logic.

Mode III-B is the non-acquisitive portion of Mode III. Once satisfactory reception has been established with the high gain steerable antenna, the CCS will command the Mode III logic to shift to the Mode III-B operation by transferring K5. The transmitter is switched to the high gain steerable antenna through diplexer 2 and the following situations will be met by the Mode III logic.

1) Case I: The standby receiver is attached to the omni antenna and has no contact. The on-line receiver has just lost contact. The Mode III logic shifts the standby receiver to the on-line position by transferring K3 and K4. If contact is established we conclude that the on-line receiver has failed and no further switching is required. If contact is not established then we conclude that the high gain steerable antenna has lost lock due either to wrong orientation of high gain antenna or earth station shutdown. The logic then drops into the Mode II lost-contact mode, and a signal is transmitted to the CCS indicating Mode III service has been terminated.

2) Case II: The standby receiver is attached to the omni antenna and has contact. The on-line receiver has just lost contact. The Mode III logic shifts the standby receiver to the on-line position, again by transferring K3 and K4. If contact is established we conclude that the on-line receiver had failed and no further switching is required. If contact is not established we conclude that the high gain steerable antenna has lost lock and the logic reverts to Mode II operation and a signal is transmitted to the CCS indicating Mode III service is terminated. In order to re-establish Mode III service the CCS will have to transmit a command triggering the acquisition mode.

c. Mode II Logic

Figure VII-1 is a block diagram for a Mode I and Mode II system. In Mode II the logic circuit switches antennas (K1) to the transmitter and to both receivers whenever the standby receiver input is some 5 db stronger (the magnitude of preference depending on absolute signal level) than the input to the on-line receiver and the on-line receiver is inadequate, and provided this condition has existed continuously for at least one minute. (At lower signal levels, the 5 db figure is reduced --for very low levels the figure is less than 1 db.)

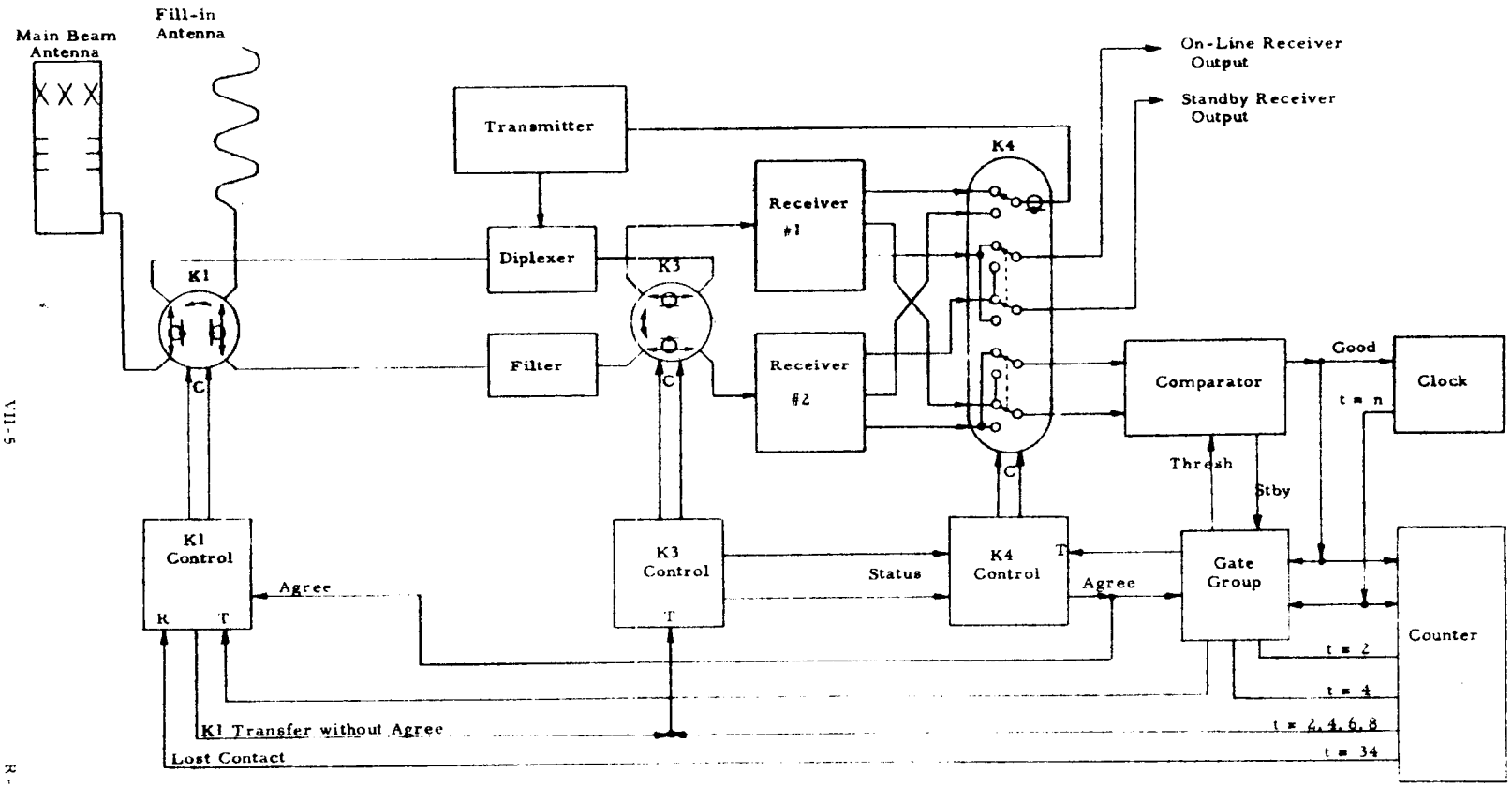

FIGURE VII-1

BLOCK DIAGRAM OF ANTENNA SWITCHING LOGIC SYSTEM MODE I AND II

If the on-line receiver fails, the logic will interchange receivers, otherwise, the same receiver remains on-line at all times.

If the standby receiver fails, the logic will revert to Mode I service,

d. Mode I Logic

A Mode I system is a truncated Mode II system. Since only one receiver is used, K4 and its control (receiver output selector) are not used, and K3 (receiver input selector) can be a SPDT relay. Simplified circuits can also be used for the comparator and gate group modules.

In Mode I, the logic retains the existing antenna selection until the (on-line) receiver reports an unacceptable signal level. If this situation lasts two minutes, the logic establishes the test mode. This means the receiver is connected to the standby antenna to determine if it is acceptable. If the standby antenna produces a strong signal (as defined by the generation of an AGC voltage above comparator threshold), the antennas are interchanges. Then the test condition is cleared to complete logic action.

At increased ranges, the normal threshold level may represent an unattainable signal level. To cover this possibility, when the above test is not satisfied within two minutes, then (at t = 4 minutes) the threshold level in comparator is dropped to a level representing marginal service only. The receiver is then returned to the original antenna (terminating first test). If the original antenna can satisfy this reduced requirement, the logic is satisfied, and returns to resting condition.

If the original antenna cannot satisfy even the reduced threshold requirement within two minutes, then (at t = 6 minutes) the test condition is restored to determine if the standby antenna can produce a usable signal level. Again, if a usable signal level is obtained while in test mode, the antennas are interchanged (to place transmitter on correct antenna) and the test condition cleared (placing receiver on same antenna as the transmitter).

If, after two more minutes have passed (at t = 8 minutes) no signal has been detected, the test mode is cleared and a waiting period is started, the assumption being a ground

station failure. This period lasts 26 minutes. Then, (t = 34 minutes) if no signal has been detected, the lost contact (LC) mode is set.

In the LC mode, transmitter and receiver are both connected to the main beam antenna. This configuration is held for 32 minutes, then the counter is reset, and test cycle is repeated to check fill-in antenna response. In effect, once established, the LC mode consists of a 66 minute cycle --62 minutes on the main beam antenna, plus 4 minutes on the fill-in antenna --repeated as often as necessary, until contact is again restored.

The comparator threshold level will normally be set low after LC mode, since only two minutes of the cycle involve use of the higher threshold level. If range allows the higher threshold level to be satisfied, then at next test cycle this level will be restored. If desired, this cycle can be initiated at once by interrupting the ground-station signal for about 2-1/2 minutes (assuming that the wrong antenna is in service).

2. Module Design

a. Comparator

The comparator is used to compare the AGC outputs of the two receivers with preset threshold levels. One comparison determines if the on-line receiver AGC is adequate. The other comparison determines if the on-line receiver AGC is adequate and greater than the standby receiver AGC. The comparator has a built-in preference for the on-line receiver of 1 db for very weak signals and 5 db for adequate signals. Figure VII-2 is a schematic of the comparator circuit.

As long as the on-line receiver is adequate (adjustable by R20) the comparator output indicates "good" and no logic action will occur. If the on-line receiver AGC is not adequate and is less than the standby receiver AGC, the comparator output indicates a "not good" and logic optimization is initiated.

b. Circuit Action

The comparator has three inputs: a DC reference (GND = LOW THRESHOLD CONTROL), the on-line AGC voltage (ON LINE AGC = IN) and the standby AGC voltage (STBY AGC = IN). There are two outputs: a signal indicating a

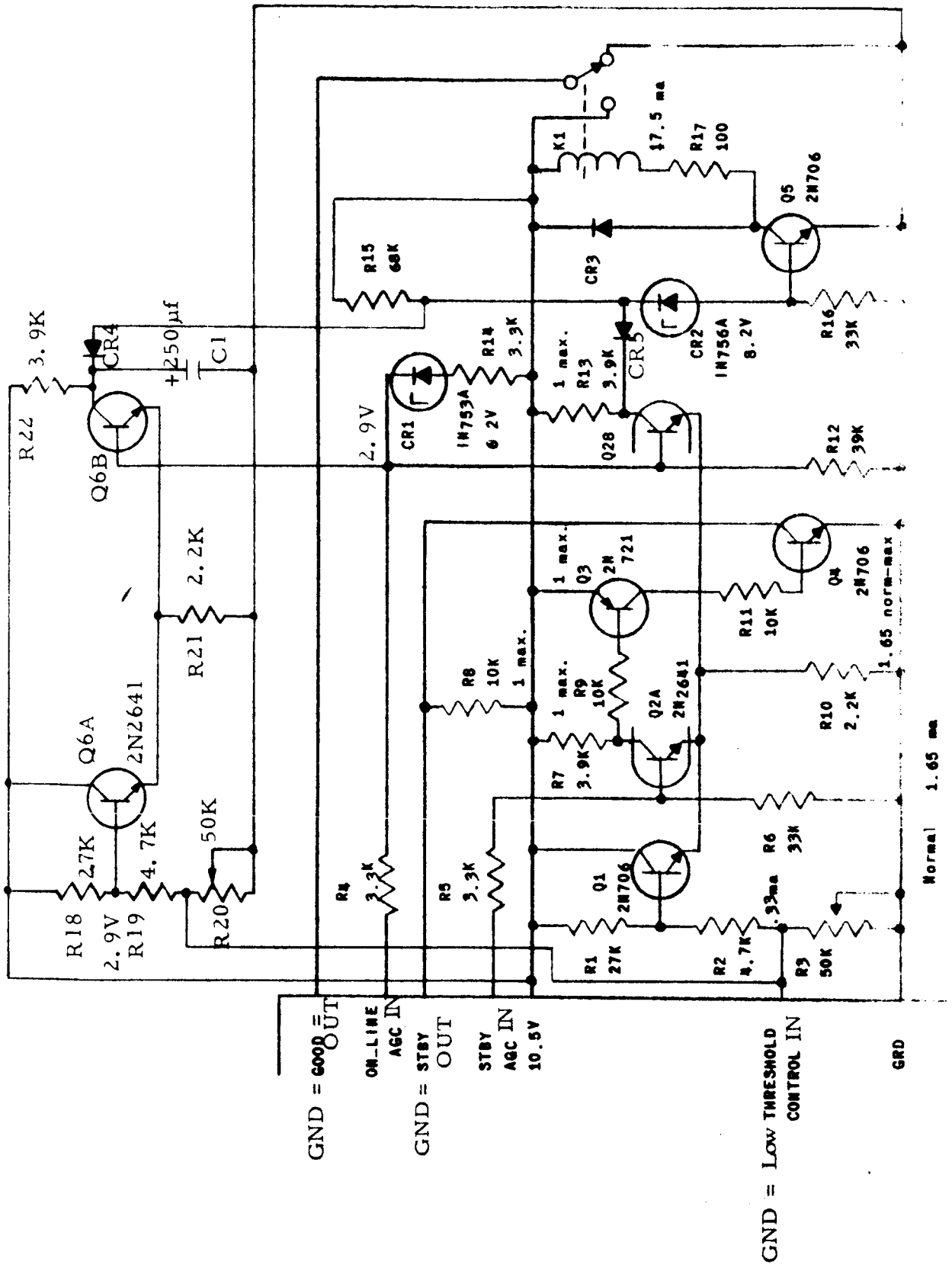

FIGURE VII-2. SCHEMATIC - COMPARATOR

good condition (GND = GOOD = OUT) and a signal indicating standby is above threshold and better than the on-line receiver (GND = STBY = OUT).

Transistors Q1, Q2A and Q2B form an analog OR circuit. Only the transistor with highest base voltage will have any collector current. The other two transistors will be cut off. Transistor Q1 is driven by the DC threshold reference signal, Q2A is driven by the standby AGC and Q2B is driven by the on-line AGC plus the preference bias network CR1 and R14. The preference bias network makes the on-line AGC appear higher as shown in Figure VII-15, page VII-36. The collector of the standby transistor Q2A is sampled by resistor R7 and amplified by Q3 and Q4 in such a manner that when the standby AGC input is greater than the DC threshold reference and the on-line AGC with preference, the collector of Q2A moves toward ground causing Q3 base current to flow and pulling collector of Q3 and base of Q4 toward +10.5 volts, which turns Q4 on hard, producing a ground standby output. At the same time, Q2B was turned off (only one of Q1, Q2A or Q2B may be on at one time) by Q2A emitter. The collector of Q2B rises to +10.5 volts and "arms" one leg of an AND gate consisting of CR4, CR5 and Q5.

Transistors Q6A and Q6B form a comparator whose purpose is to detect when the on-line receiver is adequate irrespective of the standby receiver. The output of this comparator is connected to the other leg of the AND gate consisting of CR4, CR5, and Q5. When both Q6B and Q2B are off (on-line AGC below adequate threshold and below standby AGC) then both CR4 and CR5 are connected to +10.5 volts through R22 and R13 respectively. This action permits Q5 to be turned on by current flowing through R15. When transistor Q5 is turned on, K1 closes, placing +10.5 volts on the "good" output (GND = GOOD = OUT) indicating a not good condition.

If the standby receiver AGC level is now greatest, the comparator releases the Mode II gates in the gate group module. There are two of these gates, however, one of them remains blocked by the agree/disagree circuits so that only one path is available for the clock pulse at t = 1 minute.

If the threshold voltage is greatest, both Mode II gates remain blocked, and only the Mode I logic paths can be used. (These paths are designated "Mode I" because in a dual receiver system with only one of the two receivers in operating condition, the resulting logic paths are coincident with those of Mode I. For the present discussion, it must be remembered that we are discussing a "Mode II" or dual receiver system, and are utilizing the Mode I logic paths, not Mode I logic.)

The threshold level is automatically set to its upper level (adjustable before launch to any desired value) at t = 2 so that Mode II service starts by seeking a strong signal. At t = 4 (assuming counter reaches this level before logic is satisfied and counter reset) the threshold level is reduced to a level representing marginal service. This change may permit Mode II action at t = 5 minutes, otherwise, Mode I logic paths will be utilized by testing both antennas against this low level. Once lowered, the threshold remains low until logic action is terminated, and then restarted by a new outage. If this outage is cleared by switching antennas at high threshold, the high threshold will remain in effect until circuit can no longer find an antenna to satisfy this requirement.

c. Clock

Figure VII-3 is a schematic of the clock circuit. The clock generates one pulse each minute. The circuit is composed of a multivibrator, a buffer amplifier, three step-counters and an output amplifier.

The multivibrator operates at one pulse per second. Its output is squared by the buffer amplifier to produce a constant amplitude output. The buffer amplifier drives the three step-counters in parallel.

The step-counters count by 3, 4 and 5, respectively. As a result, one input pulse in 60 (3 x 4 x 5) will produce a three-way coincident output pulse. By this means, extremely slow speed counters are avoided. Step counters are almost as period insensitive as binary flip-flops. Moreover, their higher counting ratios reduce the required number of stages --and the current drain --considerably.

The output amplifier is activated by the triple-coincident pulses only. It is made AC regenerative to give a very sharp falling edge to the output pulse. This is necessary to trigger the counter. The output pulse width is set by the step counters and is just under 20 milliseconds.

d. Counter

Figure VII-4 is a schematic of the recommended counter circuit. The breadboarded circuit consisted of only five stages, however, the added stages are certain to work (they are, like four of the present five, driven by an identical stage and at a slower rate so that no doubt as to performance exists).

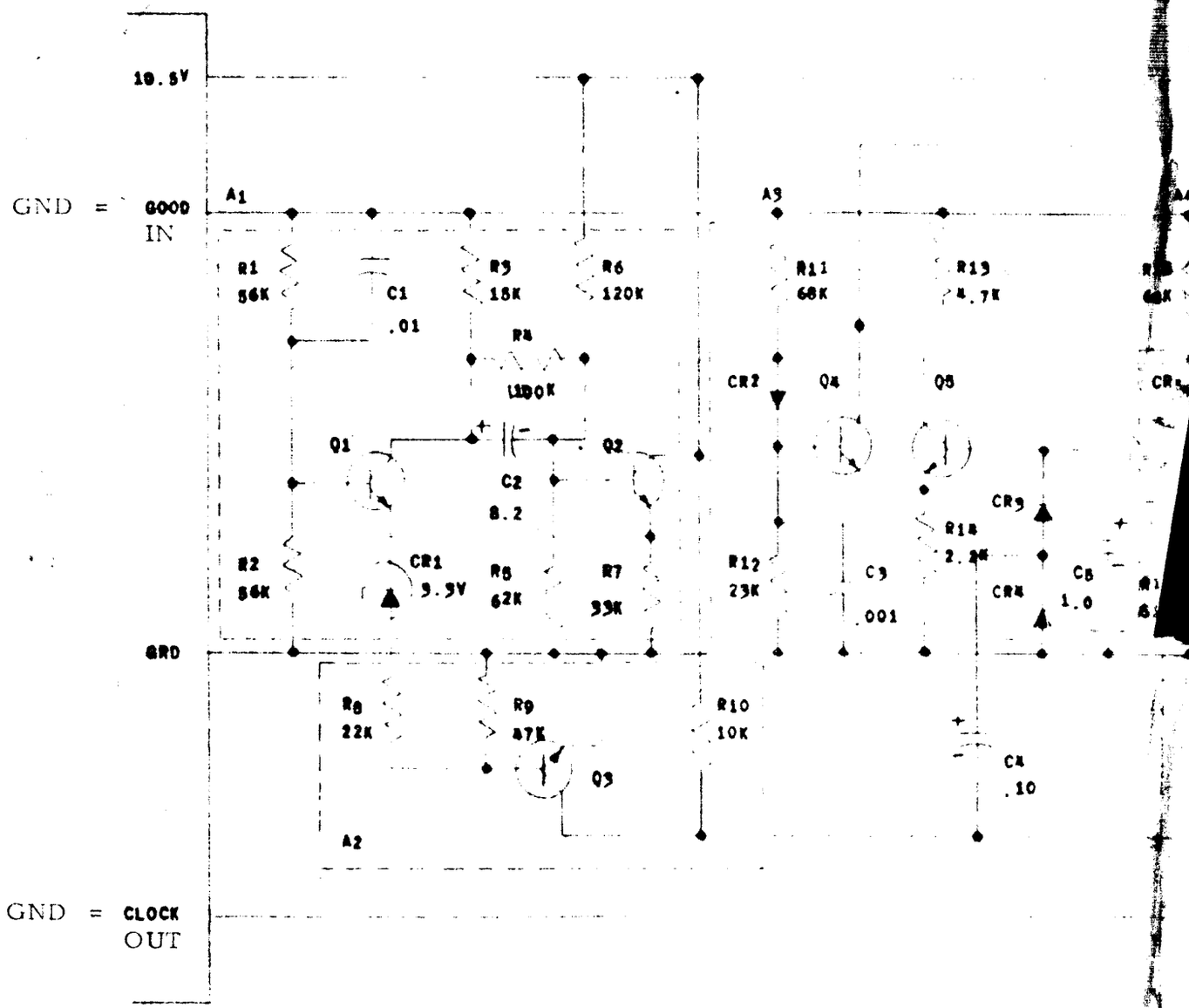

FIGURE VII-3

SCHEMATIC - CLOCK

#1

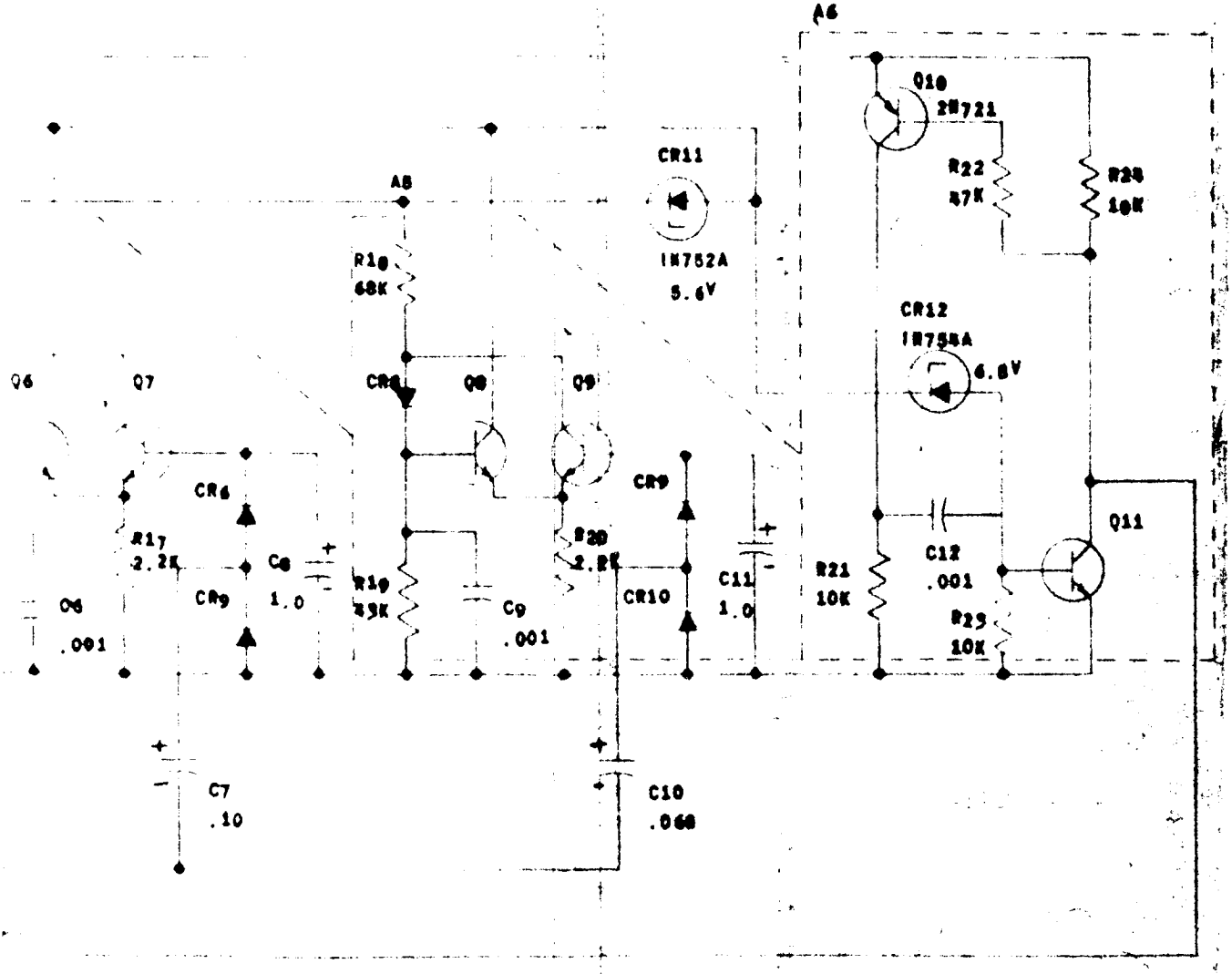
A6
Q10
2N721
R22
47K
R24
10K
CR11
1N752A
5.6V
A8
R18
68K
CR12
1N758A
6.8V
Q6
Q7
CR8
Q8
Q9
CR6
CR9
Q11
R17
2.2K
C8
1.0
R20
2.2K
C12
.001
R21
10K
CR9
R19
33K
C9
.001
CR10
C11
1.0
Q6
.001
R23
10K
C7
.10
C10
.068

#2

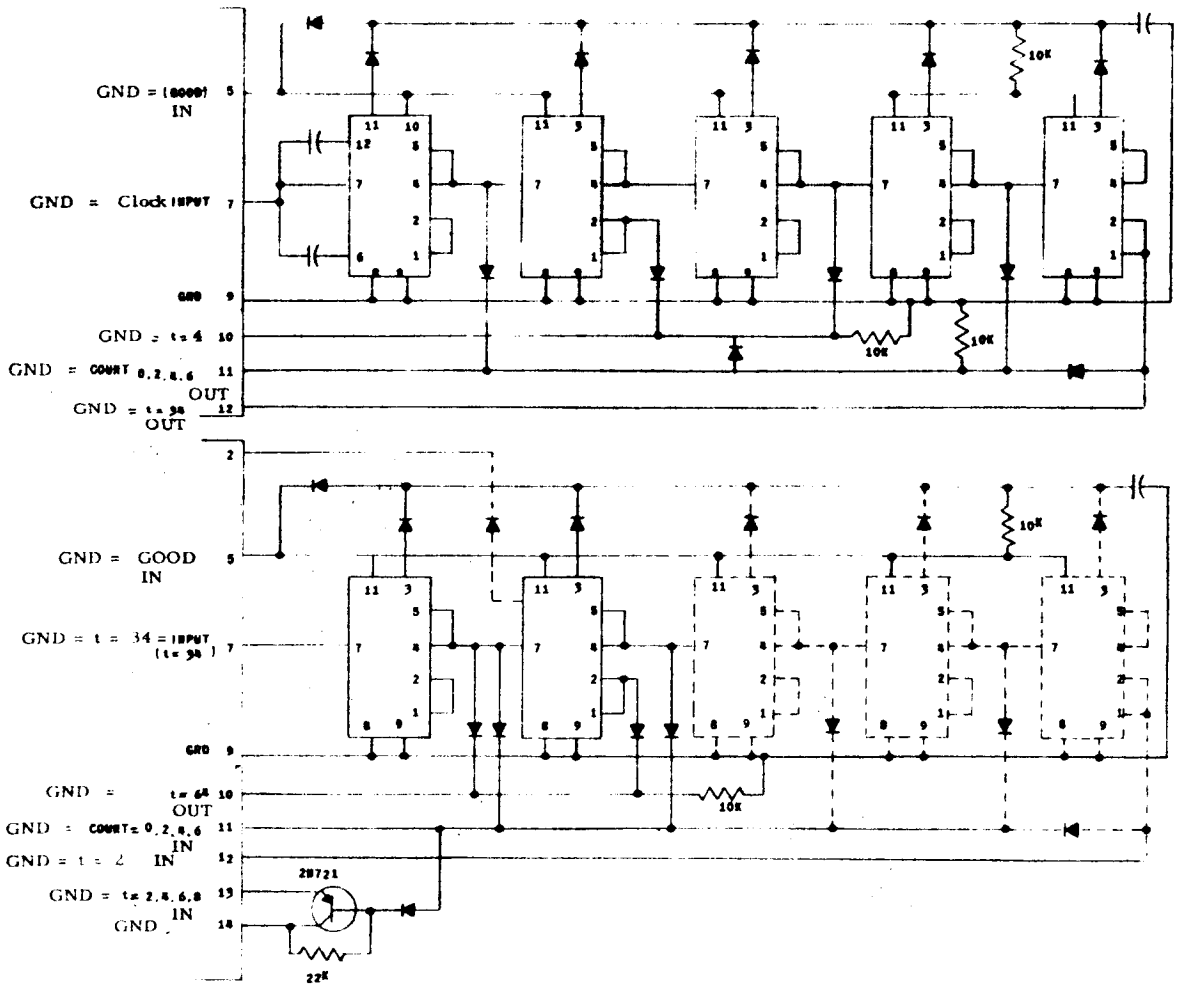

FIGURE VII-4

SCHEMATIC - COUNTER

The counter outputs (input is a 1 ppm pulse train from clock) are as follows:

1) an output at count of 0
2) an output at count of 2
3) an output at counts of 0, 2, 4 and 6
4) an output at count of 32

The first two of these outputs are used to control the comparator threshold level. The third controls the Mode I signal-seeking cycle, while the fourth output initiates the lost-contact mode.

A seven place binary chain can count to 127, however, the count is shortened in this case to 66 by feedback which resets the counter to -2 (or 126) when the count reaches 64. The counter is reset to -2 when resting since this simplifies the output circuitry.

The three stages shown dotted would be added only if timed remote operation was required; since more than five stages makes for an unreasonably large card, the counter is constructed on two identical cards. Only the components are arranged differently to distinguish between them.

e. Gate Group Module

Figure VII-5 is a schematic of the recommended gate group module. The breadboarded circuit included an additional gate, not needed with modified counter.

The gate group consists of two, triple-input AND gates used in Mode II, two double-input AND gates used in Mode I, plus an inverter and a flip-flop.

The inverter provides a negative signal, normally, to block three of the four gates in response to an affirmative input on the AGREE line. When circuit is in test mode, this input is missing, and these three gates released by inverter.

The flip-flop controls the comparator threshold. It is in turn controlled by the counter outputs at $t = 2$ and $t = 4$ minutes.

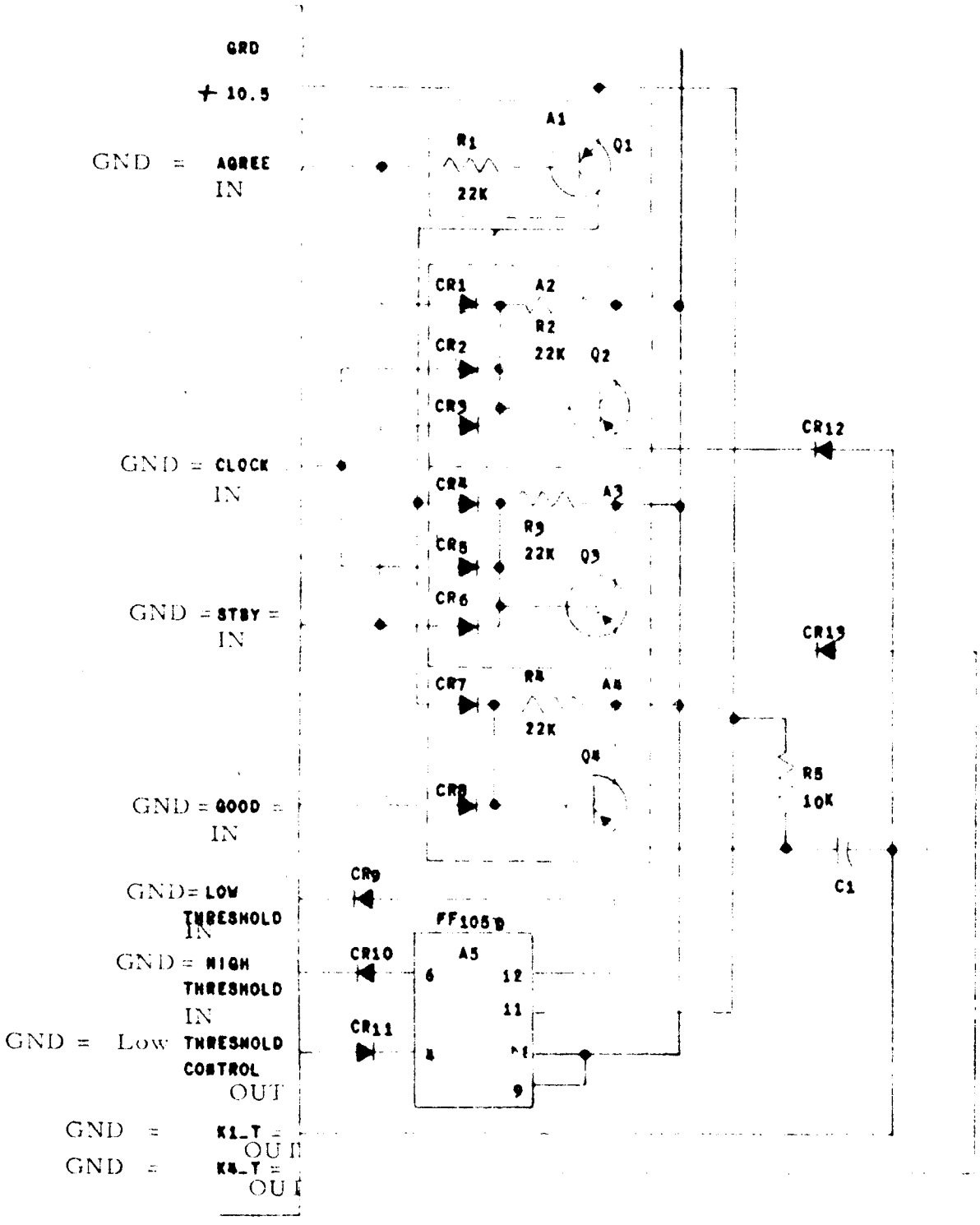

FIGURE VII-5

SCHEMATIC - GATE GROUP

f. Relay Controls

Figures VII-6A, B, C and D show a schematic of the relay control modules. The relay control modules are similar, but not identical. Three of them include a toggle input. Pulsing this input causes the controlled relay to change position without regard to initial position.

The K1 relay control also has a reset input. Grounding this point (or removing the 10.5V power, but not the 28V power) resets K1 to standard position. In addition an AND circuit on this module produces an output pulse to the K3 control module at the end of a K1 transfer if K3 and K4 disagree as to which receiver is supposed to be in service.

The K3 relay control includes no added circuitry.

The K4 relay control includes an EXCLUSIVE OR circuit that reports whether or not K3 and K4 are in agreement.

The K2 relay control is required only if Mode III service is required. The K2 relay control has no added circuitry. In fact, one diode is omitted so as to convert the toggle input to a set input.

C. Functional Operation

Figure VII-7 is a diagram showing the criteria used by the logic and the correct procedure as determined from these criteria at any given time. The following conditions are possible.

1) Normal Conditions:

Criteria I and II	Yes
Criteria III and IV	No

No action is allowed, --timer is held in reset condition.

2) Mode II Transfer:

Criteria II and III	Yes
Criteria I and IV	No

Timer is released from reset and allowed to run. First clock output pulse* (on t = n line) will pass through Gates A and E to the main antenna selector control. This control will toggle the main antenna selector relay (K1 in Figure VII-1), interchanging the two antennas. After this, normal conditions will be restored, halting the logic procedure.

* First clock output pulse occurs two minutes after timer starts to run.

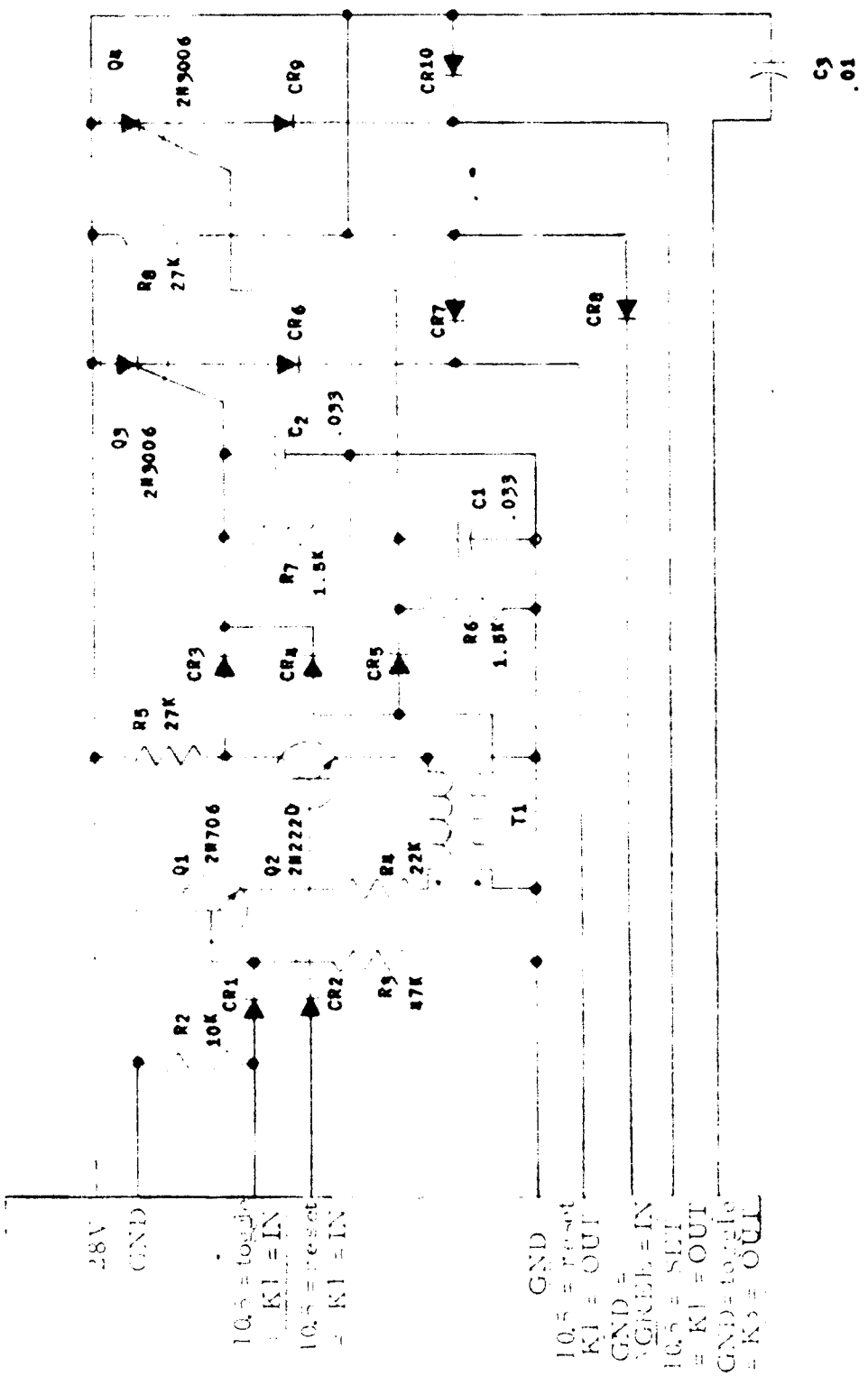

FIGURE VII-2 SCHEMATIC - K1 RELAY CONTROL MODULE

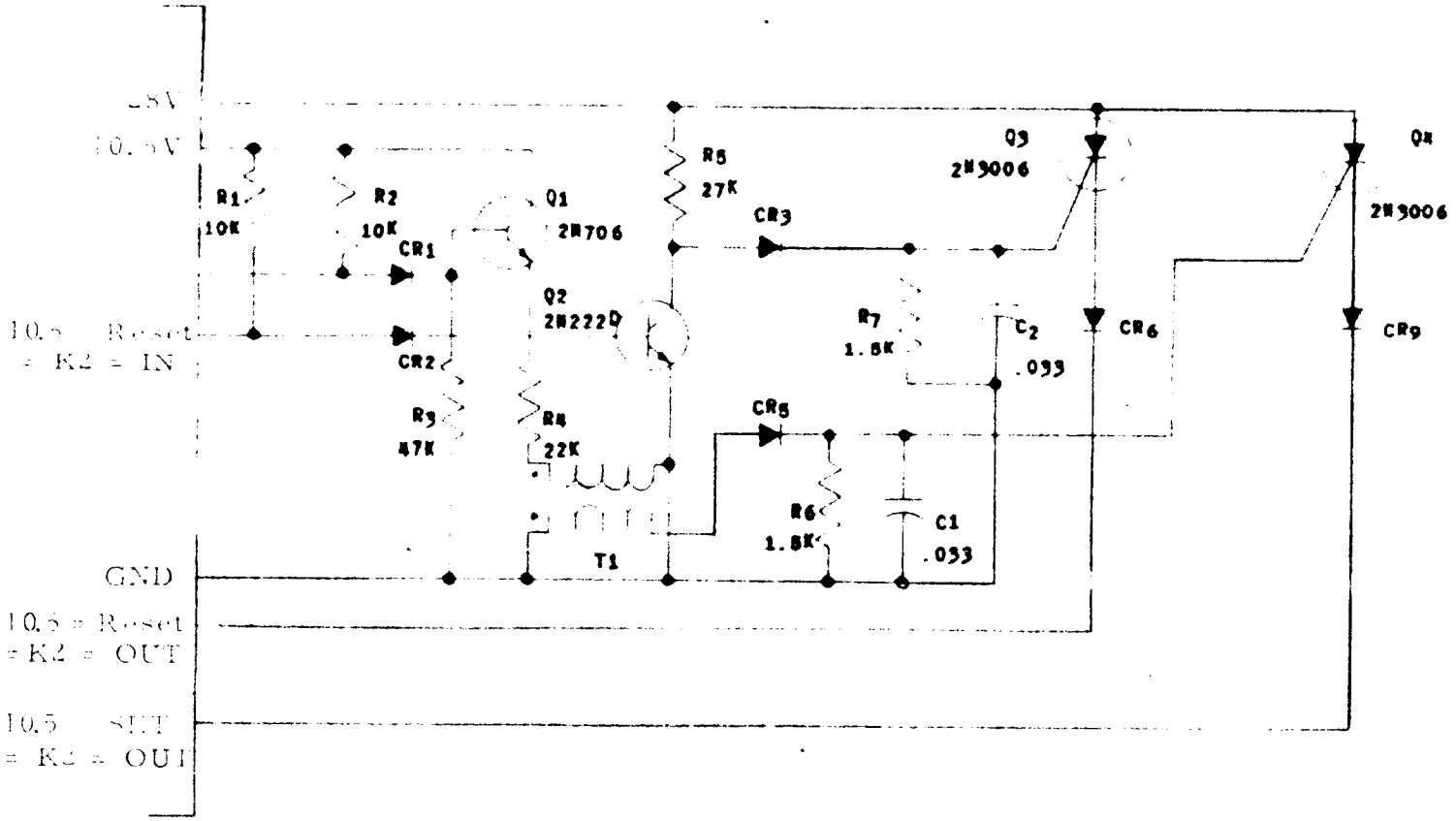

FIGURE VII-6B

SCHEMATIC - K2 RELAY CONTROL MODULE

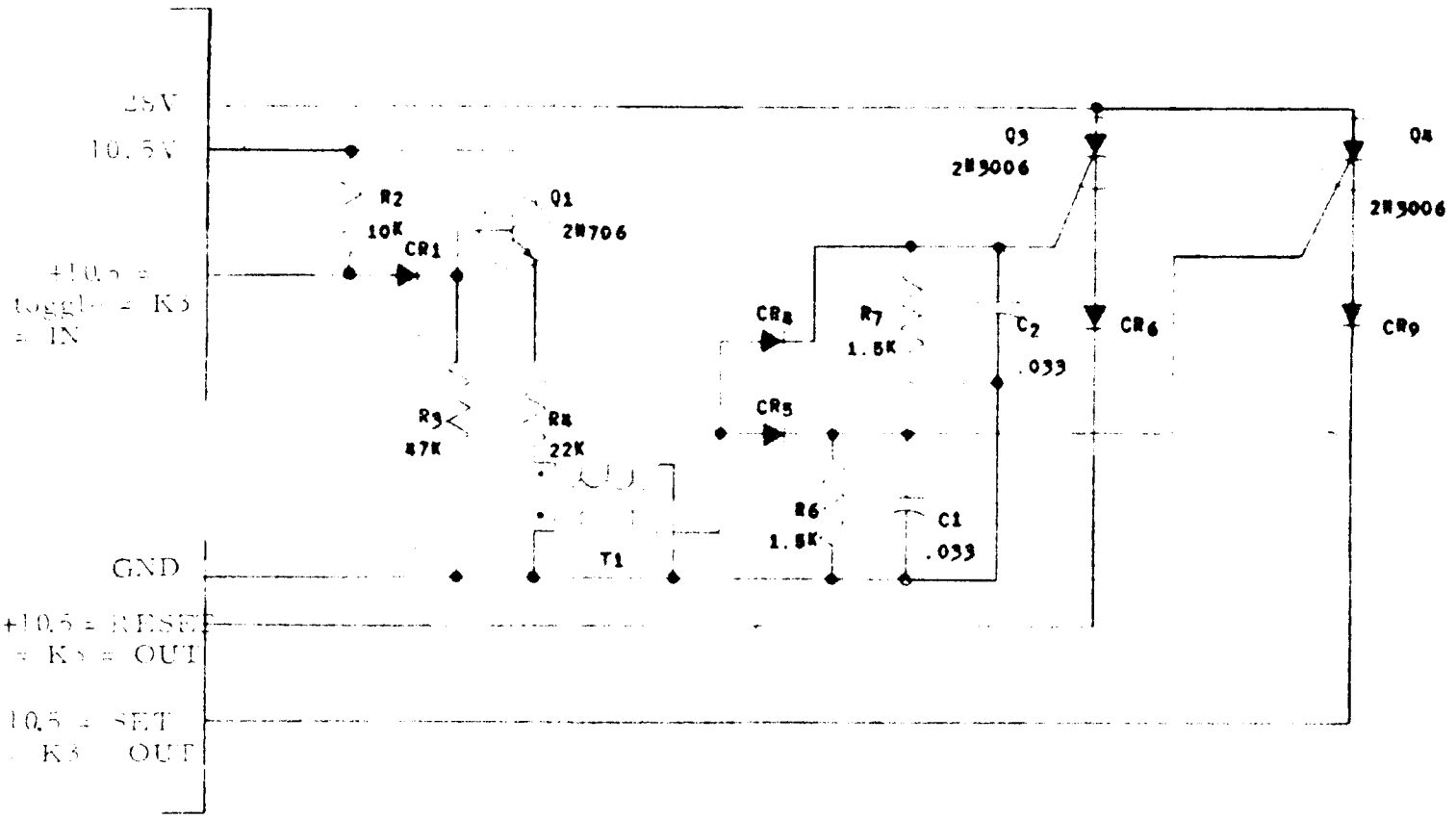

FIGURE VII-6C

SCHEMATIC - K3 RELAY CONTROL MODULE

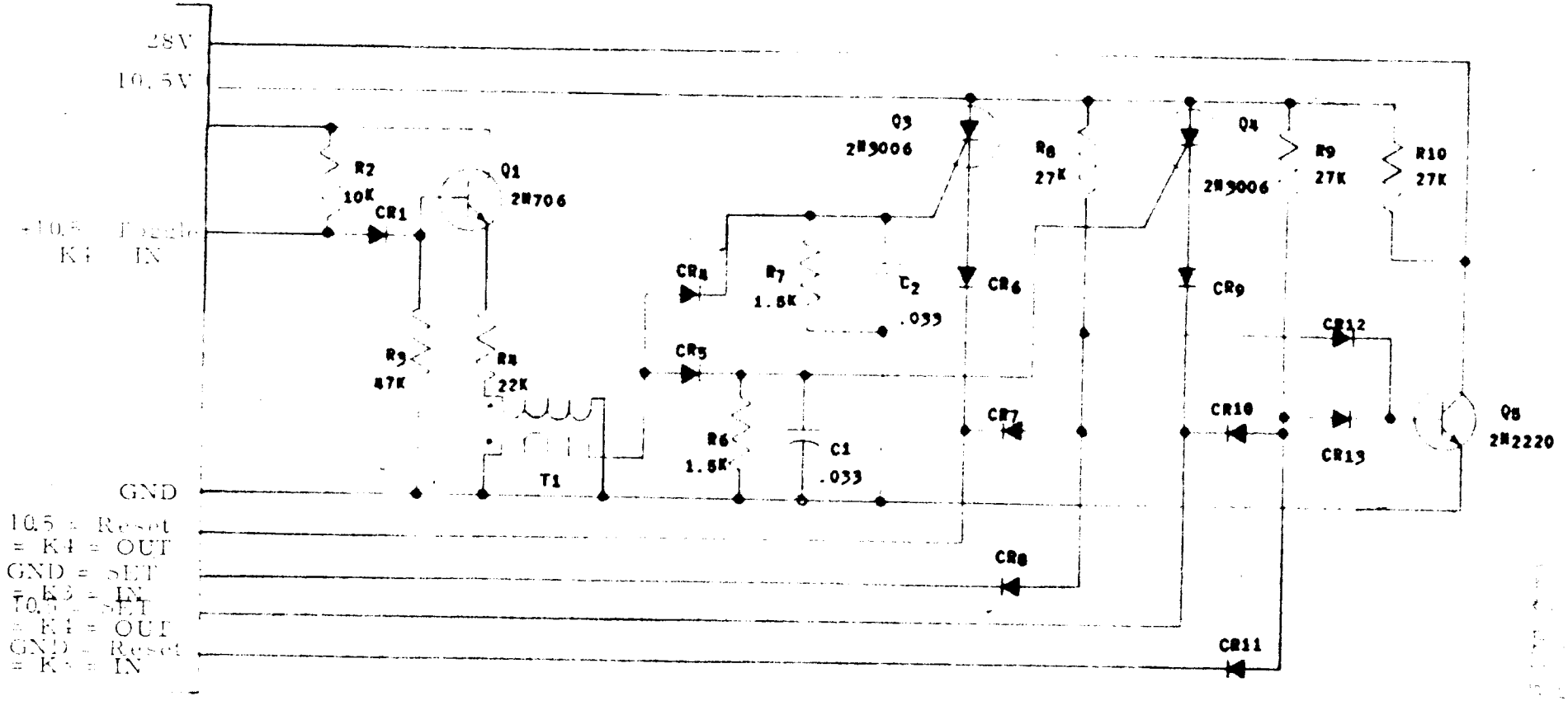

FIGURE VII-6D

SCHEMATIC - K4 RELAY CONTROL MODULE

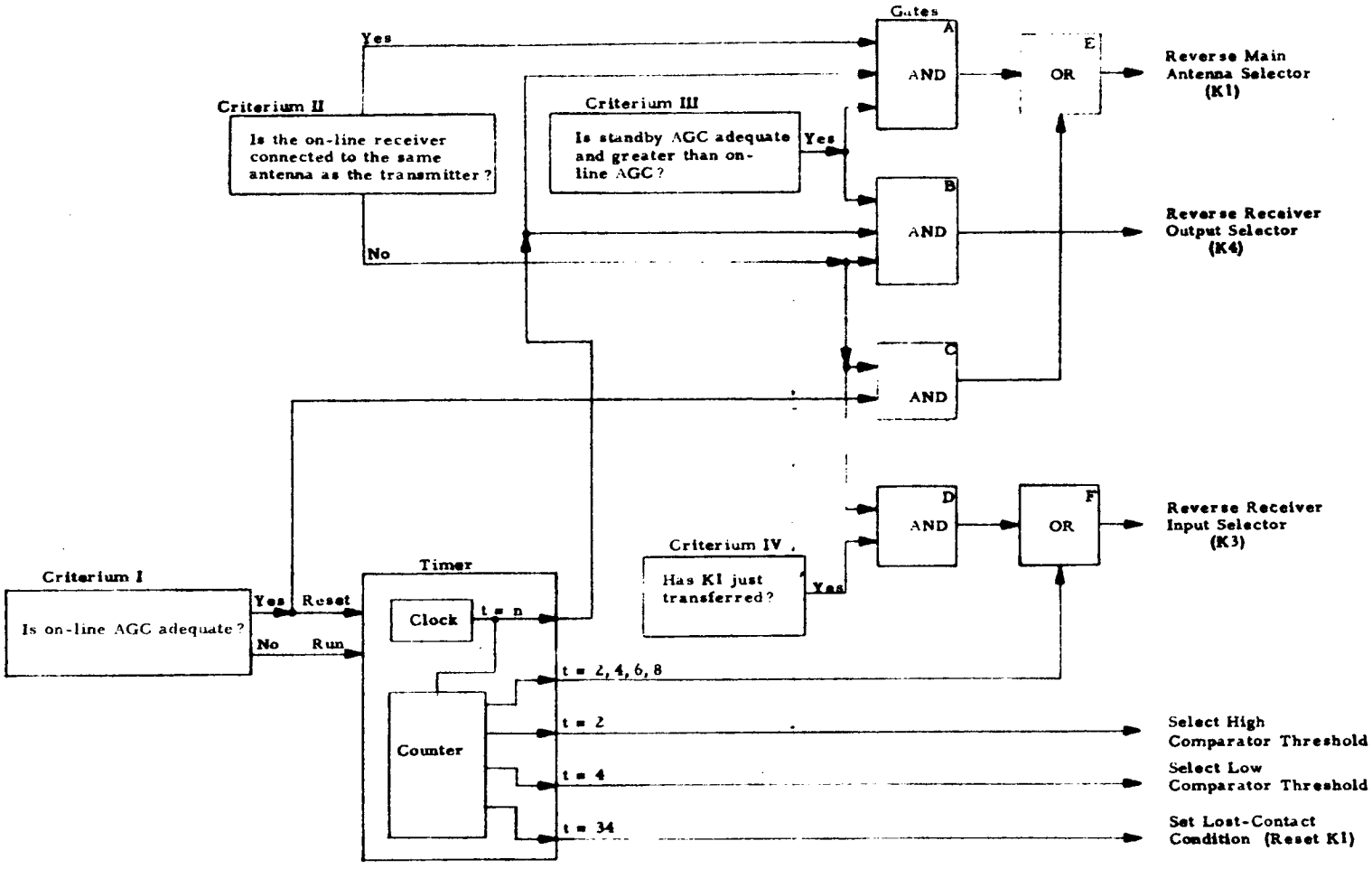

FIGURE VII-7. BLOCK DIAGRAM: LOGIC TREE

3) Mode II signal seeking procedure:

Criterium II	Yes
Criteria I, III and IV	No

Timer is again allowed to run. Criteria II and III block Gates A, B, C and D. Second clock pulse (at t = 2) causes the counter to generate outputs on the t = 2 and the t = 2, 4, 6, 8 lines. The t = 2 line pulse assures that comparator uses upper threshold level (representing a "loud and clear" signal). The other pulse is passed through Gate F to the receiver input selector control. This control causes the receiver input selector relay (K3 in Figure VII-1) to toggle, interchanging inputs to the receiver(s). At this point, a number of possibilities exist:

a) Strong signals are being received. The standby receiver has failed, or was omitted, so that Mode I service is needed to test standby antenna. In this case logic now determines:

Criterium I	Yes
Criteria II, III, IV	No

Timer is reset immediately. Reset order is passed by Gates C and E (E and F are always open) to the main antenna selector control. This control toggles K1 as in condition 2. This generates a pulse due to criterium IV, passing through Gates D and F to the receiver input selector control. This control returns K3 to its original position. Normal conditions are restored by this course of action.

b) Strong signals are being received. The on-line receiver has just failed. In this case the situation is:

Criterium III	Yes
Criteria I, II, IV	No

This means that Gates B and C open. Next clock pulse (at t = 3 minutes) will pass through Gate B to the receiver output selector control. This control toggles the receiver output selector relay (K4 in Figure VII-1). Note that receiver input selector relay has already been toggled, so this completes a receiver interchange. Normal conditions are thus restored. (Only Mode I service can be used hereafter.)

c) Strong signals are not available. In this case:

Criteria I, II, III, and IV are all No.

At t = 4, counter generates pulses on the t = 4 and the t = 2, 4, 6, 8 lines. The t = 4 line pulse switches the comparator threshold to low (marginal signals accepted). The t = 2, 4, 6, 8 line pulse results in K3 (Figure VII-1) toggling back to original position. Now, again, multiple possibilities exist.

c-1) Weak signal present. On-line receiver AGC voltage satisfies Criteria I. In this case normal conditions exist, and logic returns to resting mode.

c-2) Weak signal present. Standby receiver AGC voltage satisfies criterium III. Next clock pulse is passed to the K1 control (as in Condition 2) for normal Mode II transfer. (Mode II service will be provided now until point where outputs of both antennas simultaneously are below the relaxed requirement.) Normal conditions are restored.

If none of the above possibilities fit the circumstances, the logic continues signal-seeking. At t = 6 minutes, a pulse on the t = 2, 4, 6, 8 line again results in K3 (Figure VII-1) toggling. This connects the on-line receiver to the standby antenna again. Now,

c-3) If a weak signal is present, but the standby receiver is inoperative, conditions are read by the logic as:

Criterium I	Yes
Criteria II, III, IV	No

This is the pattern already described under 3 a. The same procedure, naturally, is used to restore normal conditions.

c-4) A weak signal is present. On-line receiver has just failed. Logic now determines:

Criterium III	Yes
Criteria I, II, IV	No

This is the pattern found under 3 b. Naturally, the same procedure is used to restore normal conditions (4 minutes later in cycle, of course).

c-5) Neither antenna/receiver combination satisfies logic. (Presumably, ground station if off the air, or line-of sight path is blocked.) This produces:

Criteria I, II, III and IV No

The counter continues counting. At t = 8 it generates a final pulse on t = 2, 4, 6, 8 line. This causes K3 (Figure VII-1) to return the circuit to the original configuration (threshold level remains at low level). This condition is maintained for 26 minutes (until t = 34) unless either criterium I or III changes to Yes. (Criterium I would reset counter --see Condition 3b for procedure if criterium III changes to Yes.)

c-6) Lost contact condition: At t = 34 the main beam antenna is selected for both the transmitter and the on-line receiver. This condition is maintained for 32 minutes (until t = 66) unless criterium I or III changes to Yes (see above).

		Condition
t = 0	Criterium I changes to No	
t = 1	(If criterium III is Yes) - main antenna selector transfers	2
t = 2	(Criteria I and III must be No, to reach t = 2)- receiver input selector transfers. High threshold in use.	3
2<t<3	(If criterium I changes to Yes) - timer reset	3a
then:	Main antenna selector transfers	
followed by:	Receiver input selector transfers	
t = 3	(If criterium III changed to Yes at t = 2) - receiver output selector transfers	3b
t = 4	(Criteria I and III must be No to reach t = 4)- receiver input selector transfer. Low threshold in use.	3c
4<t<5	(If criterium I changes to Yes). Timer reset -- no further service needed at this time. (Low threshold continued in use.)	3c-1

		Condition
t = 5	(If criterium III changed to Yes at t = 4) - main antenna selector transfers	3c-2
t = 6	(Criteria I and III must be No to reach t = 6)- receiver input selector transfers. Low threshold continues in use.	
6<t<7	(If criterium I changes to Yes) - timer reset	3c-3
then:	Main antenna selector transfers.	
followed by:	Receiver input selector transfers.	
t = 7	(If criterium III changed to Yes at t = 6) - receiver output selector transfers.	3c-4
t = 8	(Criteria I and III must still be No to reach t = 8) - receiver input selector transfers. Low threshold continues in use.	3c-5
8<t	(If criterium I changes to Yes) - timer reset-- no further service required at this time.	
t = 9, 10, ---n	(Next minute after criterium III changes to Yes)- main antenna selector transfers.	
t = 34	(Criteria I and III must still be No to reach t = 34) - main antenna selector set to main beam antenna (lost contact mode)	3c-6
t = 66	Reset timer to zero and start over.	

D. Ground Control of Antenna Switching

The ground control is available in case the spacecraft logic fails or any time manual control is desired. To initiate the ground control of antenna switching a coded signal is transmitted to the spacecraft actuating the remote relays. The block diagram is shown in Figure VII-8.

The system proposed here utilizes three input commands and four output commands. The inputs are as follows: remote start, remote stop, sequence advance, and toggle. The outputs are: comparator good, comparator standby, clock check and relay status.

The remote start command transfers logic power to an alternate power source, the switching logic to become inactivated, and the sequence logic to become activated. The remote stop command

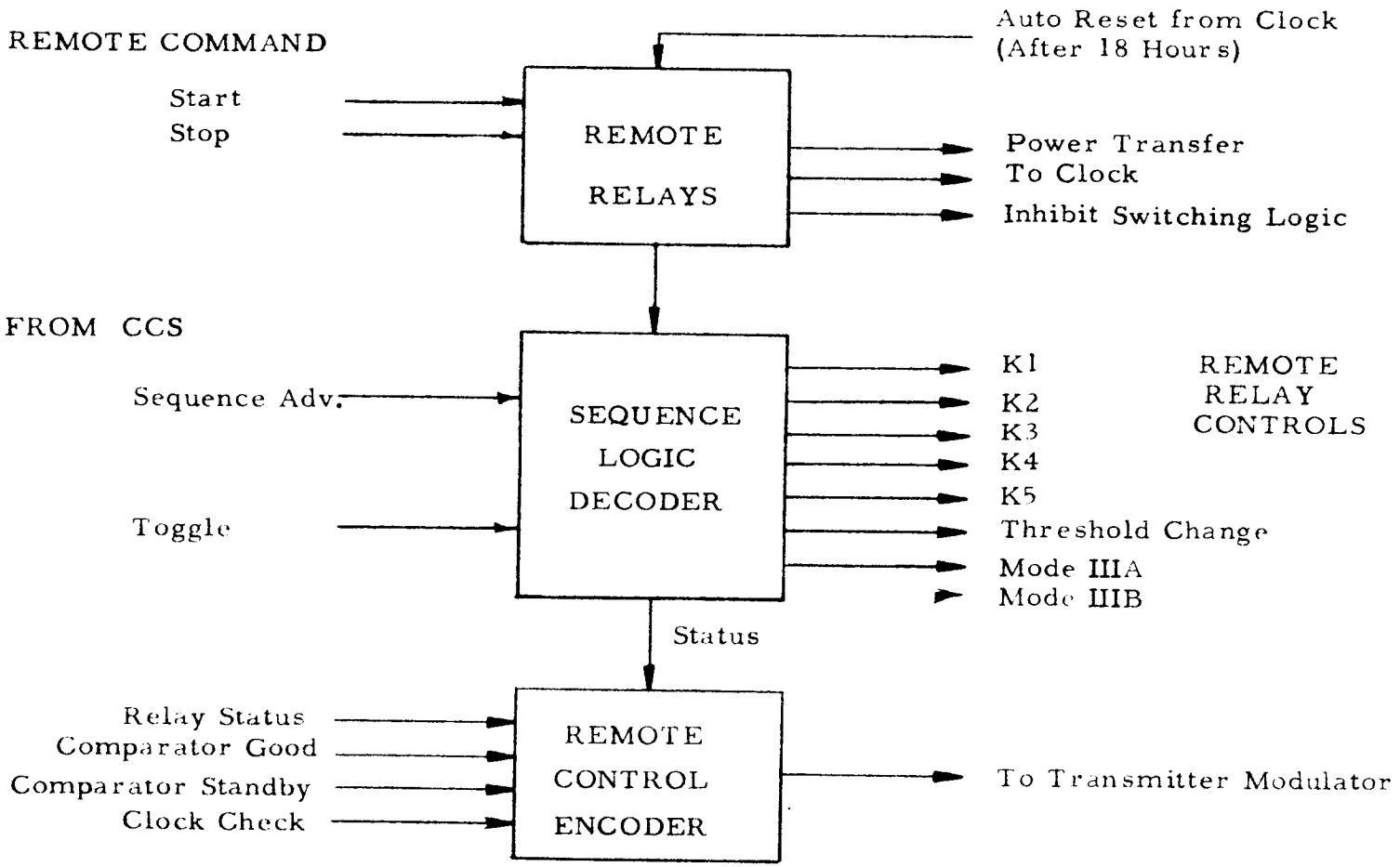

FIGURE VII-8

BLOCK DIAGRAM - REMOTE GROUND CONTROL

immediately causes the switching logic to revert to the normal condition. If a remote stop command is not transmitted, the spacecraft logic system will automatically take over control 18 hours after receipt of the remote start signal.

The sequence advance permits the ground operator to select any one of seven (more, if desired) control functions. The function chosen is determined by counting sequence advance command pulses. That is, the start command selects K1 remote function and the first sequence advance pulse moves the control to K2 relay and so on. If a change in status is desired, a toggle command is transmitted by the ground station. The function selected is then toggled.

In order to evaluate the changes in status of the receiver-transmitter system, it is proposed that the comparator "good" and "standby" status be telemetered to the ground station. These signals will permit the operator to verify that the proper decision was made. The clock check pin-points a failure in the timing circuits. The relay status signal permits the operator to determine whether a switching relay is in the set or reset condition.

E. Failure Mode

In the event of a failure of one of the receivers in a Mode II system, the logic is designed so that the system reverts to a Mode I system automatically. In the event of a comparator or other logic failure wherein an adequate signal cannot be found, the lost contact mode is initiated wherein the best antenna is connected to the best receiver (rest state). The ground control mode permits diagnostic tests to be performed by the operator to determine the effectiveness of the antenna switching system. The ground control mode offers the best insurance and recovery from a malfunction in the automatic switching system. A separate power source for ground control is proposed for added reliability.

The clock check detects a failure in the logic timing. A failure in the timing could result in a complete failure in the automatic switching system. Constant monitoring of this variable would permit immediate take-over by ground control to prevent a permanent lost contact. Another feature would be automatic transfer to a second spare set of timing circuits.

F. Logic and Switch Testing

1. Breadboard Logic

The logic system that was breadboarded differs somewhat from the system described in this report. Figures VII-9 and VII-10 are the schematics of the breadboarded counter and gate group modules respectively.

Figure VII-11 is a photograph of (from left to right) the gate group, the counter, the clock, and the comparator modules, mounted in a plastic frame for ease in testing. The modules are wired to one another, with all external connections brought to the barrier strip at top of frame. Frame is, naturally, not part of logic system. In practical cases the modules would be encapsulated for greater reliability and easier mounting. Interconnections among these four modules would probably be welded wires buried within the overall encapsulation. Space required would be about one third that used by breadboard modules. Figure VII-12 identifies the connection points of each module and the tie points on the barrier strip.

Figure VII-12 is a photograph of the relay control modules. The three relay control modules are built on identical PC boards, but differ in the component arrangements used for each unit.

The breadboard logic system includes one transfer coaxial relay--usable as either K1 or K3 in Figure VII-1, and one SPDT coaxial relay with a conventional, miniature DPDT relay wired with coils in parallel with the coaxial relay coils to simulate K4 in Figure VII-1. Actual system requires two such DPDT relays, but one is enough to demonstrate feasibility (current required is negligible, compared to the 3 ampere drain of coaxial relays). All three relay controls are included, since they differ in the auxiliary circuits included.

2. Tests Performed:

a. Modules

1) Comparator

Threshold: Adjustable 1.4 to 4.6 volts (equivalent to 1.54 to 5.04 volts at AGC line)
Input Impedance: See Figure VII-14
Bias: See Figure VII-15

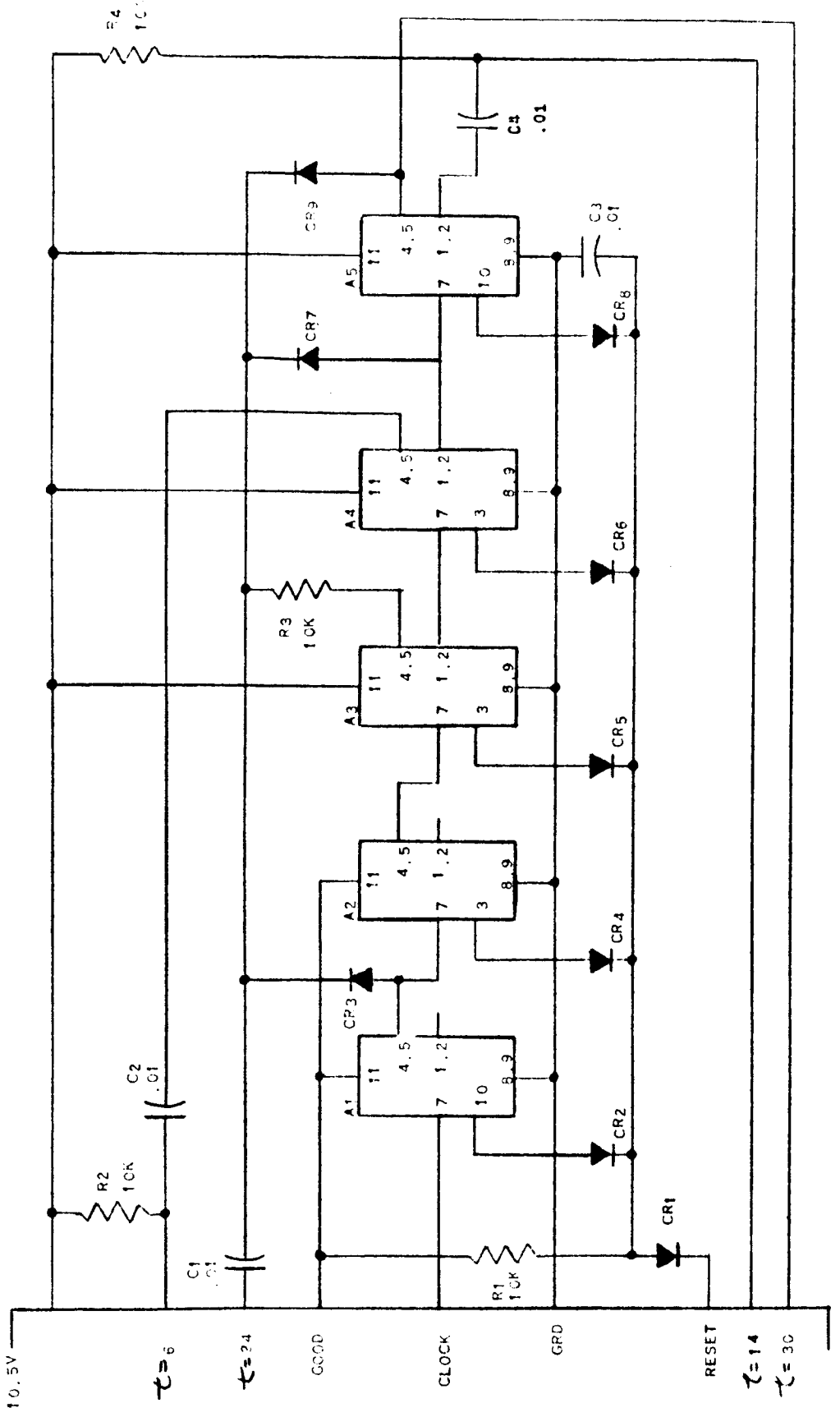

FIGURE VII-9. SCHEMATIC - BREADBOARD COUNTER

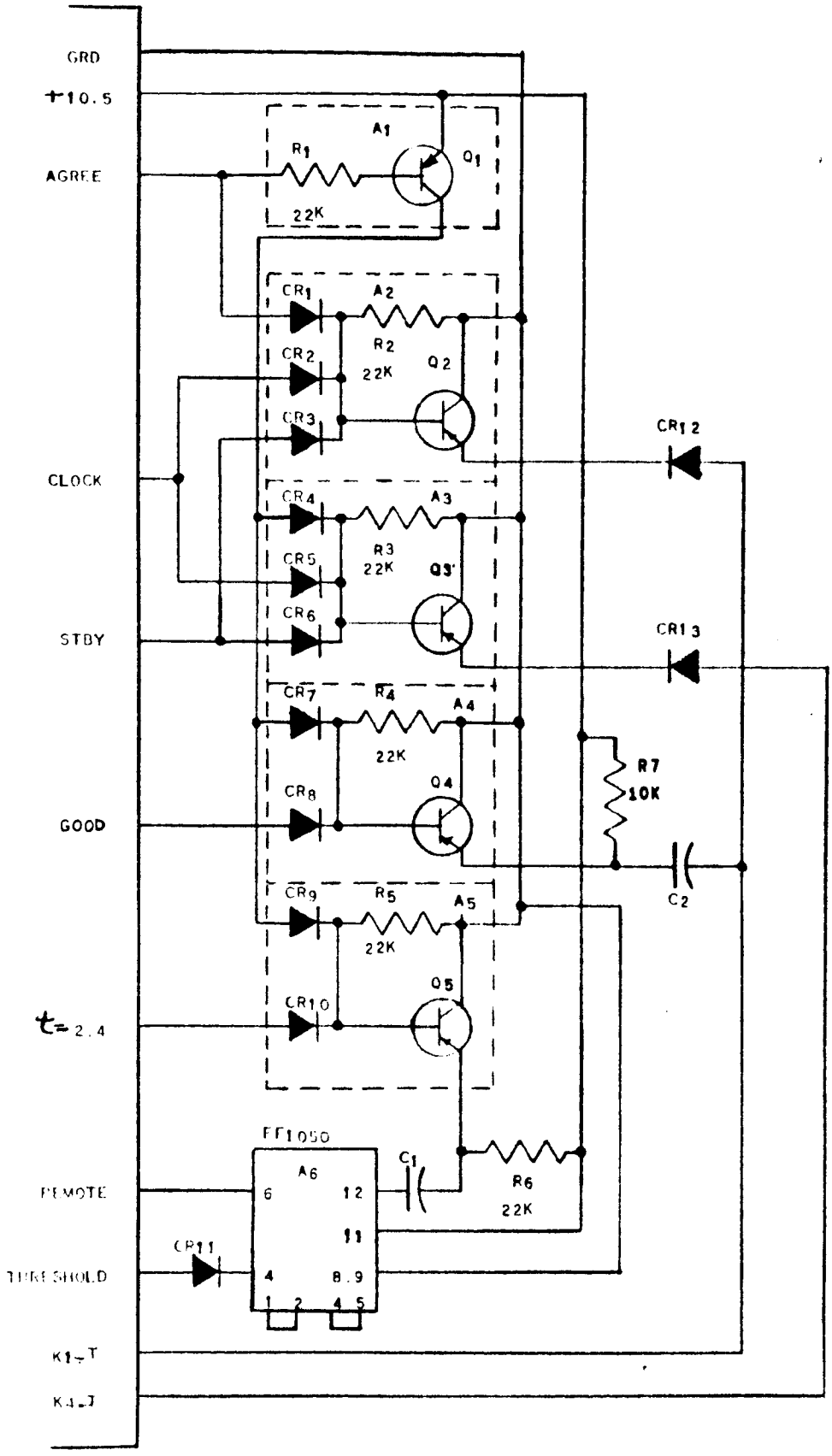

FIGURE VII-10. SCHEMATIC - BREADBOARD GATE GROUP

FIGURE VII-11

BREADBOARD LOGIC SYSTEM

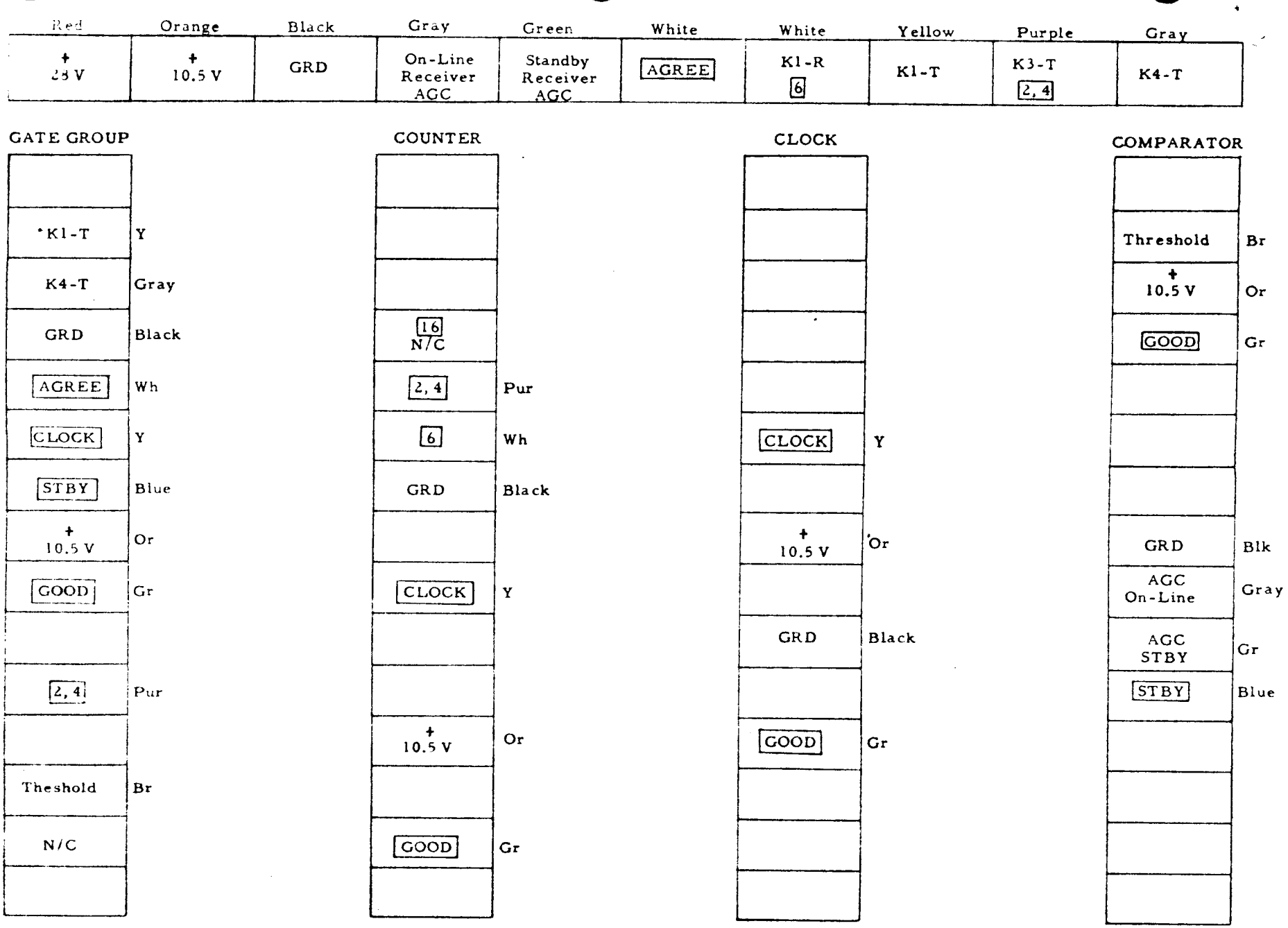

FIGURE VII-12. BREADBOARD LOGIC MODULE INTERCONNECTIONS

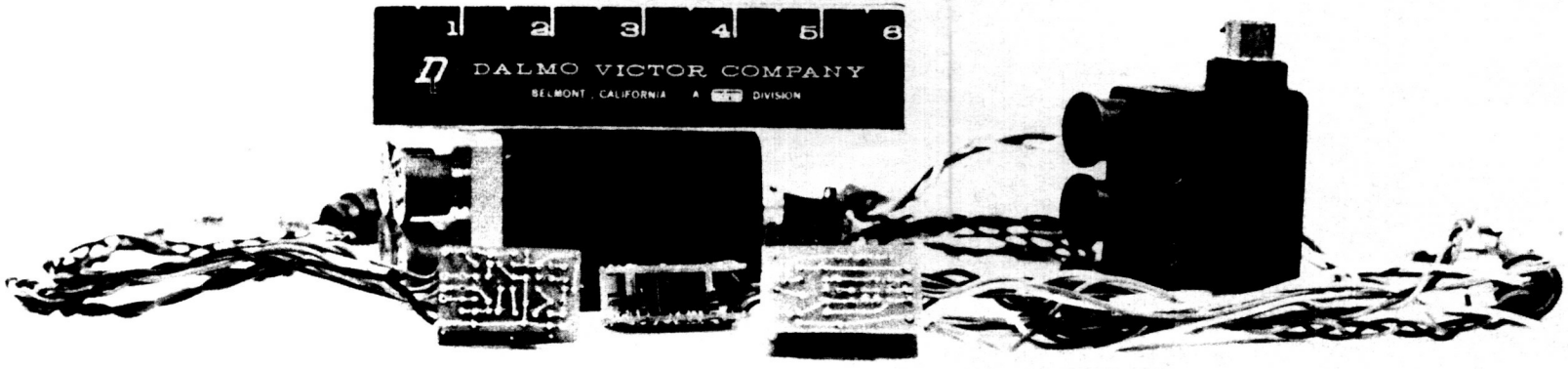

FIGURE VII-13

BREADBOARD RELAY CONTROLS

2) Clock

Period: 57 sec (could be changed to 60 sec easily)
Output: 10 volt amplitude
Leading edge negative going, 150 nsec fall time
19 msec wide

3) Counter

Checked OK -- Counts correct
Reset correct
Outputs correct

4) Gate Group

Checked OK -- Flip flop
Inverter
Gates

5) Relay Controls

Checked OK -- Toggle Circuit
Reset (K1 only)
AND (K4 only)

b. Assembled Logic

1) Comparator

Controls clock and counter.
Threshold controlled OK.

2) Clock

Operates counter.

3) Counter

Operates from clock.
Drives relay controls.

4) Gate Group

Gates commands.

5) Relay Controls

Operate from commands.

c. No Integrated Logic System Tests Were Performed

3. Implication of Tests

a. System Operation

The logic system loads the receiver AGC lines. Figure VII-14 shows the extent of this loading as a function of the AGC voltage.

The comparator is designed to give a preference for the on-line receiver. The standby receiver must exceed the on-line performance by an amount determined by the comparator bias characteristic in Figure VII-15. The input is the on-line AGC level in volts and this is plotted against the "extra" volts required by the standby AGC to cause the comparator to switch. The extra volts are given by on-line AGC minus standby AGC volts at the switching point.

Figures VII-16, 17, and 18 are curves indicating the degree of preference built into the breadboard comparator. These curves are obtained as follows: Take the 40 db above threshold point on the sample receiver curve, --this corresponds to -99 dbm on Figure VII-21. The AGC voltage at that point is approximately 4.35 volts. The AGC voltage at -96 and -94 dbm is 4.40 and 4.44 volts respectively. The difference between the operating point -99 dbm for the on-line receiver and the -96 dbm or the -94 dbm for the standby receiver results in the bias required for 3 db and 5 db preference respectively. These are plotted as points (1) and (2) on Figure VII-18. The AGC voltage at the 40 db above threshold point (-99 dbm) is 4.3 volts. Referring to Figure VII-15, find that 4.3 AGC volts corresponds to an actual comparator bias (designed into the comparator) of 0.1 volts. This is plotted on Figure VII-18 as point (3). From this, one concludes that at a receiver level of (-99 dbm) or 40 db above threshold, the built in preference is a little over 5 db of input RF signal.

Figure VII-19 shows the (approximate) responses of the two antennas as a function of vehicle orientation of the line-of-sight path. (These curves are average responses --minor variations with vehicle spin are not shown.) Figure VII-20 shows the AGC voltages the sample receiver would produce for various signal levels (as measured by an isotropic antenna). The dotted lines indicate the points at which logic would initiate the procedure to transfer to the alternate antenna providing on-line receiver was less than adequate as defined in Section F.3.b (actual transfer would occur one minute later). Thus, assuming a low tumbling rate, the hysteresis would be only slightly greater than the indicated 20° to 30° (depending on signal strength).

b. On Receiver Mismatch

If the receivers have a mismatch with respect to AGC characteristics, this mismatch appears as an error function to the logic. Refer to Figure VII-21. The mismatch between

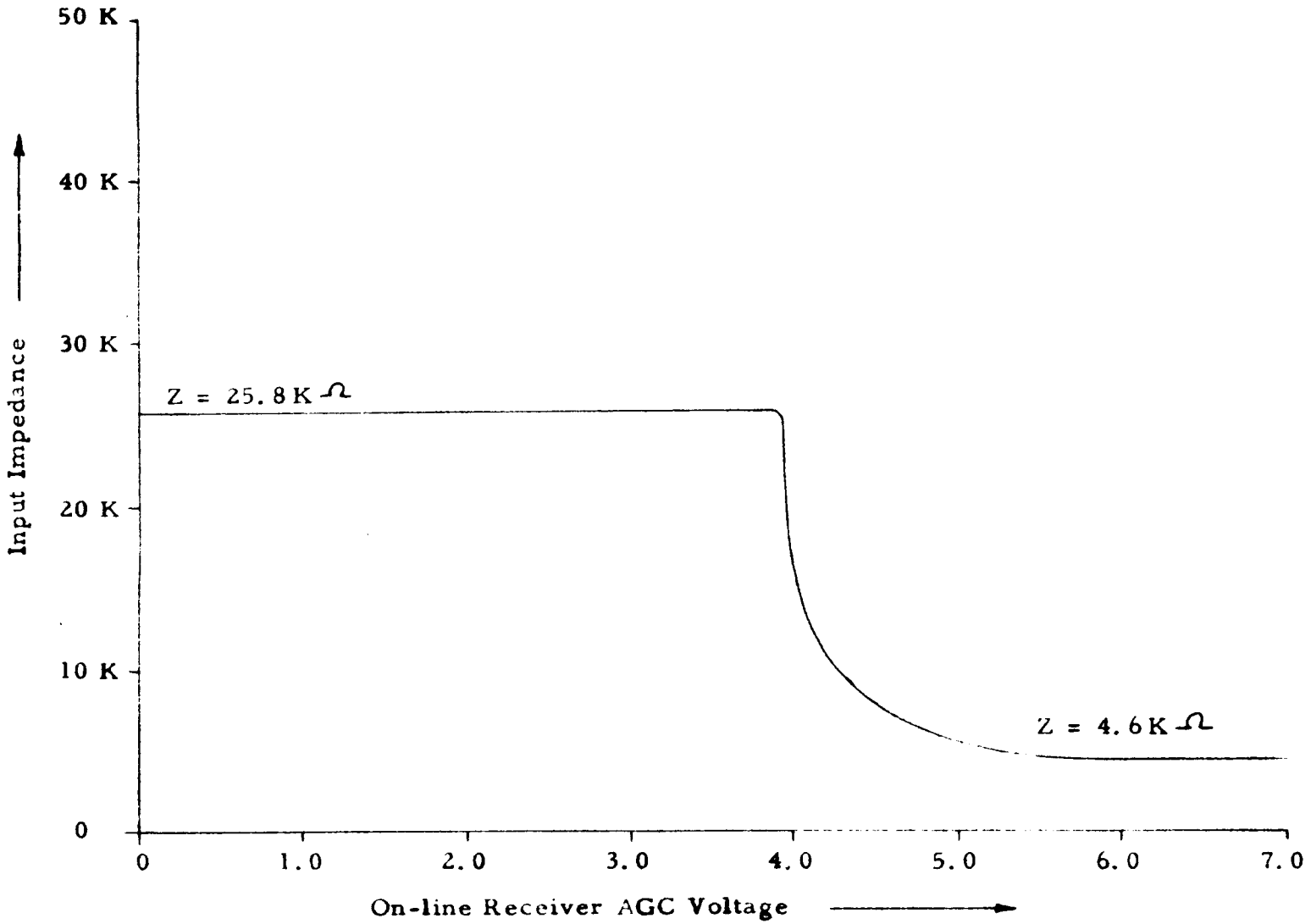

FIGURE VII-14. COMPARATOR INPUT IMPEDANCE

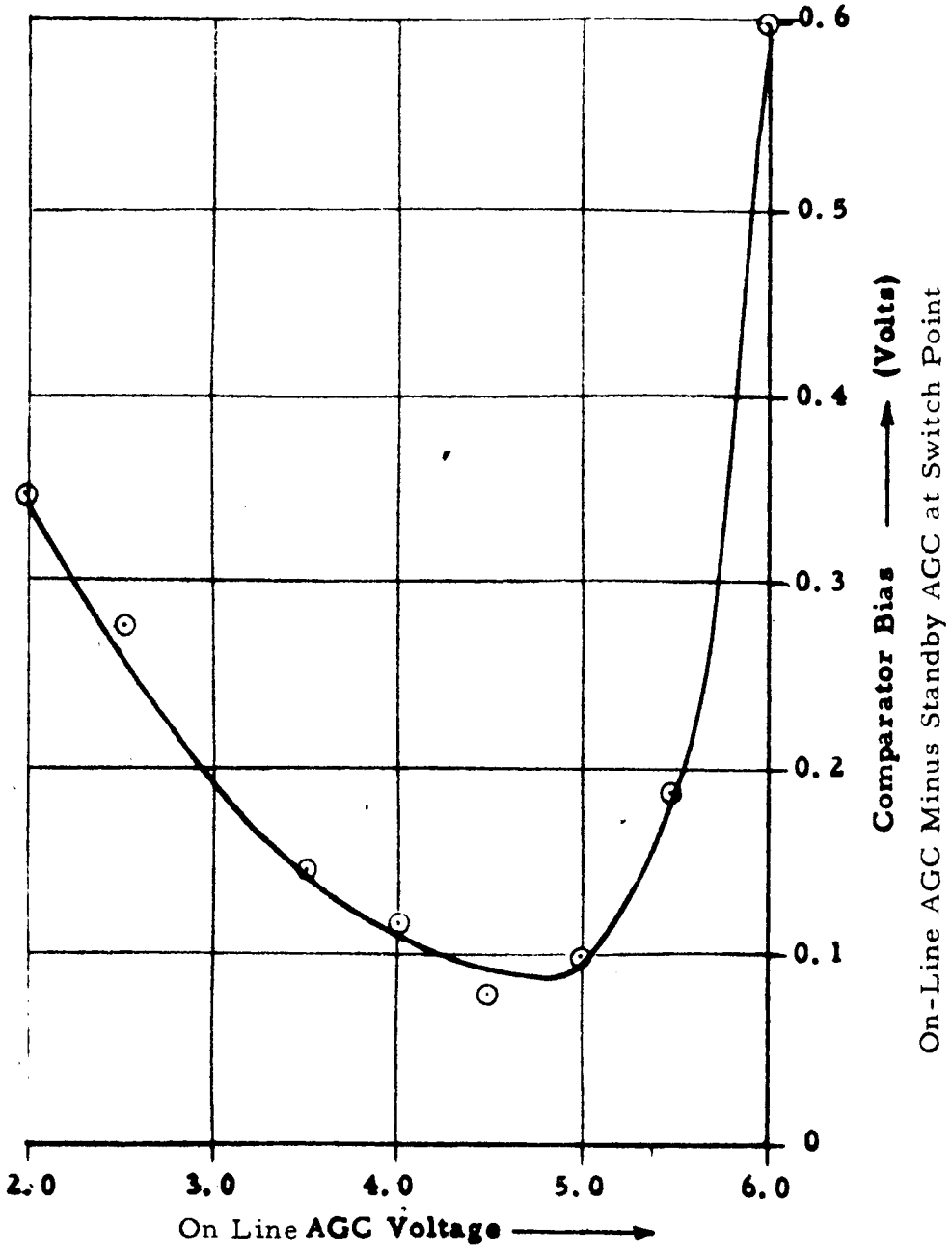

FIGURE VII-15

COMPARATOR BIAS CHARACTERISTIC

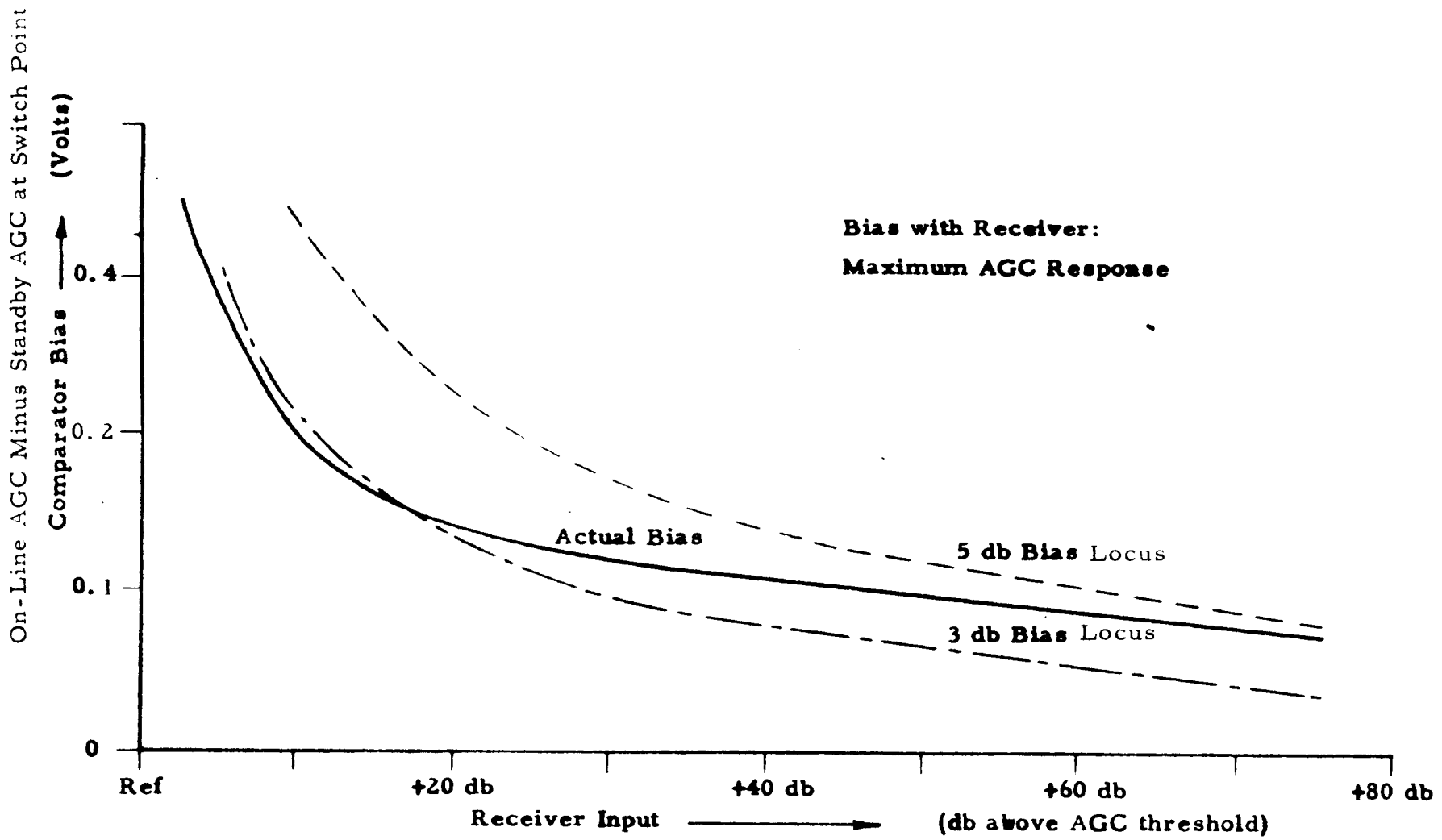

FIGURE VII-16. COMPARATOR BIAS VS. RECEIVER INPUT LEVEL

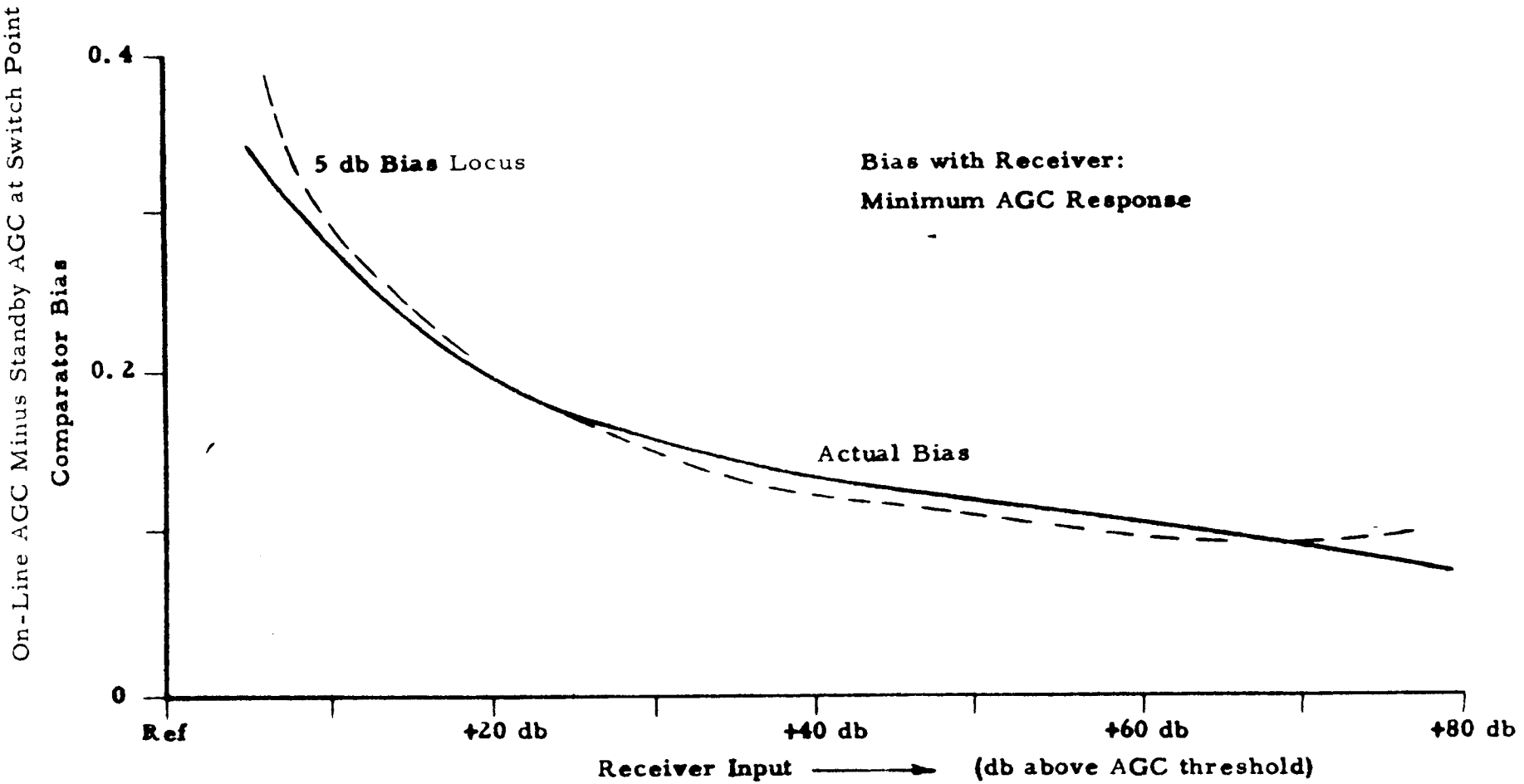

FIGURE VII-17. COMPARATOR BIAS VS. RECEIVER INPUT LEVEL

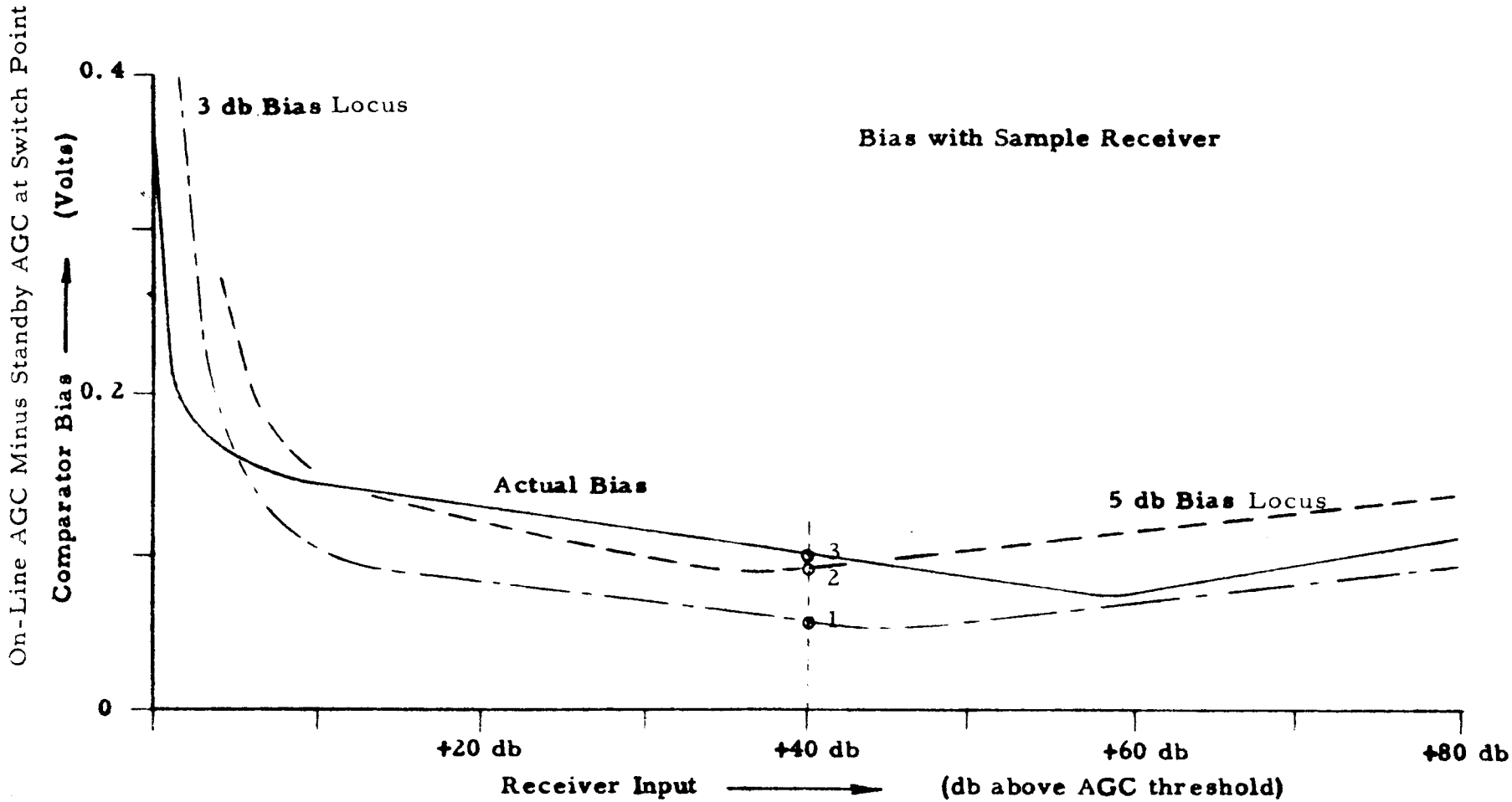

FIGURE VII-18. COMPARATOR BIAS VS. SIGNAL LEVEL

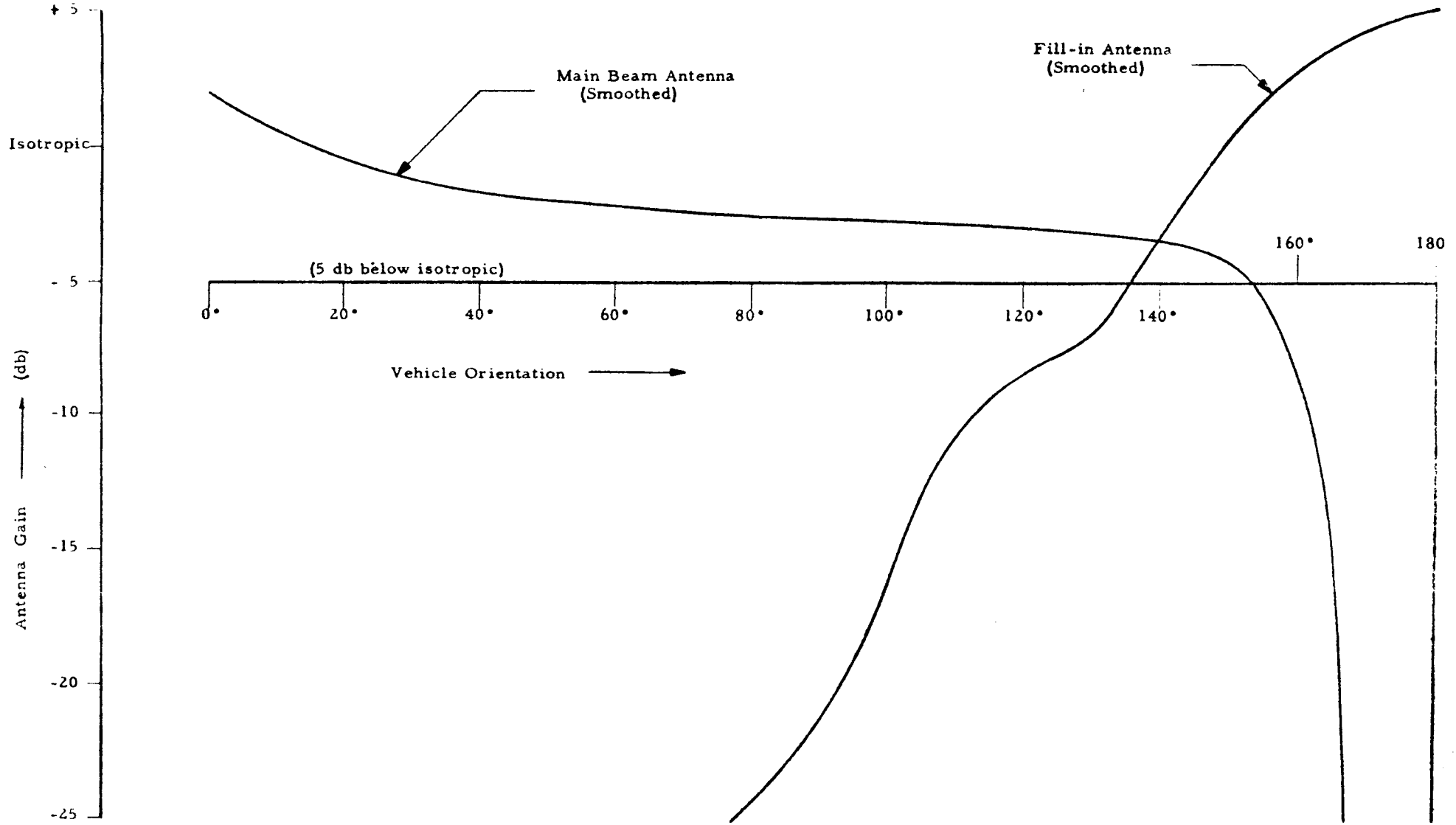

FIGURE VII-19. ANTENNA PATTERNS

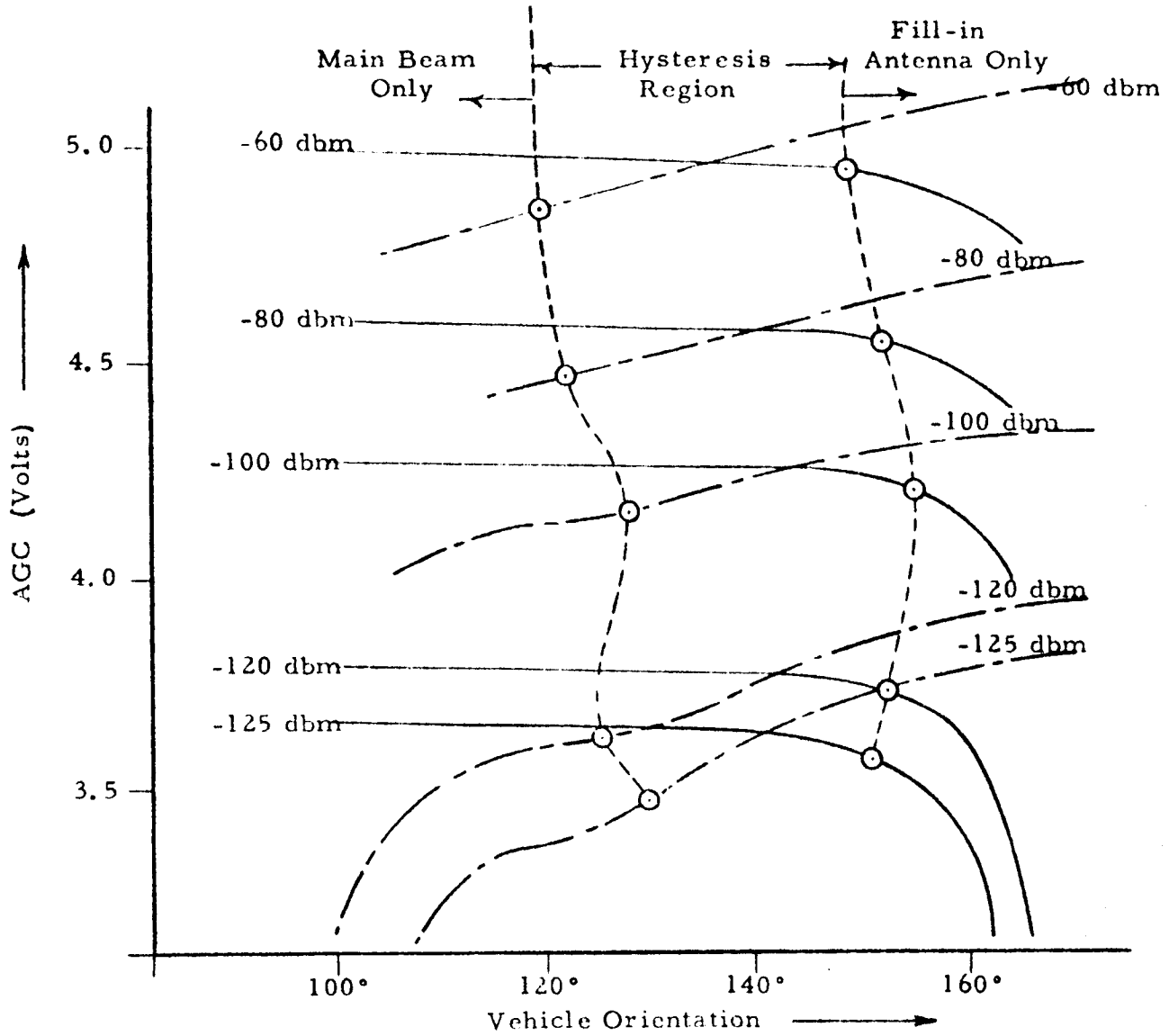

FIGURE VII-20. ANTENNA SELECTION VS. ORIENTATION

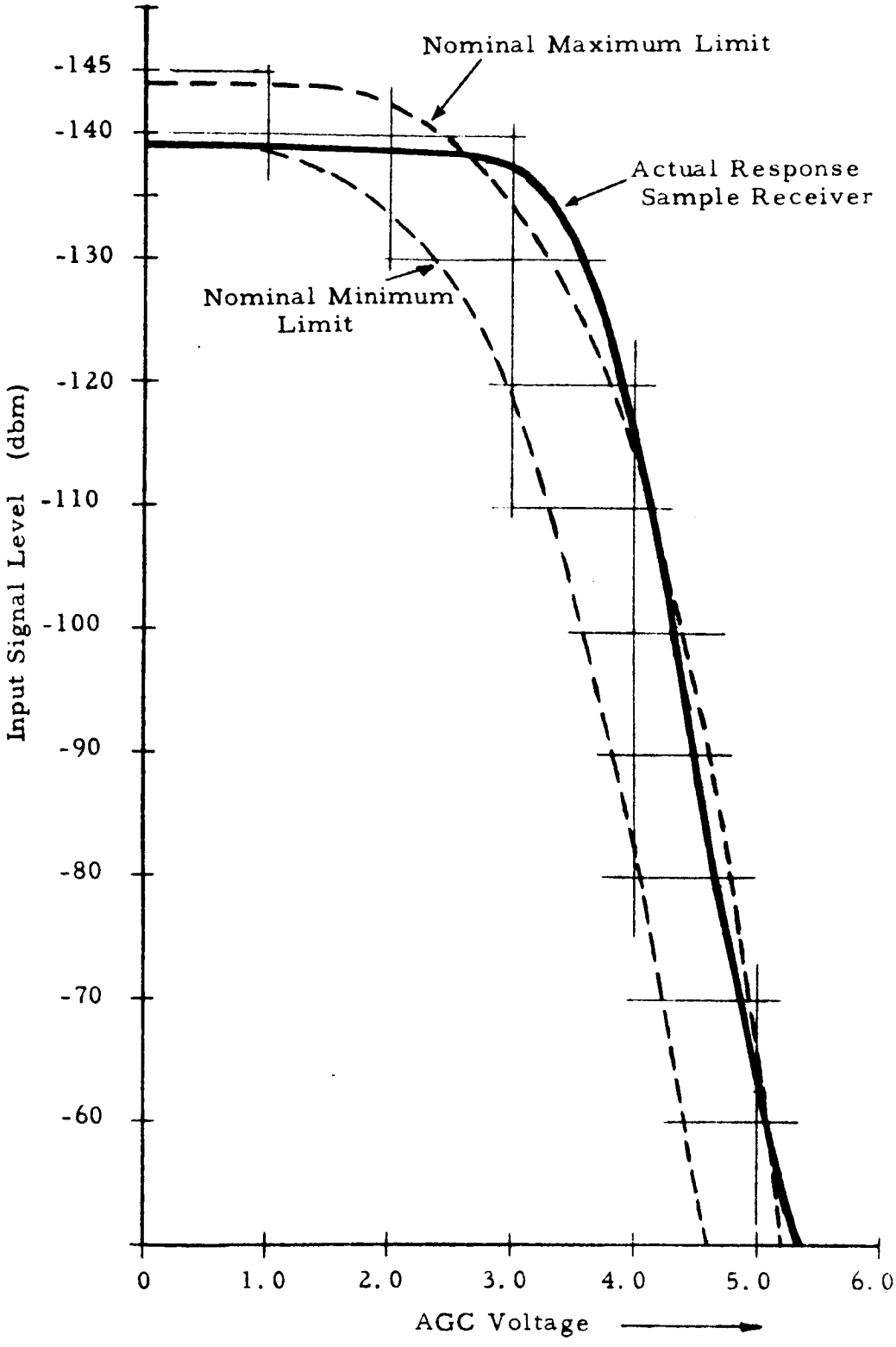

FIGURE VII-21. AGC LEVEL VS. INPUT SIGNAL STRENGTH

the Nominal Maximum Limit, the Sample Receiver, and the Nominal Minimum Limit are so great that the logic would be compromised. For example, when the receiver represented by Nominal Lower Limit is 20 db above threshold (-119 dbm) the AGC voltage is 3 volts. The Nominal Maximum Limit voltage does not drop to 3 volts until -134 dbm or 5 db above threshold. A 15 db error is introduced by the AGC mismatch.

A simple offset matching technique will permit sliding the AGC curves to the left or right to achieve a best fit with a nominal AGC curve. A circuit that will achieve this result is shown in Figure VII-22. The details of the offset DC voltage injection circuitry can take many forms and should be integrated into the receiver design. This technique was applied to the receiver characteristics of Figure VII-21 by overlays and the improved set of curves shown in Figure VII-23 resulted. If we concern ourselves with only those signals less than 30 db over threshold, the worst case error is about 2 db.

The range of AGC comparisons can be limited by the "adequacy" comparator (see comparator VII-5). Adjusting R20 of Figure VII-2 determines the range over which the automatic switching logic is active. The philosophy here is that if a signal is above a certain level (defined as adequate) no optimization is required. The remaining 2 db of uncertainty is eliminated by the built-in preference in the comparator.

By the simple expedient of including an AGC offset adjustment (adding or subtracting a fixed DC voltage) in the receivers the AGC curves of Figure VII-21 were adjusted so that only 2 db of preference was required to eliminate unnecessary or false switching commands.

c. System Power Consumption

System power requirements are shown below. The logic is designed to operate from +10.5 VDC, except for the coaxial relays plus a small drain by the relay controls at +28 VDC. The NORMAL figures apply when logic is satisfied; the ACTIVE figures when logic is not satisfied --timer is running, and the relays may be operated during this period.

Module	Normal	Active
Comparator	1.65 ma at 10.5V	23.0 ma at 10.5V
Clock	0.60 ma at 10.5V	6.0 ma at 10.5V
Counter	15.75 ma at 10.5V	55.0 ma at 10.5V
Gate Group	12.78 ma at 10.5V	12.0 ma at 10.5V

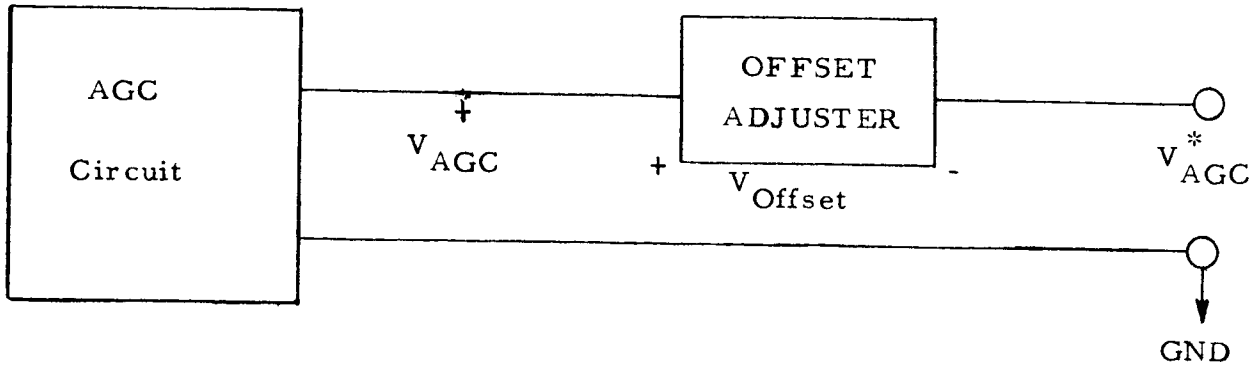

$$V^*_{AGC} = V_{AGC} + V_{Offset}$$

V^*_{AGC} = Corrected AGC Voltage

V_{AGC} = Uncorrected AGC

V_{Offset} = DC Offset Correction Voltage

FIGURE VII-22

AGC OFFSET CORRECTION VOLTAGE

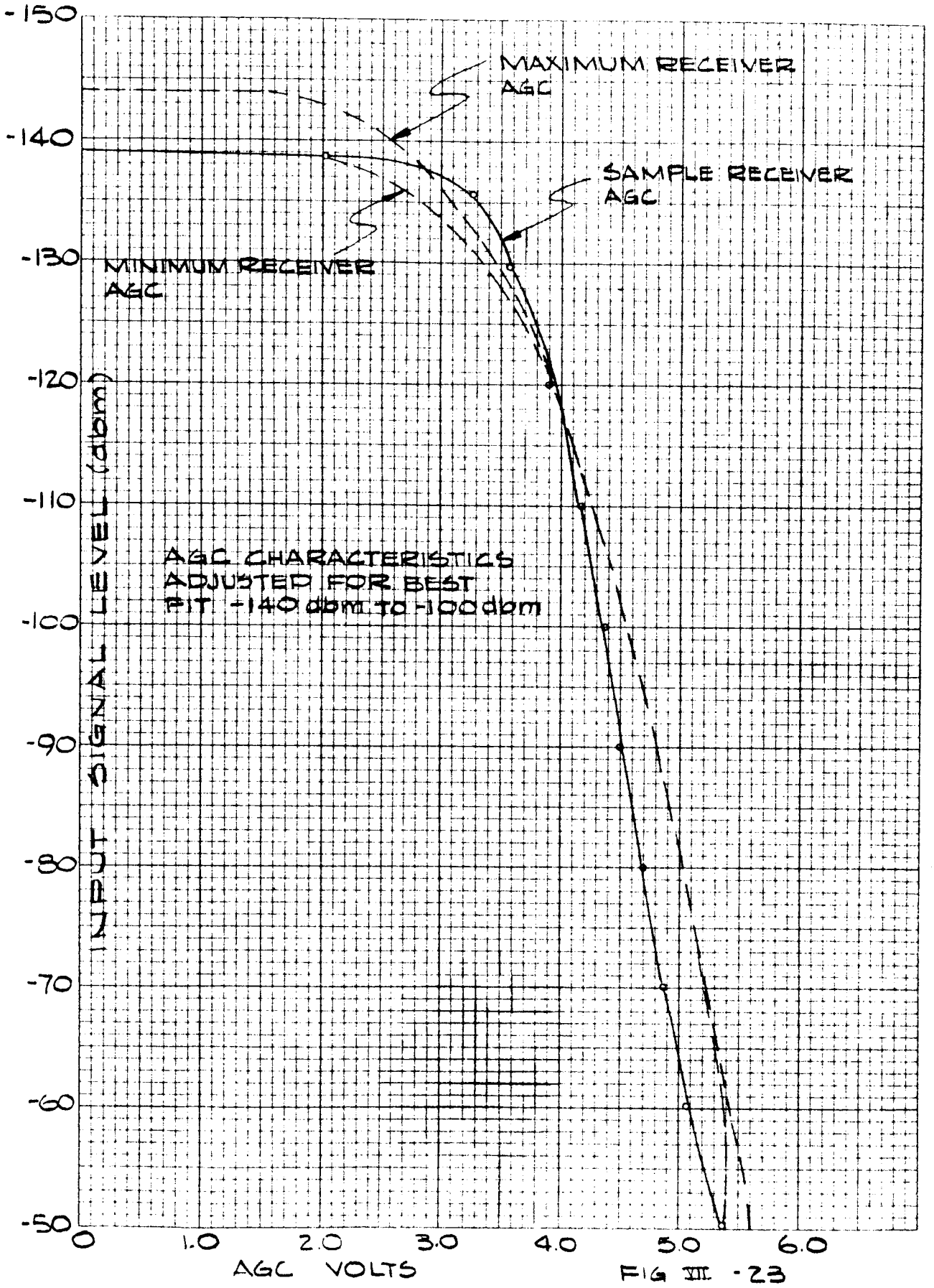
MAXIMUM RECEIVER AGC
SAMPLE RECEIVER AGC
MINIMUM RECEIVER AGC
AGC CHARACTERISTICS ADJUSTED FOR BEST FIT -140 dbm TO -100 dbm
INPUT SIGNAL LEVEL (dbm)
-150
-140
-130
-120
-110
-100
-90
-80
-70
-60
-50
0
1.0
2.0
3.0
4.0
5.0
6.0
AGC VOLTS

FIG VII-23

Relay controls do not require fast rise pulses, so they can be located so as to minimize the 28 volt line lengths (3 ampere pulses flow here). The remainder of the logic is best grouped at any convenient location in vehicle --currents are small, but relatively fast pulses are involved. Shielded lines should be used for the AGC lines and the relay control command lines to protect them.

Module	Normal	Active
Relay Controls (ea. of 3)	5.00 ma at 10.5V	4.0 ma at 10.5V
	2.00 ma at 28V	3.0 ma at 28V (1 minute average)
Total Drain	45.7 ma at 10.5V	108.0 ma at 10.5V
	6.0 ma at 28V	9.0 ma at 28V

Total power requirement, at 10% over normal voltage:

0.785 watts normal
1.677 watts active

F. Recommendations

The Mode II system is far superior to the Mode I where reliability is important. Compared to a fixed configuration, a Mode I system is mainly useful in obtaining initial contact to an orbiting satellite, since over-all reliability is substantially set by the receiver and transmitter. This basic level is much higher in a Mode II system, and the probable service life is extended by a factor of almost three. Thus this system gives the advantages of a Mode I system, plus the probability of maintaining contact to a greater range.

If power consumption appeared to be a critical factor, a modification, intermediate between Modes I and II, is possible. In this case, one receiver could be turned off normally, together with all the logic other than the comparator. When a Mode I signal seeking procedure was called for, the second receiver would be energized together with the logic circuitry. This would extend receiver lifetime as well as save power. Another option would be Mode II, remotely changed to this pattern after launch and subsequent maneuvers were completed.

The use of field effect transistors in the comparator is clearly indicated. This would reduce loading on the AGC lines. High gain is not needed here, nor high frequency gain, but stability is important. Field effect transistors are somewhat better in this respect, also.

The counter circuit recommended is designed to fit easily into a timed-remote system. Construction of the full, timed-remote system is recommended where loss of contact is expected at regular intervals. The capture of control feature appears particularly wise, unless protection is desired against control commands originating at unfriendly stations (this is another problem altogether).

Relay controls do not require fast rise pulses, so they can be located so as to minimize the 28 volt line lengths (3 ampere pulses flow here). The remainder of the logic is best grouped at any convenient location in vehicle --currents are small, but relatively fast pulses are involved. Shielded lines should be used for the AGC lines and the relay control command lines to protect them.

VIII. RELIABILITY

Failure rates have been separately computed for the various modes of action possible to the logic. These are

Mode I logic	$F = 32.04 \times 10^{-6}$/hour
Mode II logic*	$F = 19.41 \times 10^{-6}$/hour
Receiver interchange	$F = 29.87 \times 10^{-6}$/hour
Total logic system	$F = 40.21 \times 10^{-6}$/hour

There are many parts used for more than one of the above, and in addition the risk of failure in an unused component disabling the system has been incorporated in the above numbers.

From the above failure rates, the probability that the various modes of logic will survive 2000 hours operation can be computed, as $P = e^{-2000\,F}$

Mode I logic	$P = 0.938$
Mode II logic*	$P = 0.961$
Receiver interchange	$P = 0.942$
Total logic system	$P = 0.923$

Likewise, the mean time before failure can be computed as $MTBF = 1/F$ However, a more meaningful number is the expected service time in a given mode. This depends on the receiver and transmitter reliability figures as well as that of the logic.

Given, for 2000 hours operation:

$$P_{xmtr} = 0.951$$

$$P_{rcvr} = 0.789$$

The probability that a transmitter and two receivers will all be available is $(P_{xmtr})(P_{rcvr})(P_{rcvr})$ or

$$(0.951)(0.789)^2 = 0.592$$

This is the probability that a Mode II system is available for perfect logic reliability. Including logic failures gives

$$(0.951)(0.789)^2(0.961) = 0.569$$

---

* Mode II logic used here to represent those circuits unique to Mode II and not common to Mode I.

The difference between the above two figures, or 0.023, represents the probability that with transmitter and both receivers operational, the logic will fail in Mode II. There remains the possibility that Mode I logic is still functioning, however. Due to overlap between the Mode I and Mode II logic components, there is only a 50 per cent chance that Mode I will be available under these circumstances. Thus, the probability of having Mode I service here (after a mode II failure) is

$$(0.023)(0.50)(0.93) = 0.011$$

This leaves, of the original 0.592, just 0.012 which is assigned to logic failure.

A second possibility is that one receiver fails, but the other receiver and the transmitter are operational. The probability of this is that since either receiver can be the one to fail,

$$P = 2(0.951)(0.789)(1-0.789) = 0.317$$

Half the time, on-line receiver will fail, requiring a transfer; hence, the probability that receiver on-line is good comes to

$$(0.317)(1/2)(1 + 0.942) = 0.307$$

Now, this number can be combined with the figures for Mode I logic to get the probability of Mode I service.

$$P = (0.307)(0.938) = 0.288$$

As before, the difference, or 0.019, represents logic failure in an otherwise usable system.

Thus the total figures are:

Mode II	P = 0.569
Mode I	P = 0.299
Total logic service	P = 0.868
Static mode	P = 0.031

From these figures the MTBF of each system can be computed, giving:

Mode II	MTBF = 3,552 hours
Mode I or II	MTBF = 14,178 hours
Any usable	MTBF = 18,879 hours

From this, it appears that a Mode II (at launch) system will provide:

Mode II service	3,552 hours
Mode I service	10,626 hours
Static service total	2,350 hours
Total	16,528 hours

A perfect logic system would give:

Mode II	3,815 hours
Mode I	17,061 hours
Total	20,876 hours

On the other hand, a system without logic could use only one receiver, and one antenna (plus a transmitter). Such a system would have a probability of surviving 2000 hours of

$$P = (0.951)(0.789) = 0.750$$

and a MTBF of 6963 hours. Assuming a random vehicle orientation and an antenna which covered 85 per cent of space, the service life of this system would come to 5919 hours.

The above computations are all based on random vehicle orientation. If vehicle orientation is controllable, the antenna selecting portion of the logic can be disabled after control is established to assure retention of correct antenna. They also assume 100 per cent reliability for cabling and the antennas. Since these elements are totally passive, this appears a reasonable assumption. In any case, such portions would affect any system equally and would not enter into comparisons significantly.

IX. WEIGHT ESTIMATES

The total Mode II - Case I system is to weigh 28 pounds or less. The specified weights for one transmitter and two receivers is 20 pounds, leaving 8 pounds for the antennas, switches, logic, cables, connectors, and wiring. The table below summarizes the weights that were estimated for a Mode II - Case I system, as described in this report, if it were designed for space flight.

Omni Antenna	1-3/4 lbs.
Helix	3/4 lb.
RF Cabling	1-1/4 lbs.
RF Connectors	3/4 lb.
RF Switches (K 1, 3 and 4)	2-1/2 lbs.
Logic and Wiring	1 lb.
Total	8 lbs.

A Mode III system would require approximately one additional pound plus the weight of the additional antenna and RF cabling.

A Mode I system eliminates one receiver (9 pounds) and considerable RF cabling and connectors as well as requiring only one SPDT RF switch. The total saving in weight for a Mode I system is estimated at 12 pounds.

X. SUMMARY

A. Antennas

A pair of antennas that meet the requirements necessary to provide right circularly polarized spherical coverage with maximum reliability for a closed loop spacecraft telemetry system have been developed. Possible choices for antenna designs to provide two different types of pattern coverages are described.

Detailed theoretical analysis and results of hardware development are presented for one of the designs. The principal antenna was designed for maximum possible coverage with right circular polarization and the null region is covered by the secondary antenna, a simple axial mode helix. The principal, or omni antenna, consists of eight sets of dumbbell loaded crossed slots located on a circumference of a circular waveguide which is supporting a circularly polarized standing wave. Extremely good agreement between the theoretically predicted and the measured performance was obtained for both antennas. The application of these antennas to a Ranger type spacecraft and measured patterns on a Ranger mockup are detailed in Appendix I.

B. Switching Logic

In summary, the logic selects the most sensitive receiver for use on-line. It switches to the alternate antenna from that in use if the on-line antenna receiver combination is not adequate and the standby antenna receiver combination is superior.

The condition specified above must continue for two minutes before transfer occurs.

If both antennas yield inadequate signals based on original requirements, these requirements are relaxed to allow use of marginal signals. If even this relaxed level cannot be met, the logic selects the principal antenna and operates with it until the signal strength recovers. Then the logic returns to service at original or relaxed levels, whichever can be met.

A ground control method of antenna switching is proposed wherein the operator can assume complete manual control in case of failure or desire to do so. The status of all switching functions as well as the comparator status is telemetered as data to ground control. Through the CCS, ground control can toggle any switching function.

the principal antenna and operates with it until the signal strength recovers. Then the logic returns to service at original or relaxed levels, whichever can be met.

Remote control of the various RF switches can be readily added. The only change in logic required is a method to turn the logic on and off by ground command. The only common components are the coaxial relays and the remote-local relay contacts. Remote control will not, of course, aid in establishing contact, but once established, it could be used to extend logic lifetime and save on power consumption.

REFERENCES

1. H. F. Mathis, "A Short Proof that an Isotropic Antenna is Impossible," Proceedings of the IRE, Vol. 39; August, 1951, p 970

2. H. F. Mathis, "On Isotropic Antennas," Proceedings of the IRE, Vol. 42; December, 1954, p 1810

3. Dalmo Victor Staff, "Proposal for a Spacecraft Omnidirectional Antenna for Jet Propulsion Laboratory," Appendices I and II; July, 1962

4. H. R. Riblet, "A Broadband Spherical Satellite Antenna," Proceedings of the IRE; April, 1960

5. J. T. Bangert, et al, "The Spacecraft Antennas," Bell Systems Technical Journal - Telstar Issue, Part I; July, 1963, pp 869-897

6. D. S. Bugnolo, "A Quasi-Isotropic Antenna in the Microwave Spectrum," Transactions of the IRE on Antennas and Propagation; July, 1962, pp 377-383

7. D. S. Bugnolo, "A Quasi-Isotropic Antenna in the Microwave Spectrum," Transactions of the IRE on Antennas and Propagation; July, 1962, pp 377-838

8. A. J. Simmons, "Circularly Polarized Slot Radiators," Transactions of the IRE on Antennas and Propagation; January, 1957, p 31

9. H. Jasik, "Antenna Engineering Handbook," McGraw-Hill, New York, New York; 1961, Chapter 7

10. J. D. Dyson, "Equiangular Spiral Antenna," Transactions of the IRE on Antennas and Propagation; October, 1959, p 329

11. J. A. Kaiser, "The Archimedian Two-Wire Spiral Antenna," Transactions of the IRE on Antennas and Propagation; May, 1960, p 312

12. S. Silver and W. K. Saunders, "The Radiation from a Transverse Rectangular Slot in a Circular Cylinder," Journal of Applied Physics, Vol. 21; August, 1950, pp 745-749

REFERENCES (Cont'd)

13. A. J. Simmons, "Circularly Polarized Slot Radiators," Transactions of the IRE on Antennas and Propagation; January, 1957, p 31

14. N. Marcuvitz, "Waveguide Handbook," MIT Radiation Laboratory Series, Vol. 10, McGraw-Hill, New York, New York; 1951

15. A. F. Stevenson, "Theory of Slots in a Rectangular Waveguide," Journal of Applied Physics, Vol. 19; 1948, pp 24-38

16. S. Silver, "Microwave Antenna Theory and Design," MIT Radiation Laboratory Series, Vol. 12, Chapter 9, McGraw-Hill, New York, New York; 1949

17. S. Silver and W. K. Saunders, "The Radiation from a Transverse Rectangular Slot in a Circular Cylinder," Journal of Applied Physics, Vol. 21; August, 1950, pp 745-749

18. See Reference 17.

19. A. Ksienski, "Maximally Flat and Quasi-Smooth Sector Beams," PGAP; September, 1960, pp 476-484

20. A. Ksienski, "Derivative Control in Shaping Antenna Patterns," Hughes Aircraft Company Scientific Report No. 35086; September, 1959

21. G. L. Ragan, "Microwave Transmission Circuits," Radiation Laboratory Series, Vol. 9, McGraw-Hill, New York, New York; 1948, p 344

22. A. J. Simmons, "Phase Shift by Periodic Loading of Waveguide and Its Application to Circular Polarization," Transactions of the IRE on Microwave Theory and Techniques, Vol. MTT-3; December, 1955, pp 18-21

23. S. Silver, "Microwave Antenna Theory and Design", MIT Radiation Laboratory Series, Vol. 12, McGraw-Hill, New York, New York; 1949, p 296

24. A. J. Simmons, "Circularly Polarized Slot Radiators," Transactions of the IRE on Antennas and Propagation; January, 1957, p 31

25. See Reference 24.

65-430

APPENDIX I

Appendix I includes complete free space patterns and all of the antenna-on-spacecraft patterns for various spacecraft configurations. Due to its bulk, it is under separate cover.

REVISION SHEET

Section	Revision	Page	Date
I, C	Completely revised.	I-2, I-3	4/13/65
VII	Entire section revised.	VII-1 thru VII-47	4/13/65
	Figure VII-1A added.	VII-3	4/13/65
	Figure VII-1 revised.	VII-5	4/13/65
	Figure VII-2 schematic revised.	VII-8	4/13/65
	Figure VII-3, callouts added	VII-11	4/13/65
	Figure VII-4, callouts added	VII-12	4/13/65
	Figure VII-5, callouts added	VII-14	4/13/65
	Figure VII-6A added.	VII-16	4/13/65
	Figure VII-6B added.	VII-17	4/13/65
	Figure VII-6C added.	VII-18	4/13/65
	Figure VII-6D added.	VII-19	4/13/65
	Figure VII-7 revised.	VII-20	4/13/65
	Figure VII-8 replaced with new figure.	VII-25	4/13/65
	Figure VII-14 revised	VII-35	4/13/65
	Figure VII-15, callouts added.	VII-36	4/13/65
	Figure VII-16 revised	VII-37	4/13/65
	Figure VII-17 revised	VII-38	4/13/65
	Figure VII-18 revised	VII-39	4/13/65
	Figure VII-22, new figure.	VII-44	4/13/65
	Figure VII-23, new figure.	VII-45	4/13/65
VIII	Footnote added to first page of section.	VIII-1	4/13/65
X, B	Section rewritten.	X-1	4/13/65
Revision B -	Page retyped --no revision.	VII-1	6/30/65
VII	Last paragraph revised.	VII-7	6/30/65
	Figures VII-3, VII-5, VII-6A, VII-6B, VII-6C and VII-6D resubmitted in blueline form; figures unchanged.	VII-11, 14, 16, 17, 18, 19	6/30/65